Electrical Conductivity And Elastic Moduli Of Pressure-sintered Lithium Substituted Nickel-oxide.

70-1735

NOTIS, Michael Richard, 1938-

ELECTRICAL CONDUCTIVITY AND ELASTIC MODULI OF PRESSURE-SINTERED LITHIUM SUBSTITUTED NICKEL OXIDE.

Lehigh University, Ph.D., 1969
Engineering, metallurgy

University Microfilms, Inc., Ann Arbor, Michigan

ELECTRICAL CONDUCTIVITY AND ELASTIC MODULI OF PRESSURE-SINTERED LITHIUM SUBSTITUTED NICKEL OXIDE

by

Michael Richard Notis

A Dissertation

Presented to the Graduate Faculty

of Lehigh University

in Candidacy for the Degree of

Doctor of Philosophy

in

Metallurgy and Material Science

Lehigh University

1969

CERTIFICATE OF APPROVAL

Approved and recommended for acceptance as a dissertation in partial fulfillment of the requirements for the degree of Doctor of Philosophy.

16 May 1969
(date)

Walter C. Hahn, Jr.
Professor in Charge

Accepted, 16 May 1969
(date)

Special committee directing the doctoral work of Mr. Michael Notis

Walter C. Hahn, Jr.
Co-Chairman

Richard M. Spriggs
Co-Chairman

Howard M. Cohen

George P. Conard III

Richard N. Tauber

Acknowledgements

I wish to express my sincere thanks to Professor Walter C. Hahn for his guidance and advice during the entire course of this work. His constant patience and sense of humor have made my life as a graduate student both educationally valuable and enjoyable. I am greatly appreciative for the interest and assistance received from Professor Richard M. Spriggs who has led one more metallurgist into the field of ceramic science.

I am also grateful for assistance from the following:

To the remaining members of my committee, Dr. H.M. Cohen, Dr. G. P. Conard II, and Dr. R. N. Tauber, for their interest and assistance during the course of this work.

To the CDC6400 computer for making a seemingly impossible task possible.

To Dr. O. L. Anderson and Mr. P. Mattaboni at the Lamont Geological Observatory of Columbia University for the use of the Pulse Transmission and Sphere Resonance equipment without which many of the results could not have been obtained.

To the National Science Foundation for sponsoring the research under N.S.F. project grant number GK1763, and for the N.S.F. Fellowship provided to me.

To Dr. J.I. Goldstein, Mr. P. LaRussa, and Mr. R. Korastinski for their advice and assistance during several phases of the experimental work.

To my parents for their loving guidance and understanding throughout the years.

Finally, I would like to thank my parents-in-law for my wife, Ruth, who has given moral support and understanding during periods of discouragement.

TABLE OF CONTENTS

LIST OF FIGURES

LIST OF TABLES

ABSTRACT

Polycrystalline nickel oxide and lithium substituted-nickel oxide alloys ranging from 0.12 to 8.23 atomic percent lithium were prepared by vacuum pressure sintering. Changes in particle texture and shape, increased relative density, larger final grain size and a shifting fracture mode were observed with increased lithium content. This sintering behavior was interpreted in terms of enhanced oxygen diffusion caused by either a decrease in the chemisorptive surface properties or by an increase in the "mobility" of a coupled anion vacancy-electron hole complex.

Pure nickel oxide was found to tend very close to stoichiometric proportions, deviations from stoichiometry being predominantly caused by the impurity-affected surface properties of the material. The composition of 99.999% pure nickel oxide used in this investigation was found to be $NiO_{1.000003\pm0.0003\%}$. Iodometric titration analysis showed the concentrations of Li^{+1} and Ni^{+3} to be equal in pure single phase $Ni^{+2}_{1-2x}Li^{+1}_{x}Ni^{+3}_{x}O$. Analysis also indicated the absence of any detectable metallic nickel and showed no detectable lithium loss during pressure sintering. The discrepancy between these findings and those previously

reported in the literature indicates previous difficulty in the careful preparation and characterization of these materials.

The measurement of Young's modulus as a function of temperature for the lithium-nickel oxide alloy system was found to be a very sensitive method for the determination of the variation of the Néel temperature with composition. The low temperature value of Young's modulus was found to increase with increased lithium content and the temperature of the modulus anomaly was found to decrease linearly with increased lithium content. This behavior was interpreted in terms of Van Vlecks'(1) localized-electron theory of antiferromagnetism.

Resistivity measurements made on well characterized pressure-sintered polycrystalline lithium-nickel oxide alloys agreed with the reported results on single crystal material. These include a break at the Néel temperature, a lower activation energy at higher temperatures than at lower temperatures, and a decrease in the low temperature activation energy with increasing lithium content. The combined trends in the modulus and resistivity as a function of temperature and impurity level were interpreted in terms of Toyczawa's(2) electron-acoustic mode interaction model which predicts an inverse relation between the elastic modulus and the energy difference between the self-trapped

and activated electron states. It was concluded that the success of a quantitatively correct localized electron model appears to depend on the development of a theoretical approach which would simultaneously account for both optical mode and acoustic mode interactions.

REFERENCES

1. "Recent Developments in the Theory of Antifferomagnetism" J. H. Van Vleck, J. Phys. Rad. 12, 262-274 (1951)

2. "Self-Trapping of an Electron by the Acoustical Mode of Lattice Vibration. I." Y. Toyozawa, Prog. Theo. Phys. 26, 29-44 (1961)

I. INTRODUCTION

The transition metal oxides represent a group of high melting point materials which have electrical properties ranging from that of an insulator, such as pure stoichiometric nickel oxide (1), to excellent metallic conduction, such as is found in TiO and V_2O_3 (2). In the years 1948 through 1950, Verwey and coworkers (3,4) demonstrated that the addition of suitably sized, fixed valence impurity ions to the oxide of a transition metal that possesses variable valence can cause extremely large changes in conductivity. These changes are accomplished without the creation of vacant lattice defects and thus, as a group, these materials represent electronic conductors of high stability. These authors noted that the resistivity as a function of temperature could be represented by an activated process, and they ascribed the activation energy to the ionization of the electron-hole and its removal from the vicinity of the trivalent cation-monovalent impurity source. Verwey proposed the use of these materials as thermistors, but further extension of the same approach to impurities which increase the resistivity, such as Cr_2O_3 (5),could result in their use as stable balanced resistors over wide temperature ranges.

Heikes and Johnston (6) reasoned that if carrier generation was the activated process and if the activation energy was the work required to separate a trivalent transition metal ion (T^{+3}) from a monovalent impurity ion (M^{+1}), then the activation energy should vanish at approximately 10% M^{+1} (each transition metal ion having at least one impurity ion nearest neighbor). Because their experimental results indicated that the activation energy did not disappear, they concluded that the mobility, rather than the carrier generation, was the activated process. They expressed the resistivity as

$$\rho = \rho_o T \, e^{\varepsilon/kT} \qquad \text{where}$$

$$\rho_o = \frac{a\,k\,c}{q^2 \nu_o X}$$

a = lattice constant

k = Boltzmann's constant

q = charge on an electron

ν_o = lattice vibration frequency

X = mole fraction impurity ion

c = constant related to the entropy of activation

and ε = mobility activation energy.

The trivalent cation has a smaller ionic radius and a higher effective charge than the divalent cation and, therefore, causes a localized collapse of the anion lattice. The trivalent cation is thus "self-trapped" by the lattice pol-

arization or the elastic lattice distortion. A qualitative description of the Seebeck effect in hopping conductors was provided by Heikes (7) by assuming one-half of the energy for a jump to be absorbed at the initial site and one-half at the final site. In order to obtain a more quantitative description of the transport properties of low mobility materials it has been found necessary to provide a more sophisticated model. If the lattice is assumed to remain perfect and the polarization or lattice distortion is instead "quantized" and associated with the electron-hole, then a hypothetical "polaron" may be used to obtain more rewarding information.

Polaron models based on electron-optical phonon interactions have been developed by Yamashita and Kurosawa (8), Sewell (9), and Holstien (10), while Toyozawa (11,12) and Schnackenberg (13) have treated electron-acoustic phonon interactions. At low temperatures the electron-optical phonon interaction models yield a picture of a heavy particle moving in a narrow band ("polaron band") while at higher temperatures, the models predict localization of the polaron and a thermally activated mobility. The development of the polaron theories also made possible the explanation of experimentally observed Hall effects which could not be explained by the simple hopping model. The difficulty with the polaron theories is that the necessary sim-

plifying assumptions (such as either only optical mode or acoustic mode interactions) yield incomplete results.

It is interesting to note that after almost thirty years of intense investigation the controversy as to the nature of the conduction mechanism in low mobility solids has still not been solved. In a recent volume of Solid State Physics, Adler (14) states that:

> "Five years ago, a review of the electrical properties of the transition metal oxides would have concluded that the dominant mode of transport was by means of uncorrelated hopping of small polarons. It now appears that this is never the case..."

In the same volume, Appel (15) asks:

> "Is there experimental evidence for localized small polarons and for their phonon-activated hopping motion? The answer to both parts of this question is yes!"

Part of the reason for this problem is the lack of a clear quantitative theoretical basis for all but the normal wide band semiconductors and part is the nature of the material itself. Many of the transition metal oxides have fairly large deviations from stoichiometry (16) and thus specimen preparation plays a large role in the ultimate magnitude of the electrical transport properties which they exhibit. The refractory nature of the oxides makes the growth of large stress-free perfect crystals very difficult and susceptible to contamination, while at the same time causing problems such as non-uniform segregation of

doping impurities during crystal growth. In addition, uniformly high alloy concentrations are almost impossible to achieve due to the nature of the growth process itself. Thus, many of the published works on transition metal oxides are based on the use of poorly characterized polycrystalline samples (17).

Recent advances in purification techniques such as zone refining (18,19) and in the fabrication of high density polycrystalline ceramics (20) offer the opportunity of producing polycrystalline oxide materials capable of being used as reliable and economic electronic materials. The purpose of this work is to elucidate the elastic and transport properties of lithium substituted nickel oxide and to show the capability of fabricating well characterized polycrystalline electronic materials.

II. EXPERIMENTAL PROCEDURES

A. Powder Preparation

The chemical composition of the materials used in this investigation are given in Table 1. Except where specifically noted, the Johnson-Matthey 99.999% pure nickel oxide powder was used for preparation of the alloy powders. The nickel oxide powder and the alloy doping additions were weighed out in 100 gram charges, mechanically mixed for ten minutes and then air fired at 900°C for 10 hours in a covered high purity alumina crucible. The porous slug was then ground in an alumina mortar and pestle until the powder passed through a 325 mesh sieve. The alloy powder was then washed in hot distilled and deionized water until the solution indicated a neutral pH. The powder was then dried for 24 hours at 140°C.

B. Vacuum Pressure Sintering

Pressure sintering was performed in a Model 1-2300 vacuum pressure sintering furnace manufactured by Vacuum Industries, Somerville, Massachusetts (Figure 1). This unit consists of a cold wall vacuum furnace equipped with a 15 kw - 9600 cycle per second induction heating unit and is capable of reaching 1500°C. The pressure is supplied

through two vertical rams, the lower ram rigidly mounted to the frame and the upper ram connected to a hydraulic actuator that is mounted on the top of the frame.

The hydraulic pressure in the original system was controlled by a pneumatically-operated static pump which allowed the ram force to vary by ± 1200 pounds (21). Due to the high initial densification rates observed in this study during sintering, this variation caused the specimens to crack as the pressure control system would cause the pressure to surge in order to keep up with the densification rate. The static pumping system was replaced with a dynamic system (Greenlee Model 1721 Hydraulic Power Pump) having an oil flow capability of 30 cubic inches per minute at 10,000 psi. The oil flow was controlled by a stainless steel needle valve which was water cooled at 13 ±4°C. The water cooling was necessary in order to remove the heat generated as the oil was pumped through a large pressure differential and to keep the orifice size from expanding or contracting due to ambient temperature changes. This system provided very smooth pressure control within ± 2 percent of any given setting.

The major disadvantage of the system was the lack of any capability for hot ejection of the specimen and the resulting concern over the difference in thermal shrinkage rate of the specimen and the die. In addition, the high

pressures used in this study necessitated the use of high strength refractory metal dies. In turn, because the lithium additions in the specimen tended to react with the metal die, a compound die design similar to that of Moss and Stollar (22) had to be used. The final die design that was used for this study is shown in Figure 2. It consisted of a 1" I.D. X 1/4" wall high purity, high strength WEAROX (*) alumina tube inserted within a 1-1/2" I.D. X 3" O.D. T.Z.M. (†) die, and a 1/8" thick X 1" diameter alumina spacer inserted between the specimen and each of the T.Z.M. plungers. The wall thickness of the alumina insert was chosen so that it would be thick enough to avoid cracking of the wall at an applied pressure of 20,000 psi, but thin enough so as to provide maximum T.Z.M. die wall thickness for coupling to the induction heating system and for safe operation of the die system at high pressures. In addition, two Pt-Pt 10% Rh thermocouples were inserted in the T.Z.M. die wall and graphite susceptors were placed around the T.Z.M. die and each of the plungers. The temperature difference between the two thermocouples was never greater than 10°C and previous radial temperature profiles with a similar die system (23) indicated a maximum temperature dif-

---

(*) Trade name of Western Gold and Platinum Co., Belmont, Calif.

(†) Proprietary name of Climax Molybdenum Co., Coldwater, Mich. for a Mo-0.5% Ti-0.08% Zr wrought alloy.

ference of 15°C at 1300°C.

The operational sequence was such that approximately 25 grams of loose alloy powder was loaded into the die system and the powder was then compacted by the plungers at a pressure of 80 psi. The vacuum furnace was then closed, pumped down, and the temperature was raised to and held at 550°C ± 50°C for 30 minutes. The control temperature setting was then increased and pressure was slowly applied to the specimen so that the full operating pressure was reached before the temperature of the system reached 750°C ± 50°C. The temperature was then increased to the desired sintering temperature and held at that temperature for 90 minutes. The pressure was then released, the ram was raised, and the system was cooled at a rate of approximately 175°C per hour to 600°C and then all power was turned off and the system allowed to cool overnight. The specimen was unloaded and cut out of the alumina insert with a diamond blade by making two longitudinal cuts 180° apart along the axis of the insert.

The upper cross-frame of the pressure sintering unit was equipped with a linear variable differential transformer (Sandborn 7-DCDT). The core of the L.V.D.T. was attached to the upper ram and the signal from this system was fed to a Varian F-80A X-Y recorder. Thus a relative measure of the rate of densification was obtained from the

ram displacement. A time equal to twice the time when ram motion ceased, 90 minutes at temperature and pressure, was chosen for all of the remaining runs.

The ambient vacuum level within the chamber was allowed to decrease to slightly less than 100 microns before initial heat was applied, was held to approximately 20 microns during heating to maximum temperature, and was held at approximately 0.1 micron during pressure sintering and the cooling part of the cycle. Some of the pure nickel oxide specimens were observed to have two phase structures (less than 1% metallic nickel). These specimens were fired in air at 1350°C for 24 hours, were then reexamined, and found to possess single phase structures near theoretical density.

C. Chemical Analysis

Lithium was analyzed by using flame photometric methods. Lithium standards were prepared by drying reagent grade lithium carbonate (Table 1) at 120°C for 24 hours and then dissolving 4.945 grams of the dried powder in 300 ml of distilled and deionized water (*). Carbon dioxide was then released by the addition of 15 ml. of concentrated HCl,

---

(*) All analyses and washing operations were carried out with distilled water passed through a mixed-bed ion-exchange resin column.

and the solution was then diluted to 1 liter. This provided a stock solution equivalent to 4,000 ppm Li. The stock solution was diluted to 1/4, 1/3, 1/16, 1/32 of the original stock concentration for calibration solutions. The sample solution was prepared by dissolving approximately 0.5 grams of unknown in 7.5 ml of hot concentrated HCl and then diluting to 25 ml (the sample weight or concentration was readjusted in a second run if the original sample did not fall approximately midway between the calibration solutions). Analyses were performed on a Beckman Model DU Flame Photometer using a Model 4030 Medium Bore Atomizer-Burner with gas pressures of 3.5 psig for the acetylene and 8.5 psig for the oxygen. The slit width was set at 0.15 mm and the 670.8 mμ lithium line was monitored (24). The standard calibration procedure for the instrument was modified in order to use the full width of the transmission scale. After adjusting the sensitivity and burner controls in the normal manner, the following sequence was used:

(1) With the shutter closed, adjust the dark-current milliameter to zero.

(2) Place the highest concentration calibration solution in the burner, open the shutter, and vary the wavelength until maximum response is indicated. Set the transmission scale to 100 and balance the instrument by adjusting the sensitivity control.

(3) Place a "blank" of deionized water in the burner and adjust dark current to zero.

(4) Repeat steps (2) and (3) until "blank" reads zero and highest standard reads 100 on the transmission scale.

Previous reports have indicated anomalously high readings with H_2SO_4 solutions (24, 25) and low lithium results in the presence of nickel (25). Prior to establishment of the above procedure, lithium standards were run in both HCl and H_2SO_4 solutions and in the presence of nickel (as nickel chloride). No evidence of any change in the readings was indicated.

The lithium content in the nickel oxide alloy sample, expressed as mole fraction lithium, was calculated from the equation:

$$X = \frac{(W_L)(74.71)}{[(36.9455)(W_S) + (W_L)(51.77)]}$$

where W_S = Weight of sample per liter

W_L = Equivalent weight per liter of Li_2CO_3 for equal transmission.

Trivalent nickel was analyzed by iodometric titration. A schematic representation of the dissolution equipment is shown in Figure 3. Due to its extended length, the exact procedure is outlined in Appendix I. All of the analyses were performed with the same lot of concentrated (36.5 to

38 per cent) hydrochloric acid (*). A "blank" run using this acid gave no indication of the formation of free iodine. In practice, a minimum amount (2 to 7 ml) of acid was used to dissolve the sample, and the sample weight was varied (0.1 to 0.5 grams) in order to maintain the volume of 0.01N standard sodium thiosulfate (†) titrating solution within reasonable working limits. The sample powders were passed through a #325 mesh (44μ) screen prior to analysis.

D. Modulus Measurements

Young's modulus as a function of temperature for both pure and doped nickel oxide specimens was measured using a three-part "composite oscillator" method. The furnace was constructed from a 3 inch I.D., 1/4 inch wall thickness, 10 inch long Norton "Alundum" refractory tube wound with 20 gauge Nichrome V wire, with six turns per inch over the central seven inches of the tube. The winding was coated with "Alundum" cement and then the assembly was placed inside a four inch I.D., 1/8 inch wall thickness type 304 stainless steel furnace shell. The gap was packed with

---

(*) A.C.S. Reagent Grade Hydrochloric Acid, Fisher Scientific Co., Lot 772438, Maximum Limits of Impurity: Free Cl - 0.0000%, Sulfites (SO_3) - 0.00008%, Sulfates (SO_4) 0.00008%, Heavy Metals (as Pb) - 0.0001%, Residue on Ignition - 0.0004%, Fe - 0.00001%, As - 0.000001%, NH_4 - 0.0003%.

(†) Sodium Thiosulfate ($Na_2S_2O_3$), Baker "Dilut-it", 0.01N ± 0.1%, Lot #000-15283-3594.

"Alundum" insulating powder and type 304 stainless steel end pieces were used to seal the powder in and to hold the refractory tube in place. A thin walled iron tube was placed inside the refractory tube in order to provide a more uniform temperature profile; electrical contact was maintained between the inner iron tube and the outer stainless shell both of which were grounded directly at the vertical input of the oscilloscope. A.C. line voltage was controlled by a 0 - 10 ampere Powerstat and monitored by a General Radio Type 1806-A Electronic Voltmeter connected across the furnace input terminals. Furnace profiles indicated that a temperature variation of ± 2°C was maintained in the central two inches of the furnace at intermediate temperatures (room temperature to 250°C), ± 5°C at higher temperatures (250°C to 450°C) and that a temperature variation of ± 1.5°C was maintained in a one inch furnace length over the entire temperature range.

The driver and gauge transducers for the composite oscillator consisted of two "X-cut" piezoelectric quartz crystals (*). Each of the quartz crystals had a 1/4" X 1/4" cross-section, its Y-axis oriented along the length of the crystal, and the X- and Z-axes perpendicular to the other faces. The X-cut faces were vapor plated (†) with chromium,

---

(*) Purchased from Piezo Co., Carlisle, Pa.

(†) Courtesy of Bell Telephone Laboratories, Allentown, Pa.

for good adherence, and gold, for good electrical contact under high temperature conditions. This orientation has been found to provide high intensity pure longitudinal vibrations with good temperature stability (26).

The "Lavite" (*) holding fixture for the composite oscillator supported four 1/4 inch wide, 1-1/4 inch long, 0.015 inch thick stainless steel spring strips. A fine tungsten point with a 0.001" tip radius (†) was passed through a small hole in the upper end of each of the flat springs and was then silver-soldered to it. The spacing in between each set of points was set at 3/16" so that they would maintain a positive holding pressure on the 1/4" quartz crystals. Stainless steel wire leads were silver-soldered to the lower part of each of the spring strips. These leads emerged from the furnace through "Lavite" end pieces and provided electrical contact to the assembly. A 1/4" x 1/4" x 2" long "Lavite" bar with a 1/8" diameter x 1" deep hole along its length axis was cemented to the center of the top surface of the holding fixture. Temperature readings for all of the runs were read from a Pt-Pt 10% Rh thermocouple (#) placed inside this bar. Prior to any of

---

(*) American Lava Corp., Chattanooga, Tenn.

(†) Semimetals, Inc., Westbury, Long Island, New York.

(#) All thermocouples were calibrated in boiling distilled water and read 100.375°C $\pm$ $^{.000}_{.125}$ °C.

the experimental runs, a second bar identical to that described above was placed between the tungsten points, and the temperature difference between the oscillator position and the "monitor" thermocouple position was determined over the temperature range 0 - 390°C. The "equilibrium" temperature gradient was found to be less than 1 °C over most of the range, and this value was reached within 15 to 20 minutes after temperature changes of 25 to 50 °C were made. An inert gas atmosphere of CO_2 or pre-purified N_2 was maintained within the furnace for these and all succeeding runs.

The quartz crystals were frequency matched within 0.7 per cent. Matching of the specimen and the crystals will be discussed in the Results and Discussion section. Calibration curves for the frequency versus temperature response of each of the crystals were determined by placing marked and identified crystals in the composite oscillator holder inside the furnace but without the specimen cemented between them. The composite oscillator was then prepared by cementing a specimen of similar cross section between the crystals with GA-60 (*) epoxy strain gauge cement. Pressure was applied as the system was being cemented together in order to squeeze as much cement out of the joint as possible. A thin cemented joint was desired in order to produce good coupling between the various components of the oscillator.

(*) Automation Industries, Instrument Div., Phoenixville, Pa.

The assembly was baked in a drying oven at 120°C for one hour and then placed in the holding fixture so that the quartz crystals were in the same position as when they were calibrated. The assembly was positioned so that the center of the specimen fell directly over the center of the monitor thermocouple block and the tungsten points held the quartz crystals at their respective centers (nodes). The holder was then situated so that the center of the specimen fell at the center of the thermal flat within the furnace.

A schematic of the measuring equipment is shown in Figure 4. The signal from a 2c-2mc General Radio type 1310-A Variable Frequency Oscillator was monitored with a General Radio Type 1150-BPH Digital Frequency Meter which had an internal 100 kc test crystal. Frequency control of 1 cps in 200,000 cps was achieved by placing a three turn 1.5-5 picofarad variable capacitor across the main frequency control of the oscillator. The 600 ohm output of the oscillator was modified by the addition of a 0 - 2.5 megohm potentiometer so that the output could be controlled at 0.2 volts over the entire frequency range. The output was then fed to a 20c - 3 mc General Radio Type 1233-A Power Amplifier. The constant 0.2 volt input produced maximum output and no signal distortion from the power amplifier. The output from the amplifier was monitored by a General Radio Type 1806-A Electronic Voltmeter, and was connected to the

driving crystal of the composite oscillator. The signal from the gauge crystal of the composite oscillator was fed directly to the vertical input of a Hewlett-Packard Model 130-B oscilloscope. Electrical ground was maintained throughout the system by grounding the shielded cable at each input and output terminal, connecting the grounded side of both crystals together, and carrying this ground connection directly to the scope. A clear undistorted signal was then obtained, and resonance was determined by varying the oscillator until maximum peak height was achieved on the scope. The furnace temperature, resonant frequency, magnitude of the output signal from the amplifier, and the peak-to-peak voltage from the scope were recorded and used to calculate the modulus and relative acoustic loss.

E. Resistivity Measurements

Four point probe dc resistivity measurements as a function of temperature were made on the same samples as were used for the modulus measurements. A schematic diagram of the measurement circuit is shown in Figure 5. Measurements were made inside a platinum wire-wound vertical quartz tube furnace that was insulated with Johns-Manville "Min-K" high temperature quartz fiber. The specimen was cut into a rectangular bar approximately 0.1 inches thick, 0.15 inches wide and 0.5 inches long, and then placed on a fused quartz microslide at the end of an alumina multibore tube. The

physical arrangement of the fixturing is quite similar to that used for previous investigations and is adequately described in the literature (27, 28). Platinum leads were attached to the specimen with 80% Au-20% Pt alloy paste (*), and the contacts were sintered at 800°C for one hour.

Measurements made with wide variations in the current indicated the contacts to be ohmic. A switching network was provided so that current flowed through the specimen only while a measurement was being made and current and voltage reversals made during each run indicated the absence of any measureable thermoelectric effects. A monitoring Pt-Pt 10% Rh thermocouple placed in contact with the quartz microslide and directly under the specimen indicated a temperature within 2 degrees of that indicated by the furnace control thermocouple placed 1/2 inch away from the specimen. The temperature was slowly increased from room temperature to 400°C over a six hour period and then allowed to cool at a similar rate (1.1°C/min).

(*) Squeegee Gold Alloy Paste #A-1199, Engelhard Ind., East Newark, N.J.

III. DISCUSSION AND RESULTS

A. The Ni-O System

The only known investigation of the Ni-O phase system was performed by Bogatskii (29) whose results are shown in Figure 6. There is a small region where solid solutions of O_2 in Ni are formed at concentrations up to one weight per cent O_2. The liquidus curve drops from approximately 1450°C for the melting point of Ni to a eutectic at 1438°C and 1.5 weight per cent O_2, then rises to approximately 1650°C at the compound NiO. The curve then drops off almost vertically, levelling off at the melting point of Ni_2O_3 and again at NiO_2.

In addition to being thermodynamically incorrect, the region between NiO and O_2 points out the argument that has existed since the early 1900s as to the existence of anhydrous higher nickel oxides.

In 1926, LeBlanc and Sachse (30) gave the analysis of the products of $NiCO_3$ calcination as NiO, Ni_2O_3, active oxygen and water, when calcined in air. They used an iodometric titration technique in order to find the concentration of Ni^{+3} present and then expressed this as Ni_2O_3. In another investigation (31), LeBlanc and Sachse attempted to

form Ni_2O_3 or NiO_2 but found only nickel oxide with up to ten per cent excess oxygen ($NiO_{1.1}$). Lunde (32), in 1927, reported that slow heating of $Ni(NO_3)_2$ produced a black powder having an analysis nearly that of Ni_2O_3 but with the x-ray pattern of NiO. Commenting on Lunde's work, LeBlanc and Sachse (33) argued that his material was probably a mixture of NiO, active oxygen, water, with possibly only a maximum of ten per cent of higher nickel oxides. Lunde then proposed (34) that the material could also be a hydrated higher nickel oxide such as $NiO_2 \cdot XH_2O$.

Holtermann (35) reported that higher oxides were extremely unstable and that only the monoxide could be identified, while Bogatskii (29) reported that NiO_2 was stable under "high pressure" and that Ni_2O_3 had a crystal structure and unit cell very close to that of NiO. In 1954, Shimomura and coworkers (36) reported that nickel oxide with up to 20 per cent excess oxygen still had the NiO structure and that no higher compounds could be found. In 1956, Rode (37) observed nickel oxides with up to 32 per cent excess oxygen without any evidence of anhydrous Ni_3O_4, Ni_2O_3 or NiO_2, although hydrides of higher oxides were definitely thought to be present. Based on a very thorough study of reaction products from nickel cathodes in electrolytic cells, Briggs and Wynne-Jones (39) also concluded that no anhydrous higher oxides could be identified. In addition,

based on a study of x-ray fine structure, Tsutsumi (40) stated that compounds identified as Ni_2O_3 were actually NiO plus $NiO_2 \cdot XH_2O$. However, in 1957, Finch and Sinha (41) identified a complex nickel spinel $Ni_{28}O_{32}$, and in 1959, Bogatskii and Mineeva (42) again identified both NiO_2 and Ni_2O_3 which decompose at 50°C and 350°C respectively.

Finally, Labat (43) made an extensive review of the conflicting information and concluded that although the existence of higher anhydrous nickel oxides was largely doubted, it seemed to be well established that their hydrates or combinations with alkali or alkali-earth oxides were well established. Tuomi (44) came to similar conclusions in 1965.

The extent of non-stoichiometry in nickelous oxide has also been the source of much controversy. In 1930, LeBlanc and Sachse (45), performing the first work with bulk material rather than powder, found that NiO dissolves only a "small" quantity of oxygen without forming higher oxides. In 1931 they measured the conductivity of these bulk samples (46) and found that "pure" NiO had a conductivity of 10^{-8} $(ohm\text{-}cm)^{-1}$ while NiO with 5 per cent excess oxygen ($NiO_{1.05}$) had a conductivity of 10^{-3} $(ohm\text{-}cm)^{-1}$. Klemm and Haas (47) noted a wide variation in magnetic susceptibility and the presence of metallic nickel in their work on powdered materials and proposed that stoichiometric nickel ox-

.ide was unstable and would break down to $NiO_{1.005}$ and metallic Ni. Baumbach and Wagner (48) found a maximum deviation from stoichiometry of $NiO_{1.0005}$ to $NiO_{1.005}$ working with oxidized nickel foil, and Boswell and Iler (49) found a maximum of $NiO_{1.006}$ when working with sintered but porous specimens. Even with oxygen pressures up to 300 atmospheres, Holtermann (35) was able to obtain a maximum deviation from stoichiometry of $NiO_{1.07}$ with powder material, while Shimomura and coworkers (36) obtained results between $NiO_{1.02}$ and $NiO_{1.2}$ at 0.21 atmospheres pressure. In 1962, Perakis (50) found a maximum deviation from stoichiometry of $NiO_{1.0196}$ and a minimum of $NiO_{1.0007}$ in equilibrium with metallic nickel. In 1964, Blaise and Lefevre (51) gave an analysis of $NiO_{1.00098}$. In 1965, Cherkashin (52) reported a range of $NiO_{1.00013}$ to $NiO_{1.0224}$, and in 1966, Gravelle, Shobaky and Urbain (53) reported an analysis of $NiO_{1.00016}$, all on powdered materials. In 1968, Fender and coworkers (54) reported an analysis of $NiO_{1.000\pm0.002}$ for spectrographically standardized powder obtained from Johnson-Matthey Chemicals (metallic impurities less than 15ppm).

The above discussion is summarized in Table 2. There appears to be a striking correlation between the nature of the sample (powder versus bulk material), the year of investigation (or realistically the purity), and the observed maximum deviation from stoichiometry. Gossel (55,56) has

made the observation that the nonstoichiometry of nickel oxide is mainly a surface property and that surface conditions affected the excess oxygen content to a much greater extent than did variations of temperature and atmospheric conditions. LeBlanc and Sachse (31) and Charman and coworkers (59) both found a rapid change in color from black to green when nickel oxide powder was placed in an acid-KI titration solution, which suggested that excess oxygen was present only at the surface. The surface properties and catalytic activity of nickel oxide have been quite extensively studied by many investigators (55-61) and since, in general, the study of the chemistry and physics of surfaces becomes a science unto itself, it will not be dealt with here except for one experimental observation in the next paragraph.

"Pure" reagent grade nickel oxide from Fisher Scientific or Baker Chemical Company having an clive green color, 99.9% pure nickel oxide from Atomergic Company having a grey color, and 99.999% pure nickel oxide from Johnson-Matthey Company having a bright "Kelly Green" color were all fired in cleaned high purity silica or alumina crucibles at temperatures between 800°C and 1000°C. While all the other powders tended to change to a lighter green color, the Johnson-Matthey powder remained the same green color. In addition, the same powders fired in crucibles contaminated

with small amounts of lithium all formed sintered "cakes" that were black on the outside but bright green towards the center. Keeping in mind that all previous investigations have associated the bright green color with nearly stoichiometric nickel oxide, it is concluded that the extent of deviation from stoichiometry (or the quantity of excess oxygen) is an impurity affected-surface controlled effect (see Table 1 for chemical analysis of powders).

The early development of the quantitative relationship between imperfections, the departure from stoichiometry, electrical conductivity, matter transport and chemical reactions in the solid state can largely be attributed to the work of Schottky (62), Wagner (63), Mott (64), Hauffe (65) and Kroger and Vink (66). Using the law of mass action as first applied to this type of system by Wagner, and the relationship between the self diffusion coefficient of Ni^{+2} and nickel vacancies as given by Mott, the concentration of vacancies has been given by Mitoff (67) as:

$$[V_{Ni}''] = 7.8 \times 10^{-3} P_{O_2}^{1/6} \exp(-11{,}400/RT) \text{ vacancies per ion pair.}$$

Based on work by Eror (68) which indicated that a $P_{O_2}^{1/4}$ dependence might be more appropriate, Price (69,70) has restated Mitoff's relationship as:

$$[V_{Ni}''] = 8.97 \times 10^{-3} P_{O_2}^{1/4} \exp(-11{,}400/RT) \text{ vacancies per ion pair.}$$

Using Mitoff's approach, but with different diffusion data, Eror (68) gives the concentration of nickel vacancies as:

$[V_{Ni}] = 4.58 \times 10^{-5} \exp(+5000/RT)$ vacancies per ion pair

in air (P_{O_2} = 0.209). Recently, Sockel and Schmalzried (71), using a coulometric titration method with calcia stabilized zirconia as a solid electrolyte, have again found a $P_{O_2}^{1/6}$ dependence of vacancy concentration, and extrapolation of their results at 1200°C to P_{O_2} = 0.209 would give $[V_{Ni}] \simeq 3.1 \times 10^{-4}$. Finally, Ormont (72), using binding energy theory and experimental data existing in the literature found $[V_{Ni}] \simeq 2 \times 10^{-11}$ at 25°C. A tabulation of the above results is given in Table 3 for 1200°C and 25°C where possible.

Comparison of these values with corresponding vacancy concentrations in CoO and MnO would also be indicative of the relative differences in magnitude for the three compounds. Carter and Richardson (73) found a value of 8×10^{-3} for $[V_{Co}]$ at 1150°C and one atmosphere oxygen pressure during oxidation studies with cobalt foil, and Fisher and Tannhauser (74) reported a value of 1×10^{-2} under similar conditions. Eror (68) also reported a value of 1×10^{-2} vacancies per ion pair, and extrapolation of Sockel and Schmalzried's work gives the same. As for MnO, Davies and Richardson (75) reported a range of stoichiometry from $MnO_{1.000}$ to $MnO_{1.045}$

at 1650°C with varying pressure, and Eror (68) reported a value of 2×10^{-3} vacancies per ion pair at 1200°C and a partial oxygen pressure of 7×10^{-10} atmospheres. Although Eror's work involved the thermogravimetric analysis of NiO, CoO and MnO, he presented no results for NiO because the change in weight was smaller than the sensitivity limit for his equipment.

The iodometric titration results of the present investigation (discussed in detail in a later section) show a precision of ±0.0003 per cent (Table 4) for the lower Ni^{+3} concentrations while the "blank" HCl run and both of the unalloyed 99.999% pure nickel oxide powders (as received, and fired) gave no indication of any reaction with KI solution. The analysis of the pure nickel oxide used for this investigation may thus be given as essentially $NiO_{1.000003}$ ±.0003%. This is in excellent agreement with Fender and coworkers'(54) results on the same powder but with a less accurate method. Comparison of this value with those given in Table 3 indicates good agreement, realizing that even under extremely slow cooling the powder would not be able to reach the equilibrium vacancy value but would rather have a "frozen-in" vacancy concentration corresponding to the higher temperature range. Referring back to the color change observations, it might now be stated that pure nickel oxide tends very close to stoichiometric proportions

and that deviations from stoichiometry are caused only by the impurity-affected surface conditions of the material.

Although electrical conductivity or conductivity type per se is not enough to successfully describe a transport mechanism, a knowledge of both permits some approximate judgments as to the relative position of phase boundaries and the stability of certain types of defects in the lattice. Thus the fact that wüstite in equilibrium with iron at 900°C was determined (76,77) as $FeO_{1.05}$ and wüstite in equilibrium with Fe_3O_4 was determined as $FeO_{1.125}$ while the electrical conductivity has been shown to be p-type only (78,79) indicates that the wüstite phase field is shifted from the nominally stoichiometric compound and that conductivity involves the formation of cation vacancies and higher valence cation states. On the other hand, manganous oxide has been observed with either excess metal or excess oxygen (75,80) and possesses both n-type and p-type conductivity (68,81-83). The phase region for manganous oxide therefore overlaps the stoichiometric compound, has a fairly wide stoichiometry range (75) and conduction may be either by cation vacancies (p-type) or by cation interstitials (n-type) or by anion vacancies (n-type). Cobalt oxide has been reported (83) to have a sign reversal in the slope of the thermoelectric power vs. oxygen partial pressure curve, while neither the thermoelectric power nor conductivity have a sign reversal

themselves. Thus, as mentioned before, cobalt oxide has a fairly small compositional variation near the stoichiometric compound, and also possesses a conductivity type dominated by cation vacancies but with the possibility of small amounts of interstitial cobalt or anion vacancies at very low pressures or at high temperatures (74).

Despite the large number of investigations which have found nickel oxide to possess only p-type conduction, there are a few reports in the literature indicating n-type conductivity. However, due to conflicting experimental observations, all of these reports appear to be highly questionable. Takeuchi and Igaki (84) reported n-type conductivity, but later reported (85) this as "semimetallic conduction accompanied by ferromagnetic behavior." Schlosser (86) noted that nickel oxide doped with gallium was n-type for 0.6 atomic per cent gallium or greater, but Rooksby and coworkers (87) noted the formation of $NiGa_2O_4$ spinel even with very small gallium additions, and El Shobaky and coworkers (88) have noted the increased tendency for the formation of metallic nickel with gallium additions. In 1965, Snowden and Saltzburg (89) reported n-type conductivity through Seebeck-coefficient measurements at room temperature but also reported a sign reversal at 380±30°C (the Curie point of nickel). Recent work (90, 91) on the Seebeck coefficient of nickel oxide single crystals as a

function of temperature and pressure indicated no change of sign from p-type conduction, but indirect experimental evidence does exist for an n-type component for the carrier mobility term (92 - 95). This component has, however, been interpreted as being related to an anomalous effect due to internal magnetic fields (92,93), rather than as caused by a second carrier component.

The above discussion thus provides a picture of nickel oxide as having an extremely small deviation from stoichiometry (narrow phase field) shifted to the oxygen excess side but including the nominally stoichiometric compound, NiO. The conductivity may be described as heavily dominated by the formation of cation vacancies and higher valence cations.

B. NiO-M_xO_y Alloy Systems

A tabulation of the extent of solid solubility of MxOy oxides in NiO at various temperatures and pressures is given in Table 5 , along with known stoichiometric compounds, common valence and size deviation (in per cent) between R_{Ni}^{+2} and R_M. The ionic radii used for this tabulation were taken from Pauling (96) because they represent the most complete and consistent set of both divalent and trivalent empirical radii available. In particular, Pauling gives the following pertinent radii:

Element & Valence	Ionic radius, A°
O^{-2}	1.4
Li^{+1}	0.6
Mg^{+2}	0.65
Ni^{+2}	0.72
Ni^{+3}	0.62
Co^{+2}	0.74
Co^{+3}	0.63
Fe^{+2}	0.76
Fe^{+3}	0.64
Cr^{+3}	0.69
Cu^{+2}	0.69
Zn^{+2}	0.74

Using Pauling's value of $R_O{}^{-2}$ = 1.4A°, and the average Ni^{+3} - O^{-2} interionic distance of 2.02A° in $Li^{+1}Ni^{+3}O_2$ given by Dyer and coworkers (97) a value of $R_{Ni^{+3}}$ = 0.62A° is obtained which is in excellent agreement with Pauling's tabulation. The observation that $R_{Mg^{+2}}$ lies between both $R_{Ni^{+2}}$ and $R_{Ni^{+3}}$, and $R_{Co^{+2}}$ and $R_{Co^{+3}}$, might also be made. This fact has been used by Oakey (98) to hypothesize a "pre-relaxation" effect in $Li_xMg_yCo_{(1-x-y)}O$ alloys.

The $NiO-M_xO_y$ systems seem to provide excellent agreement with the Hume-Rothery solid solution rules (99,100). The oxides of Group IA, IIA, IB, IIB show a definite trend towards high solubility when the deviation between cation

radii is less than 20% (SIZE EFFECT). Solubility is generally restricted for almost all systems showing intermediate phase formation (ELECTRONEGATIVE VALENCY EFFECT) such as Group IA and IIIA, or for those oxides with much higher cation valence such as the oxides of the IIIB, IVB, and VB groups. The NiO-ZnO and NiO-CuO systems with up to 35 mole per cent CuO or ZnO soluble in NiO but with almost no NiO soluble in CuO or ZnO(101-103) seem to demonstrate an ELECTRON CONCENTRATION EFFECT (Ni^{++} = $[Ar]^{18}3d^{8}$, Cu^{++} = $[Ar]^{18}3d^{9}$, Zn^{++} = $[Ar]^{18}3d^{10}$).

The seeming abnormality in the solubility of Cr(<1%), Mn(100%), Fe(<10%), Co(100%) oxides in NiO may be explained by referring to Figure 7 which is a plot of the free energy of formation (stable oxygen pressure) versus temperature for the compounds of interest. The stable phase field for NiO has wide overlap with the CoO and MnO phases and hence the large solubility, while there is no overlap for the Cr system and therefore low solubility. It may be observed that there is no overlap between the NiO and FeO phases but that the phase fields are fairly close. Indeed, for small additions of FeO to NiO (low activity) the upper stability limit would fall within the NiO stable phase field because of the higher allowed oxygen pressure, while the lower stability limit for FeO would fall even lower because of the lower allowed oxygen pressure before the appearance of

a metallic iron phase. Thus, the stable FeO phase field is wider and overlaps the NiO phase field for low iron concentrations and therefore enables some solubility of the two components.

The first work with the $NiO-Li_2O$ system was published in 1948 by Verwey and coworkers (3) who found lithium to be soluble in nickel oxide in amounts as great as ten mole per cent and then later (4,104) to be soluble to less than 40 per cent. Kohler and Jamison (105) reported the solubility limit at 28 atomic per cent lithium in thin nickel oxide films, and Heikes and Johnston (6) found difficulty in dissolving more than 15 per cent lithium in the lattice. The compound $LiNiO_2$ was identified by Dyer, et al (97) and again later by Johnston and coworkers (106). Perakis and coworkers (50,107-109) reported various degrees of ferromagnetism for the system but Fensham (110) working with single and two phase alloys with up to 50 atomic per cent lithium found metallic nickel present whenever ferromagnetic behavior was exhibited. In addition, Janusz, et al (111) and Johnston, Heikes and Sestrich (112) duplicated the sample preparation technique of Perakis but found no evidence of ferromagnetism down to liquid nitrogen temperature.

In 1958, a thorough investigation of the magnetic and crystallographic properties of the system was made by Goodenough and coworkers (113,114) and then essentially con-

firmed by Bronger, et al in 1964 (124) and by Bade, et al in 1965 (125). Their results show that, for values of x between zero and 0.3 in $Li_xNi_{1-x}O$, the material is a random solid solution possessing a sodium chloride type structure (MnO magnetic cell). For $0.3<x<0.5$ the material possesses a rhombohedral α-$NaFeO_2$ structure with a definite ferrimagnetism caused by ordering of Li^{+1} and Ni^{+3} on alternate 111 planes. The strongest ferrimagnetic effect is found for $x \simeq 0.38$ (Bronger) and corresponds quite well with the ordering parameters given by Goodenough (zero ordering for x=0.3, maximum order for x=0.5) predicting maximum magnetization in the middle of the phase region. At x=0.5 the ordered compound $LiNiO_2$ is formed and for $0.5<x<0.67$ the material is paramagnetic and possesses a monoclinic structure.

The Japanese literature seems to indicate a parallel development of the knowledge concerning the solid solution region of the NiO-Li_2O system but from a more chemical viewpoint. Takeuchi (25) obtained alloys containing up to 8 mole per cent lithium oxide at 700°C (kinetically limited) and made a very careful study of the flame spectroscopy methods for analyzing lithium. Iida and coworkers (126-129) investigated the kinetics of the solid state solution reaction for 4 weight per cent lithium (18 atomic per cent) and found that solution formation started at temperatures as low as 300 to 500°C and then reached a maximum solubility at 800-

1000°C because of the volatility of lithium oxide. These same authors later combined their chemical techniques with x-ray methods (115-117) in order to determine the variation of lattice constant with lithium content and then established the limiting solubility at 25-28 atomic per cent. Many other investigators (112-114, 118-123) have determined the lattice parameter variation with composition and these are shown as the volume of the chemical cell versus composition in Figure 8. The data of Goodenough and coworkers (113,114) covers the widest concentration range, is fairly linear and falls midway in the range.

The NiO-MgO system exhibits complete solid solubility (130-132) and has been shown by Hahn and Muan (133) to be an ideal solid solution following Vegard's law. It is interesting to note, however, that even though the Li^{+1}-Mg^{+2} cation size deviation is only 7.7 per cent as opposed to 17 per cent for Li^{+1}-Ni^{+2}, less than one per cent lithium oxide is found to be soluble in MgO.(139, 140, 142, 143) Inspection of the following ionization potentials for Li, Mg, and Ni,

	I	II	III
Li	5.4	75.6	122.4
Mg	7.6	15.0	80.1
Ni	7.6	18.2	35.2

shows the second ionization potential of lithium to be ap-

proximately the same as the third ionization potential of magnesium but much higher than the third ionization potential of nickel. If the charge neutrality condition is looked upon as an additional degree of freedom for the system, it might be proposed that the high solubility of lithium in nickel oxide and the low solubility in magnesium oxide are the expected results. In effect, this combination of small deviation of cation size in conjunction with ease of ionization of one of the component cations is the cause of the formation of the group of materials called "controlled valence" compounds. (4)

C. The Ni-NiO Phase Equilibria

Various experimental observations have been made in the literature (47,50,53,58,88,110,144-149) that indicate the presence of metallic nickel in nickel oxide. Almost all of these studies report the use of very high surface area oxides (150-300 m^2/g) prepared by thermal dehydration of $Ni(OH)_2$ at 200-300°C under a pressure of 10^{-6} mm Hg as originally developed by Teichner and coworkers (144,145). These reports seem to be in conflict with studies of thermochemical equilibrium for the Ni-NiO system (133-138) as shown in Figure 9. Alternatively, investigations using lower surface area powders prepared at high temperatures in air (146) do not show the presence of metallic nickel, while

those prepared at high temperatures in vacuum (110) do show the presence of nickel, both observations being in agreement with simple thermochemical considerations.

Using a value of ΔG° = -46,500 cal/mole NiO at 250°C (Figure 7), $P_T = 10^{-6}$ mm Hg, $P_{O_2} = 0.21\ P_T$ (in atmospheres), $\Delta G_{BULK} = \Delta G^\circ - \frac{RT}{2} \ln P_{O_2}$ = -35,000 cal/mole NiO = -470cal/gram NiO.

If a value of $\gamma = 10^3$ erg/cm^2 is chosen for the surface energy of nickel oxide (150) and 225 m^2/gram for the surface area, then

$$\Delta G_{SURFACE} = \frac{10^3 \frac{erg}{cm^2} \cdot 225 \frac{m^2}{gram} \cdot 10^4 \frac{cm^2}{m^2}}{4.185 \times 10^7 \frac{erg}{cal}} = 53.8 \text{ cal/gram NiO.}$$

Thus the surface energy effect cannot be neglected when considering very high surface area powders. A second possible explanation for the appearance of metallic nickel at low temperatures would be the presence of retrograde solubility as has been demonstrated for the PbS system (151), but no evidence of such behavior has been reported for any of the transition metal oxide systems.

The conditions of temperature and pressure under which the present pressure sintering investigation was carried out (approximately 1100°C at 0.1 micron Hg total pressure) would indicate that they fall close to the Ni-NiO phase boundary (Figure 9). The presence of metallic nickel

(1 to 2 per cent) as shown by metallographic inspection for the as pressed 99.999 per cent nickel oxide specimens indicates that they were on the nickel side of the boundary. However, under similar conditions, the lithium doped specimens did not show evidence of a two phase structure. An initial explanation of this behavior might be given by considering the variation of the activity of nickel oxide with lithium doping level. As lithium oxide is added, the mole fraction of nickel oxide and therefore its activity should decrease. If the activity of nickel oxide decreases, the equilibrium oxygen partial pressure for equilibrium between nickel and nickel oxide decreases, or the doped nickel oxide is stable at a lower oxygen pressure.

The difficulty with the above explanation lies in the realization that despite experimental variations in pressure and temperature around the "nominal" conditions, all of the pure 99.999 per cent nickel oxide specimens gave two phase structures, while even extremely small lithium additions (0.1 mole per cent) eliminated the presence of metallic nickel. The fairly large (28 to 30 mole per cent) solubility of lithium in nickel oxide would seem to predict either adherence to or a slightly positive deviation from Raoult's law for the nickel oxide solvent phase for small lithium additions (152). Thus, for an alloy with $N_{NiO} = 0.999$ (0.1 per cent lithium) the activity, α_{NiO},

would be equal to or greater than 0.999. The resulting shift in the Ni-NiO phase boundary for $Ni_{0.999}Li_{0.001}O$ would be small in comparison with the variation of experimental conditions and a two phase structure might still be expected for this alloy and possibly $Ni_{0.995}Li_{0.005}O$ as well. The single phase structures obtained with pressure sintered sub-micron 99.9 per cent pure nickel oxide (Atomergic C1435) eliminate the possibility of a kinetic effect related to the surface area (300 fold difference in the particle size between the two powders) and point to an effect related to sample purity.

The widening of the stable phase field for pure and doped non-stoichiometric binary semi-conductor compounds such as PbS, PbSe, and PbTe has been investigated by R.F. Brebrick (153,154). Brebrick extended the qualitative approach to imperfection chemistry developed by Kroger and Vink (66) into a quantitative theory through the application of a simple non-degenerate band type semiconductor model. The assumptions made during his theoretical development are:

1. The predominant point defects present in the two sublattices are vacancies,
2. Clustering of point defects is unimportant,
3. Each M or N vacancy is associated with an acceptor or donor level,

4. Non-degenerate statistics may be used, and

5. The phase coexisting with solid MN compound is one or the other of the pure elements.

The net electron or hole concentration, n-p, is used to express composition because experimental results are usually expressed in these terms rather than as mole fraction of either of the components. For an N rich, pure compound, the net relative hole concentration, n-p, is given as:

$$2RT \left\{ \sinh^{-1} \frac{n-p}{2\sqrt{k_s}} + \sinh^{-1} \frac{n-p}{2n_i} \right\} = \Delta G^*_{MN} + A$$

where

n_i = intrinsic carrier concentration

k_s = Schottky constant = $[V_M]\,[V_N]$

ΔG^*_{MN} = Gibbs free energy change of formation of one mole of compound from the elements.

A = Bond strength parameter.

This equation indicates that the magnitude of (n-p) will be larger (the stability range is wider) the larger the free energy of formation of the compound.

Although this analysis has been applied mainly to IV-VI semiconducting compounds, there is very good reason to believe that the approach is directly applicable to the transition metal monoxides (155). As a group, they tend to

favor singly or doubly ionized cation defects with no evidence of clustering. In particular, pure nickel oxide tends close to stoichiometry, has a eutectic system with almost pure nickel and vaporizes primarily by dissociation to the elements (135). Investigators that have adopted a band approach for pure nickel oxide variously give the band gap as 2 - 5 electron volts in width with the Fermi level 0.5-1 electron volt above the valence band (86,58,156,157). Comparison of the free energy of formation of each of the divalent transition metal oxides (Figure 7) with the experimentally determined maximum deviations from stoichiometry gives good qualitative agreement with Brebrick's analysis. Kroger (158) has recently used the same approach to explain the assymmetry in the stable phase field for both divalent and trivalent transition metal oxides.

Brebrick (159) gives the chemical potential of the metal component, M, as:

$$\mu_M - \mu_M^i = RT \sinh^{-1}\left[\frac{(n-p)-(N_D-N_A)}{2\sqrt{k_s}}\right] + (E_f - E_f^i)$$

where N_D, N_A = concentration of ionized donors or acceptors

μ^i, E_f^i = chemical potential and Fermi level of intrinsic material

Whether a hopping model (where each Li^{+1} ion produces a Ni^{+3} mobile hole) or an exhaustion region extrinsic band model is chosen makes no difference in the applicability of the previous analysis to the present work. For a pure

p-type semiconductor such as nickel oxide, $n \simeq N_D \simeq 0$ and $p \simeq N_A$. The first term in the above equation therefore goes to zero, and the result is simply

$$\mu_M - \mu_M^i = E_f - E_f^i.$$

The reported drop of Fermi level to 0.2 - 0.3 electron volts with even the smallest lithium doping concentrations (86) thus causes a very sharp drop in the chemical potential of Ni in NiO, decreases the activity precipitously and rapidly widens the stable phase field for nickel oxide. This results in a large negative deviation from Raoult's law (as opposed to a slight positive deviation proposed initially) and gives a good qualitative explanation of the present experimental observations.

D. Chemical Analysis

The iodometric titration method (Bunsen-Rupp Technique) was first used (38,141,160-163) in order to measure the quantity of "excess oxygen" or "oxidizing power" of chromium and manganese oxides. Verwey and coworkers (3,4) used the method to show that "within certain limits of Li content, the Ni^{+3} content is equivalent to the amount of Li added to the system." In 1961, Deren (164), and in 1962, Bielanski and coworkers (165) showed approximate equivalence of Ni^{+3} and Li^{+1} up to 0.8 atomic per cent lithium and er-

ratic results between 1.4 and 2.5 atomic per cent lithium. In 1965, Hayashi and Iida (116-117) showed approximate equivalence over the range 0 - 28 atomic per cent lithium. However, in 1966, Gravelle and coworkers (53,166), using a modified method similar to that of Charman (59) (combined HCl and KI solutions in same flask), found large discrepancies between Li^{+1} and Ni^{+3} for the range 2 - 10 atomic per cent lithium. Many of the above investigators have shown that partial dissolution of the sample or vacuum baking of the sample prior to analysis indicates a non-homogeneous distribution of Ni^{+3}. These results have been attributed to either a non-homogeniety in the lithium distribution, or to a tendency for the "excess oxygen" to remain at the powder surface. More accurate methods for the chemical analysis of surface layers, such as surface reduction by aqueous hydrazine (167), indicate that the amount of surface excess oxygen decreases monotonically with increasing calcining temperature and with increasing lithium concentration.

The iodometric titration method used for this work is similar to the improved technique developed by Panthony and Siddiqi (168) and has been described earlier. The major advantages of the present arrangement (Figure 3) over previous techniques is that the HCl feed system allows the introduction of HCl <u>after</u> the system has been purged of air,

and permits continuous gas flow throughout the system after the gas inlet tube in the reaction flask has been clogged by the dried residue.

The combined results of Ni^{+3} iodometric and Li^{+1} photometric analyses are given in Table 4. Inspection of the table shows a consistently larger difference between Li^{+1} and Ni^{+3} (in both the starting powder and the pressure sintered samples) for the unwashed 5% Li alloy than for any of the other samples. The pH of this powder was found to be basic, and therefore all further analyses and pressure sintering work was performed on washed powders. This indication of incomplete solution of lithium in nickel oxide is the most likely explanation of previously reported discrepancies between Li^{+1} and Ni^{+3}.

A comparison of the lithium and Ni^{+3} content for the starting alloy powders and the pressure sintered samples indicates that there was little or no lithium loss during vacuum pressure sintering. This is quite surprising since many reports of lithium loss during sintering in air exist in the literature (4,98). These reports of lithium loss might be related to small amounts of second phase material, which would not be detectable by standard x-ray techniques, but which were removed by the extended washing process of the present investigation.

The dissolution of nickel oxide powder is a result of the reaction

$$Ni^{+3} + Cl^{-} \rightarrow Ni^{+2} + \frac{1}{2}Cl_{2(g)}$$

and the formation of free iodine is a result of the displacive reaction

$$\frac{1}{2}Cl_{2(g)} + I^{-} \rightarrow Cl^{-} + \frac{1}{2}I_{2}.$$

The presence of metallic nickel in the reaction flask would also cause the reaction

$$Ni^{\circ} + Cl_{2} \rightarrow 2Cl^{-} + Ni^{+2}$$

and therefore the quantity of $Cl_{2(g)}$ entering the KI solution will be a function of the difference in Ni^{+3} and free nickel. Thus, in addition to showing the equivalence of Li^{+1} and Ni^{+3} concentrations, the present results indicate the lack of detectable metallic nickel.

E. Sintering of Pure and Doped Nickel Oxide

The first extensive investigation of the sintering behavior of pure and doped nickel oxide was performed by Iida (169) and Iida and Ozaki (170). They observed that the sintering rate of nickel oxide was greater in vacuum than in air. Because an increased vacuum level should decrease the number of cation vacancies and hence decrease the sintering rate, these authors concluded that densification is not predominantly affected by a lattice defect mechanism. However Blackman (171) observed the sintering rate of nickel oxide to be greater in oxygen than in nitrogen and in 1965, Brown (172) noted that normal grain growth was always observed during the sintering of nickel oxide. Brown proposed that the departure from stoichiometry and hence the occurrence of lattice vacancies make the movement of ions so facile that it is impossible for either impurities or pores to build up on the grain boundaries and thus prevent discontinuous grain growth. In 1966, Wang (173) investigated the low temperature (549 - 993°K) sintering behavior of nickel oxide by monitoring resistivity versus sintering time. Through the use of Coble's intermediate stage sintering model (174) he identified the diffusion of Ni^{+2} to be the rate-determining step during sintering. On

the other hand, initial sintering studies with nickel oxide spheres (175) indicate the presence of a higher activation energy (73.3 k cal/mole) than either the activation energy for self-diffusion of Ni^{+2} cations (45.6 k cal/mole) given by Choi and Moore (176) or the activation for oxygen anion self-diffusion (57.5 k cal/mole) given by O'Keeffe and Moore (177). In addition, the observation of high creep rates in nickel oxide films (178) at temperatures as low as 850°C (well below 0.5 T_M where diffusion controlled creep is normally expected to become operative) indicates the possibility of a plastic flow contribution to sintering behavior. It is extremely likely that a multi-mechanism approach such as that recently proposed by Johnson (179) will be more fruitful in describing the early stage sintering behavior of this type of material.

Optimum final relative densities obtained by normal sintering methods are 89% (Iida [169]), 93% (Harrison [180]), and 95% (Herbst and Friedberg [181-182]) while the literature abounds with reports of poorer density materials. Pressure sintering (20) makes practical the study of the more controllable later-intermediate and final stages of sintering, and affords the possibility of both increased density and increased strength through finer final grain size. Harrison (183) reported a relative density of 96.4% for hot pressed nickel oxide, and Spriggs and coworkers

(184,185) reported the achievement of nearly theoretical density in very short times.

The relative final density of pure nickel oxide and of each of the alloys used in this investigation are shown in Figure 10 as a function of lithium content. Transmission electron micrographs of representative starting powders are presented in Figure 11, and a carbon-chrome replica of a fractured surface of each of the same pressure sintered samples is presented in Figure 12. The range of final grain sizes is given in Table 6. It is interesting to note that while there is little or no particle growth during the solid state alloying treatment, there is a definite change in the surface texture and particle shape. The surface changes from a rough hackled texture for pure nickel oxide to an increasingly smooth appearance with increasing lithium content, while at the same time the shape appears to shift from a somewhat rounded geometry to a definitely angular structure. A similar comparison of the fractographs indicates the fracture mode to shift from predominantly transgranular for pure nickel oxide, to predominantly intergranular with increased lithium content; at the same time there is a definite increase in the final grain size (Figure 12 and Table 6).

A consistent qualitative explanation of all of the observed results may be gained by interpretation of the sintering behavior with respect to the lattice defect struc-

ture of the material. As previously described, nickel oxide is a p-type, oxygen excess (cation vacancy) compound that has a strong tendency to chemisorb oxygen at a free surface. Deren and coworkers (57) have found that the quantity of oxygen which can be removed by desorption increases with increasing lithium content and Keier (186) has found the O^{18} isotopic exchange rate to increase rapidly with lithium additions. Keier proposed that lithium additions decrease the chemisorptive tendency of nickel oxide, thus making possible the formation of anion vacancies at the surface. These vacancies increase the isotopic exchange rate at the surface because they permit anion bulk diffusion. However, for a simple defect model it is illogical that electroneutrality could be maintained by the simultaneous addition of lithium (M^{+1}) and the formation of an anion vacancy, V_O, which would have an <u>effective</u> positive charge. Hoch and Szwarc (187 - 188) have proposed that the defect responsible for oxygen self-diffusion is a coupled anion vacancy-electron hole complex. In their model, although the anion vacancy concentration is constant, the "mobility" of the complex is increased by lithium additions because of the corresponding increase in the concentration of electron holes.

With respect to the present investigation, the addition of small quantities of lithium to the nickel oxide

lattice fills the available cation vacancies in the pure material and thus decreases the sinterability by removal of a possible diffusion mechanism (Figure 10). The conditions under which pressure sintering was carried out (Figure 9) were such as to place the material near the Ni/NiO phase boundary. Under these conditions the pressure and temperature dependent equilibrium defect concentration relation (Schottky defects)

$$[V_{Ni}][V_O] = K(T,P)$$

would cause the concentration of anion vacancies to be maximized. Thus, whether lithium additions enhance anion diffusion by reducing the chemisorption at the surface or by increasing the "mobility" of a complex defect, the result of increasing the lithium content should be an increase of the lattice diffusion contribution to the sintering rate. The increase of relative density with substantial lithium additions (Figure 10), the change in particle texture and shape (Figure 11) and the increasing grain size (Figure 12 and Table 6) may all be interpreted in terms of this approach. The changing fracture mode may be attributed to the loss of high chemisorption tendency (strong free surface bonds) with lithium additions.

A similar diffusion enhancement mechanism to that described above has been proposed by Rovner (189) to ex-

plain enhanced oxygen diffusion in magnesium oxide single crystals, and may be applicable to the interpretation of enhanced grain boundary anion diffusion in Al_2O_3 (190), MgO (191) and CoO (192).

F. Electron Microprobe Analysis

Microprobe analysis was performed on both pure and doped nickel oxide specimens. The samples were mounted without heating by using a low-level exothermally setting potting compound (*). They were then slowly ground on number 240,320,400 and 600 grit silicon carbide papers (under kerosene in order to prevent surface heating), lapped on a short nap felt cloth with 15 micron and 6 micron diamond abrasive and then polished on a silk cloth with 1/4 micron (maximum diameter) diamond abrasive (†) without pressure, for three hours. This procedure produced a good surface for microprobe work and held grain pullout to a minimum. The specimen was then ultrasonically cleaned with acetone and immediately placed in the microprobe. The probe was always focused adjacent to the area of interest and then shifted for the scan sequence in order to prevent prior contamination of the area analyzed. The instrument used

---

(*) Klearmount, Vernon-Benshoff Co., Inc., Albany, New York

(†) 1/4 Micron Geonite Diamond Compound, Geoscience Inst., Mount Vernon, New York

was an ARL Co. Model EMX-SM (Electron Microprobe X-ray Scanning Microscope) with a 0.2 micron beam size, and all photographs were taken at the slowest electronic scan rate (5 sec/cm).

Figure 13A shows the area scanned for the 99.999 per cent nickel oxide specimen. The trace made by the beam clearly indicates the beam location. Figure 13B shows the same area after etching for ten minutes in boiling concentrated HCl. It is evident that the beam passed through a large pore and two grain boundaries. The pore may be used as the reference point for the microprobe photographs. Figures 14,15, and 16 show both area and line scan displays for specimen current, secondary electron and back-scattered electron images. The secondary electrons are low energy electrons (less than 200 ev) and therefore respond to surface conditions and topography. The lack of response shown by the secondary electron scans (Figure 15) thus indicates the absence of a topography effect, and therefore, the positive response demonstrated in the specimen current scans (Figure 14) may be interpreted in terms of enhanced grain boundary conduction. The peak height at the grain boundary (Figure 14B) is only 4 per cent above the base line current. A similar analysis was performed on an 8.23 atomic per cent lithium sample. Figure 17 shows both a specimen-current area and line scan display for this alloy.

The specimen-current peak at the grain boundary is only 1-1/2 per cent above the base line current.

A Ni-Kα X-ray scan of the 8.23 atomic per cent lithium sample is shown in Figure 18A. For comparison, Bickelhaupt's (140) photograph of a Mg-Kα scan for a 5 atomic per cent lithium doped MgO specimen is shown in Figure 18B. Because of its low atomic mass, lithium cannot be directly detected with the microprobe, and therefore the absence of nickel (or magnesium in Bickelhaupt's work) must be used in order to indicate a variation in the lithium level. Although no quantitative data were taken, in comparison to the work performed with lithium in magnesium oxide, there appears to be no significant segregation of lithium in nickel oxide.

The possible effects of grain boundary or pore conduction in polycrystalline materials have long been a troublesome barrier to the use of these materials for reliable electronic applications. For example, Goodman (193) has found an increase in resistivity of four orders of magnitude in barium titanate at its ferroelectric Curie temperature. Hutson (17) has reviewed the possible idiosyncracies of polycrystalline materials in general, and Morin (194) has suggested the possible presence of grain boundary conduction in nickel oxide caused by higher concentrations of excess oxygen at the grain boundary than within the bulk

material. This excess oxygen causes a higher concentration of holes and hence a higher p-type conductivity. Similar results have also been reported by Nachman and coworkers (195). However, both of these investigations were performed on specimens with relative densities only 75 to 87 per cent of theoretical density and would therefore be very prone to such effects. Boseman and Crevecoeur (196) report an order of magnitude difference between dc and ac resistivities for an 8.8×10^{-2} atomic per cent lithium alloy, 93 per cent dense, cooled in nitrogen, and identical dc and ac resistivities for the same alloy cooled in air. Boseman and Crevecoeur suggested that this was due to a grain boundary effect, but recent work by Kabashima and Kawakubo (197) shows similar discrepancies between ac and dc measurements in single crystals with similar doping concentrations and similar measurement temperature ranges. In addition to the above, Thornton(198) has reported grain boundary conduction in nickel oxide bicrystals to be caused by the presence of a discontinuous metallic nickel phase at the boundary. The preparation techniques used in this work are questionable.

Microprobe analysis of the grain boundary diffusion of Ni^{+2} in MgO (199), oxygen self-diffusion in polycrystalline alumina (200), and sintering studies in alumina (201) show that the grain boundary width in oxide materials is of the order of 1 micron rather than 10 to 100 angstroms

as would be expected in most metals. Therefore, the present microprobe results on both pure and doped nickel oxide specimens, using very slow scan rates (5 sec/cm) and a small beam size (0.2 microns), give good indication that significant grain boundary effects are absent in the materials used in this investigation. This might also be expected from the high density and high purity of these samples in comparison with the polycrystalline materials used in previous investigations.

G. The Elastic Moduli and Electrical Conductivity

Various attempts have been made in the literature to relate the electrical, magnetic and elastic properties of pure and substituted transition metal oxides. Heikes and Johnston (6), who observed a higher activation energy for electrical conduction above the Néel temperature than at low temperatures for a variety of sintered transition metal oxide alloys, related the major portion of the activation energy to the localized lattice distortion which surrounds a positive hole as it jumps, or "hops", through the lattice. Since the magnitude of the lattice distortion is related to the elastic properties of a material, and because of experimental observations (202) which indicated a large increase in Young's modulus for NiO and CoO as temperature is increased through the Néel point, Heikes and Johnston argued

that the activation energy should likewise increase. Similarly, they explained the observed decrease in activation energy with increased lithium additions as caused by a decrease in the elastic constants with increased impurity concentration.

Toyozawa (11,12) proposed that, in polar materials, there should be an interaction between electrons possessing high effective mass and the acoustic (†) vibration modes of the lattice (as opposed to the simple "polaron" models which consider only optical mode interactions). Toyozawa showed that there is a sharp transition from a "band" state ($M^* \simeq M_o$) to a "localized" state ($M^* > 10^4 M_o$) when the electron-acoustic phonon coupling constant reaches a critical value, $g = g_c \simeq 1$. The coupling constant may be expressed as

$$g = \frac{1}{6} \frac{E_d^2 M^*}{\hbar^2 Ca}$$

where E_d = Bardeen-Shockley deformation potential constant $\simeq$ 2 ev.

C = effective elastic constant

a = nearest neighbor distance.

Adler (14) has recently given a more usable equivalent

(†) The acoustic mode is defined as both the cation and anion moving in phase or as the center of mass of the two ions moving with them, while the optical mode is defined as both the cation and anion moving out of phase or as the center of mass remaining stationary.

expression as

$$\left[\frac{E_d^2}{(Mv^2)\ \Delta}\right] \simeq 1$$

where M = mass per unit cell

v = velocity of sound

Δ = "band width".

Koide (122) investigated the electrical conductivity of $Li_xNi_{(1-x)}O$ single crystals and found a lower activation energy above the Néel temperature than at lower temperatures. This experimental work was interpreted in terms of Toyozawa's interaction theory, and the "band width", Δ, was equivalent to the energy difference, $\varepsilon_m = E_a - E_s$, between the self trapped state (E_s) and the activated state (E_a). Koide gives the expression for resistivity as

$$\rho = \frac{k\ a\ B}{Te^2\nu_l x} \exp\ -\left[\varepsilon_c/kT\right] \exp\left[\varepsilon_m/kT\right]$$

where k is the Boltzmann constant, a is the lattice constant, T is the absolute temperature, e is the electronic charge, ν_l is the lattice vibrational frequency, x is the mole fraction of impurity, and B is a constant. The ε_c term is associated with the ionization of holes and is important at low impurity concentrations, while the ε_m term is associated with an "activated" mobility. The lower activation energy observed by Koide above the Néel temperature is consistent with Toyozawa's model and the experi-

mental increase of the modulus at the Néel temperature.

With reference to Adler's expression for Toyozawa's model, three observations may be made:

(1) If there is a change of modulus at the Néel temperature then a change in the slope of resistivity versus temperature curve should occur at the same temperature. This change should occur at a different temperature for each composition.

(2) If the modulus <u>increases</u> at the Néel temperature then the activation energy should <u>decrease</u> above the Neel temperature ($E_{LT} > E_{HT}$).

(3) If the <u>low temperature</u> modulus <u>increases</u> with increased impurity content then the difference between the low temperature and high temperature activation energies should <u>decrease</u> (the modulus above the Néel temperature is normally expected to decrease with temperature for a paramagnetic material and is therefore a poor indicator).

The Néel temperature of nickel oxide was first measured by Foex (203) using dilatometric methods and was found to be 525°K. Many other measurement methods have been used, and the results are given in Table 7. The best value for the Néel temperature, obtained from more recent data in the table, appears to be 523°K. Because of the relatively broad susceptibility peak (50) as opposed to the sharp modulus change (202), and because of the interest in the vari-

ation of the low temperature modulus with lithium concentration, measurements for this investigation were performed using the modulus technique.

The difficulties encountered in measuring elastic moduli of small samples are outlined in Appendix 2. Careful investigation was made of the accuracy and experimental difficulties associated with each of the available methods before a specific method was adopted. The Forster free vibration method was ruled out (230) because of the need for a long specimen, while the "pulse-echo", "Phase Comparison" and "Pulse Superposition" methods were eliminated (231) due to the inaccuracy of velocity measurements associated with small samples. Although the "Pulse Transmission" and "Sphere Resonance" methods were found to give good accuracy for small specimens (232), they were similarly eliminated because of the difficulties associated with measurements at elevated temperatures. The composite oscillator method was adopted because of its applicability to small specimens, lack of complicated electronic equipment, and adaptability for high temperature measurements. However, the room temperature Young's modulus measurements were standardized against "Pulse Transmission" and "Sphere Resonance" measurements for both the pure nickel oxide and the highest lithium alloy investigated (*). A description of the mathematical

(*) These measurements were made by Messrs. M. Notis and J. Snyder at the Lamont Geological Observatory of Columbia University with the kind permission of Dr. O.L. Anderson.

basis for the composite oscillator method and a tabulation of the data are presented in Appendix 3. A description of the experimental and associated calculation procedures for the "Sphere Resonance" and "Pulse Transmission" methods is given in Appendix 2. The experimental "Sphere Resonance" data for pure nickel oxide at room temperature are given in Table 8, and all of the room temperature modulus results for each of the methods are given in Table 9.

Observations made from the data given in Table 9 might be summarized as:

(1) The shear velocity of the 8.23 per cent lithium alloy is 50 per cent higher than that for pure nickel oxide (Pulse Transmission data) while the longitudinal velocities are nearly identical.

(2) The Young's modulus values from Sphere Resonance and composite oscillator methods agree within 0.2 per cent, and Pulse Transmission and composite oscillator within 22 per cent, for pure nickel oxide. Pulse Transmission and composite oscillator measurements agree within 10 per cent for the 8.23 per cent lithium alloy.

(3) The value of Poisson's ratio, 0.443 from Pulse Transmission, and 0.416 from Sphere Resonance, for pure nickel oxide is extremely high. The value of Poisson's ratio for the 8.23 per cent lithium alloy is 0.35, and repre-

sents a very substantial decrease from the value for pure nickel oxide.

The values obtained for the room temperature moduli of nickel oxide may be compared with the pre-existing experimental work in the literature and with theoretically derived moduli. Street and Lewis (202) give the room temperature value of Young's modulus for 68 per cent dense nickel oxide (240) as 5.1×10^{11} dyne/cm^2, Belov (217) gives the Young's modulus for unidentified nickel oxide as 3.24×10^{11} dyne/cm^2 (3.3×10^3 kg/mm^2 in the original paper), and Slack (241) has given the value of C_{11} as 10.0×10^{11} dyne/cm^2. Wakabayashi and coworkers (242) have measured the effect of pressure on the lattice parameter of NiO and have expressed this as:

$$\frac{\Delta V}{V_o} = -5.4 \times 10^{-7} P + 0.6 \times 10^{-12} P^2$$

where P is the applied pressure in bars. The bulk compressibility, B_T, may be expressed as

$$B_T \equiv -\frac{1}{V}\left(\frac{\partial V}{\partial P}\right)_T \simeq -\frac{1}{V}\left(\frac{\Delta V}{\Delta P}\right)_T = -\frac{\Delta V}{V}\left(\frac{1}{P-P_o}\right)\Bigg|_{\substack{V=V_o \\ P_o=0}} = -\frac{\Delta V}{V_o}\left(\frac{1}{P}\right)$$

and since the bulk modulus is just the inverse of the compressibility,

$$K\Big|_{P=1} = -\frac{V_o}{\Delta V}(P) = -\left[\frac{1}{-5.4\times10^{-7}(1)+0.6\times10^{-12}(1)^2}\right](1)$$

$$= 1.85\times10^{6} \text{ bars} \times \frac{10^{6}\text{dyne/cm}^2}{\text{bar}} = 18.5\times10^{11} \text{ dyne/cm}^2.$$

The mean sound velocity may be derived from the Debye temperature (243) using the relation

$$\vartheta_m = \frac{k}{h}\left[\frac{3PN_A\rho}{4\pi M}\right]^{-1/3}\theta_D$$

where $k = 1.38\times10^{-16}$ erg/°K

$h = 6.6\times10^{-27}$ erg·sec

P = Number of atoms per molecule = 2

$N_A = 6.023\times10^{23}$ molecules/gram atomic weight

ρ = density = 6.806 g/cm^3

M = molecular weight = 74.71.

Seltz and coworkers (244) give $\theta_D = 404$°K and Wenner (245) gives $\theta_D = 415$°K. Using the average value of 410°K, the value of ϑ_m is 2.9×10^5cm/sec, and the Debye frequency, $\nu_D = \theta_D \frac{k}{h}$, is 8.6×10^{12}/sec.

If the infrared reflection specta for a diatomic substance is known, the bulk modulus can be determined (reference 243 equation 10) from the Szigeti (246) relation:

$$K = \frac{4\pi^2C^2\bar{m}}{6R_o\lambda_o^2}\left(\frac{\varepsilon_o+2}{\varepsilon_\infty+2}\right)$$

where C = speed of light = 3×10^{10} cm/sec

R_o = interatomic spacing = $\frac{a_o}{2}$ = 2.09A° = 2.09×10^{-8}cm

$\bar{m}$ = effective mass per ion pair =

$$\left[\frac{M_O M_{Ni}}{M_O + M_{Ni}}\right]\frac{1}{N_A} = \frac{(16)(58.71)}{(74.71)(6.023\times10^{23})} = 20.8\times10^{-24}\text{g}$$

ε_o = dielectric constant

ε_∞ = square of the index of refraction (n)

λ_o = "Reststrahlen" wavelength.

Marshall and coworkers (247) give these last three values as $\varepsilon_o = 11.9$, $\varepsilon_\infty = 4.75$ and $\lambda_o = 24.5\mu$ ($\nu_t = 408\ \text{cm}^{-1}, \lambda_o = \frac{10^4}{\nu_t}$). The above equation then gives a value of $K = 20.2\times10^{11}$ dyne/cm^2.

The mean sound velocity, ϑ_m, may be related to (243) Poisson's ratio and the bulk modulus according to the expression

$$\vartheta_m = \left[\frac{3}{\left[\frac{1+\sigma}{3(1-\sigma)}\right]^{3/2} + 2\left[\frac{2(1+\sigma)}{3(1-\sigma)}\right]^{3/2}}\right]^{\frac{1}{3}} \cdot \left[\frac{K}{\rho}\right]^{1/2}$$

The experimental and derived values of ϑ_m and K are summarized in Table 10. Where necessary, the conversion from ϑ_m to K was performed using the Poisson's ratio of σ=0.416 obtained from the Sphere Resonance method. The agreement of these values is excellent, except for the Debye value.

Young's modulus as a function of temperature for pure nickel oxide is shown in Figure 25. The two curves represent measurements made with two different sets of crystals, 92.5 kc and 118.5 kc. The specimen matched the 92.5 kc crystals at room temperature and the 118.5 kc crystals at 245°C. The maximum deviation of $f_{s(o)}$ and $f_{s(f)}$ (equation A3.4 and equation A3.3) for the 118.5 kc crystal measurements occurred at 250.5°C and was 0.57 per cent. Although the effect of sample and crystal matching is pronounced for the high temperature modulus, the low temperature modulus values agree very well and the curves overlap in the region of the anomalous modulus increase. Below the anomaly, the slow increase in modulus is caused by a decrease in spin ordering, while above the anomaly, the decreasing modulus is caused by the normal thermal decrease found in paramagnetic materials. The Néel temperature was therefore defined as the point of maximum slope in the modulus curve. This choice of Néel temperature was found to be independent of crystal-sample frequency matching for both pure nickel oxide and all alloy compositions measured with different sets of crystals. The high and low temperature modulus measurements obtained for pure nickel oxide using the 118.5 kc crystals, and the low temperature moduli for the alloy specimens represent good modulus values because of good crystal-sample matching. The high temperature modulus values obtained for the alloy com-

positions should not be taken as being representative of the absolute modulus because of poor matching of specimen and crystals in that region.

Figure (26) shows the effect of using equation (A3.3) as an approximation of equation (A3.2) for pure nickel oxide measured with 118.5 kc crystals (i.e. ignoring the $\tan^2$ term). There is a slight decrease of the low temperature modulus and an increase of the high temperature modulus, but again there is no change of Néel temperature with either choice of solution. Table 11 gives the appropriate data for the same specimen and indicates the value of the modulus obtained at room temperature and the Néel point for each solution method. Although equation (A3.2) provides a slight correction to the modulus value for reasonable deviations from matched conditions, the original starting assumptions (which were made in order to obtain an analytical expression) produced an incomplete solution. Thus, as the $\tan^2$ term approaches 1, $1-\tan^2$ approaches zero and the value of f_s obtained from equation (A3.2) increases rapidly. For this reason and in order to be consistent with other published experimental work using this method, the $\tan^2$ term was ignored.

The explanation of the anomalous modulus increase at the Néel temperature has been the source of much argument. Street and Lewis (202) originally proposed that the modulus effect was caused by changes in spin orientation, but later

(248) these same authors ascribed the anomaly to domain motion. Fine (249,250) measured Young's modulus and internal friction of CoO and explained his results in terms of domain changes related to crystal distortion. It seems logical however that the Néel temperature represents the point at which critical fluctuations in the spin system are reached, causing an interaction between acoustic lattice vibrations and the spin system. This type of interaction qualitatively accounts for the modulus change and the sharp increase in sound attenuation at the Néel point. Slack (251) observed that stresses of approximately 10^5 to 10^6 dyne/cm^2 were required to cause domain wall motion in nickel oxide single crystals. Yevtushchenko and Levitin (252) measured the moduli of MnO, CoO, and Cr_2O_3 under dynamic stress conditions of 10^4 dyne/cm^2 or less, and consequently concluded that the anomaly is attributable to either the rotation of magnetic moments within a domain or to spin rotation. Belov (253) and coworkers came to similar conclusions for NiO.

Difficulties also exist as to the correspondence of the Néel temperature and the observed crystallographic distortion. A slight rhombohedral distortion (a_o = 2.9518A°, α = 60°4.2' at 18°C) below the Néel temperature was first observed by Rooksby (254,255), and the correspondence of the Néel temperature and lattice distortion was observed in CoO and Cr_2O_3 by Greenwald and Smart (256). General agreement

with these observations was noted by Slack (251) in 1960. However, thermal expansion measurements made by Gillam and Holden (257) indicate no observable distortion until 90°C below the Néel temperature. Vernon and Lovell (258) have explained anomalies in resistivity measurements on nickel oxide single crystals as being caused by the non-correspondence of the Néel temperature and the onset of distortion. The most recent evidence (259) based on high temperature observation of domain structure in annealed nickel oxide crystals indicates correspondence of the magnetic and crystallographic transformations.

Young's modulus versus temperature data for pure nickel oxide and for five lithium alloys ranging from 0.12 to 8.23 atomic per cent lithium are presented in Figures 27 and 28. The relative acoustic loss corresponding to each of these specimens is given in Figure 29. Young's modulus versus temperature for a nominal $Li_{0.01}Mg_{0.115}Ni_{0.875}O$ alloy is presented in Figure 30. Comparison of Figures 27, 28 and 30 demonstrates the excellent repeatability of the measurement method. Inspection of Figure 27 or 28 shows a definite decrease in Néel temperature with increased lithium content and a fairly large increase of low temperature modulus with increased lithium content. Comparison of Figures 27 or 28 and Figure 29 shows that the maximum in each acoustic loss curve corresponds very closely to the anomalous modulus in-

crease. The Néel temperature for each of these alloys, obtained from the modulus curves, is plotted in Figure 31. A similar curve can be obtained from the acoustic loss.

Shimomura and Tsubokawa (213) observed that the temperature of the anomaly in the specific heat of nickel oxide -copper oxide alloys decreased with increasing copper content. Perakis (107), Bielanski (260), and Mehandjeev (121) and coworkers have all investigated the magnetic susceptibility of powdered lithium-nickel oxide alloys as a function of temperature. The susceptibility curves all show a broad maximum and, although there is a general decrease in Néel temperature with lithium content, the results indicate very erratic behavior. On the other hand, Richardson and Millegan (207) indicate a very large decrease of Néel temperature with decreasing particle size for pure colloidal nickel oxide. They attribute this behavior to a decrease in the number of spin-opposed nearest neighbors caused by the influence of increased amounts of excess oxygen as the surface area is increased. Akiyama and coworkers (261,262) report a general decrease in Néel temperature with increased lithium content but give neither composition nor T_N for any of the alloys. No other reports on the effect of impurity additions on the Néel temperature could be found.

The linear relation between Néel temperature and lithium content observed on bulk material in this investigation

can be explained in terms of a localized electron approach to antiferromagnetism. Van Vleck (263) has shown that the Néel temperature, for antiferromagnetic compounds having a sodium chloride type structure and spin alignment such as that possessed by MnO or NiO (264), may be expressed as

$$T_N = \frac{1}{4} \alpha C_M$$

where C_M = Curie constant per gram·mole = $N\mu^2/3\ k$

μ = absolute value of the magnetic moment = $\mu_B g\sqrt{S(S+1)}$ (reference 265)

g = Landé factor = 2 for pure spin magnetic moments (reference 265)

S = Spin angular momentum (in Bohr Magnetons) = 1 (reference 265)

μ_B = Bohr Magneton = 9.2733×10^{-21} ergs/gauss.

The proportionality factor, α, is given by

$$\alpha = \frac{-2[Z][A_{EX}]}{N\mu_B^2 g^2}$$

where Z = number of nearest neighbors with opposite spin

A_{EX} = "Exchange Integral."

For pure nickel oxide, each Ni^{+2} ion has six nearest neighbors of like spin and six of opposite spin so that Z = 6. If one of these thirteen Ni^{+2} ions is replaced by a Li^{+1}, a

second Ni^{+2} ion changes valence to Ni^{+3} in order to maintain charge neutrality and, then Z = 5. For this situation the lithium content would be (1/13) x 100 = 7.7%, or

$$\frac{\Delta Z}{\Delta(\%Li)} = \frac{6-5}{0-7.7} = -0.13$$

If a divalent element such as Mg were added the change of nearest neighbors would be only one-half of that for lithium since no Ni^{+3} would be produced. Thus if Z is a simple monotonic function of impurity concentration (as should be the case for a random solid solution) and if the magnitude of the "exchange integral" is constant (as should be the case for a localized electron model), the Néel temperature should be a simple decreasing linear function of impurity content.

Using the values given above, C_M for nickel oxide is found to be equal to 1, and if Z = 6 and the Néel temperature of nickel oxide is set at 523°K then the "exchange integral" is found to be

$$(A_{EX})_{NiO} = -3.6\times10^{-14} \text{ ergs.}$$

This agrees fairly well with a theoretically derived value of 1.17×10^{-14} ergs given by Nesbet (266). If the experimentally determined value of C_M = 3.1 obtained by Perakis (50) is used, then the value of the "exchange integral" would be -1.16×10^{-14} ergs. Although the agreement is excellent, it may be somewhat fortuitous because of the simple

cubic lattice used by Nesbet. If

$$Z = Z_{NiO} + \%Li \quad \frac{\Delta Z}{\Delta(\%Li)} = 6 \quad -0.13\ (\%Li)$$

then for a 10% lithium alloy Z = 4.7,

$$(T_N)_{THEORETICAL} = \frac{-(Z)(A_{EX})}{2N\mu_B^2 g^2} C = 409°K$$

or $\Delta T_N/\Delta(\%Li) = \frac{523-409}{0-10} = -11.4°K/(\%Li)$. This compares very well with the observed value of -9.1°K/(% Li) obtained from Figure 31. A similar calculation for Mg additions would give

$$\Delta T_{N/\Delta}\ (\%Mg) = -5.7°K/(\%Mg).$$

If the localized approach is correct then the total change in Néel temperature should just be the arithmetic sum of all the ΔT's from each impurity addition. This may be expressed, for lithium and magnesium additions, as

$$\Delta T_N = \Delta T_{N(Li)} + \Delta T_{N(Mg)}.$$

The experimental value of the Néel temperature of the ternary alloy $Li_{0.01}Mg_{0.115}Ni_{0.875}O$ was 461°K (Figure 30), while the contribution to the Néel temperature decrease caused by a one per cent lithium addition should have been 9.1°K. The decrease of T_N attributable to the magnesium addition is then

$$\Delta T_{N(Mg)} = \Delta T - \Delta T_{N(Li)} = (523-461) - 9.1 = 52.9°K$$

or $\Delta T_N/\Delta(\%Mg) = -4.6°K/(\%Mg)$. Again the agreement between this value and the theoretical value of -5.7°K/(%Mg) seems good. It might also be noted that the value of the experimentally observed $\Delta T_N/\Delta(\%Li)$ is almost exactly twice that of the value of $\Delta T_N/\Delta(\%Mg)$ as was predicted by the localized model.

The resistivity of each of the lithium-nickel oxide alloys as a function of temperature is given in Figure 32. The break in each curve shifts to lower temperatures with increasing lithium content, and the magnitude of the shift from pure nickel oxide to the 8.23 atomic per cent lithium alloy corresponds to the Néel temperature change shown in Figure 31. The slope of each curve (the activation energy) is lower in the high temperature region, and the slope in the low temperature region decreases with increasing lithium content. All of these trends are in qualitative agreement with the electron-acoustic phonon interaction proposed by Toyozawa(11,12)and the measurements made on lithium doped single crystals by Koide(122).The pure nickel oxide specimen shows an additional break at approximately 100°C. Similar results have recently been observed in nickel oxide single crystals and have been attributed to

ionization of localized acceptor impurity levels and inter-acceptor "hopping" (267), crystal distortion (258), thermally activated impurity tunnelling (268) and to normal band-type acceptor ionization (269). A schematic resume of the experimentally observed behavior of the resistivity of pure nickel oxide as a function of temperature is shown in Figure 33.

Resistivity measurements alone are not conclusive or even sufficient criteria upon which to base a conduction mechanism. However, the interpretation of the linear decrease in Néel temperature with increasing lithium in terms of localized-electron magnetic theory, and the interpretation of the inter-relation between the elastic modulus and the conduction activation energy in terms of an acoustic coupling effect both give support to some type of "hopping" mechanism. Experimental investigations on the optical properties of nickel oxide yield similar conclusions. Morin (157) found the spectral response of the Ni^{+2} ion in the isolated,octahedrally bound, $Ni(H_2O)_6^{+2}$ hydrated complex to be the same as in NiO; other investigators (270-272) found identical response for Ni^{+2} in MgO and Ni^{+2} in NiO. Photoelectric emission and optical reflectance work (273) show the various band models not to be applicable to the outer electron shells of nickel oxide. Finally, recent work (274) with the infra-red optical absorption spectra and

high-frequency conductivity of lithium doped nickel oxide single crystals has been interpreted in terms of the small polaron theory of Bogomolov and coworkers(275-276). One of the major difficulties with the description of localized-electron transport properties in terms of optical mode ("polaron") interactions still appears to be the explanation of abrupt changes in conduction properties across critical points (such as the Néel temperature).

To summarize the results and discussion presented in this section, it has been found that

(1) the low temperature value of Young's modulus increases with increasing lithium content and the temperature of the modulus anomaly decreases in a similar manner.

(2) The temperature of the modulus anomaly is equivalent to the Néel temperature for each of the alloys, and the linear decrease in Néel temperature with lithium content was interpreted in terms of Van Vlecks'(263) localized-electron theory of antiferromagnetism.

(3) Resistivity measurements made on well characterized pressure-sintered polycrystalline lithium-nickel oxide alloys agree with the reported results on single crystal material. These include a break at the Néel temperature, a lower activation energy at higher temperatures than at lower temperatures, and a decrease in the low temperature activation energy with increasing lithium content.

(4) The combined trends in the modulus and resistivity as a function of temperature and impurity level were interpreted in terms of Toyozawa's electron-acoustic mode interaction model which predicts an inverse relation between the elastic modulus and the energy difference between the self-trapped and activated electron states.

(5) Although more direct techniques such as resistivity, Hall effect and thermoelectric power measurements have not yet provided clarification of the conduction mechanism (primarily because of the unavailability of adequately prepared and well characterized materials) optical studies have provided strong indirect evidence for a localized model.

The success of a quantitatively correct localized electron model appears to depend on the development of a theoretical approach which would simultaneously account for both optical mode and acoustic mode interactions. Close kinship between the theoretical work and the careful preparation and characterization of materials is equally needed in order to realize critical interpretation of observed behavior.

CONCLUSIONS

1. Pure nickel oxide tends very close to stoichiometric proportions. Deviations from stoichiometry are predominantly caused by the impurity-affected surface properties of the material. The composition of 99.999% pure nickel oxide used in this investigation was found to be $NiO_{1.000003\pm0.0003\%}$.

2. The qualitatively observed shift in the Ni/NiO phase boundary with lithium doping additions was explained in terms of a sharp decrease in the Fermi energy level. In turn, this shift causes a very sharp drop in the chemical potential of Ni in NiO, decreases the activity precipitously, and rapidly widens the stable phase field of NiO.

3. The concentrations of Li^{+1} and Ni^{+3} are equal in pure single phase $Ni^{+2}_{1-2x}\,Li^{+1}_{x}\,Ni^{+3}_{x}O$. The iodometric titration results indicate the absence of any detectable metallic nickel in the oxides used for this investigation, and show no detectable lithium loss during pressure sintering. The discrepancy between these findings and those previously reported in the literature indicates previous difficulty in the careful preparation and characteriza-

tion of these materials.

4. The sintering behavior of lithium substituted nickel oxide (change in particle texture and shape, increased relative density, increased grain size and change of fracture mode) was interpreted in terms of enhanced oxygen diffusion caused by either a decrease in the chemisorptive surface properties or by an increase in the "mobility" of a coupled anion vacancy-electron hole complex.

5. Electron microprobe results on both pure and doped nickel oxide specimens indicate that significant grain boundary conduction effects are absent in the samples used in this investigation.

6. The measurement of Young's modulus as a function of temperature for the lithium-nickel oxide alloy system was found to be a very sensitive method for the determination of the variation of the Néel temperature with composition. For the lithium-nickel oxide system this variation was explained in terms of a simple localized-electron approach to magnetic properties.

7. For each of the polycrystalline alloys, the trends in the variation of resistivity as a function of temperature agree with previously reported work on single crystal material. These trends, in combination with the modulus results, were interpreted in terms of a localized electron-acoustic mode interaction.

Appendix I

Procedure for Determination of Ni^{+3}

1. Set up the apparatus as shown in Figure 3.
2. Coat all joints with Dow Corning Silicone Lubricant Stopcock Grease.
3. Before coating the joints of the reaction flask (A), weigh out sample directly into the flask.
4. Pipette 10 ml of conc. HCl into pressure equalizing funnel (B)
5. Pipette 50 ml of 20 weight per cent KI solution (*) into flask #1 and 25 ml into flask #2.
6. Cool both KI flasks in ice baths.
7. All joints are positively sealed with commercial spring clips.
8. Open all stopcocks, except stopcocks (C) and (D), and slowly pass dry CO_2 through the apparatus for 5 minutes to purge system of air (rapid flow will blow sample powder out of reaction flask).
9. Close stopcock (E), open stopcock (C) and allow 2.5 ml HCl to enter reaction flask. Close stopcocks (C) and (F).
10. Open stopcock (D) and allow CO_2 to bubble through reaction flask.
11. Heat reaction flask with boiling water until the sample dissolves. The solution will be dark green in color and should show no residue at the bottom of the reaction flask. If dissolution is incomplete, repeat steps 9 through 11.

(*) Potassium Iodide, Baker Lot 31640, Reagent Grade.

12. Remove boiling water from reaction flask and heat with a direct, but gentle, flame until the sample has been evaporated to dryness.

13. Heat glass ware between reaction flask and flask #1 to dryness.

14. Bubble CO_2 through apparatus for 5 minutes and then close stopcock (G).

15. Remove flasks #1 and #2. Test flask #2 with 2.5 ml starch solution (**). If there is a color change save the solution as it will be added to flask #1 later.

16. Wash gas diffusion tubes into their respective flasks to insure no loss of iodine.

17. The iodine in flask #1 is then titrated with 0.01N $Na_2S_2O_3$ until the solution is pale yellow. Add 5 ml of starch solution. (If flask #2 indicated the presence of a color change it should now be added to the contents of flask #1). The solution should be dark blue.

18. Slowly add $Na_2S_2O_3$ until the end point (blue to clear) is reached.

19. The weight percent Ni^{+3} is calculated from the following equation:

$$\text{weight } \%Ni^{+3} = \left(\frac{\text{ml} \times \text{N} \times \frac{58.71}{1000}}{\text{sample wt}} \right) \times 100$$

20. The atomic per cent Ni^{+3} is calculated from the following equation:

$$\text{atomic } \%Ni^{+3} = \left(\frac{\frac{\text{weight } \%Ni^{+3}}{58.71}}{\frac{\text{weight } \%Ni^{+3}}{58.71} + \frac{[100 - \text{weight } \%Ni^{+3}]}{74.71}} \right) \times 100$$

(**) 2 grams Baker's Soluble Starch Powder in 1 liter distilled and deionized water.

Appendix 2

"Pulse Transmission" and "Resonant Sphere" Elastic Modulus Measurements

The accurate determination of dynamic elastic moduli on small samples (less than one inch in length) has been found to be of utmost importance for the research and development of new materials. Standard measurement techniques, such as the Forster resonance (213) and the sonic "pulse-echo" (220) methods, have not been found to be directly applicable to small specimen measurements. The Forster method consists of resonating a "free" bar with frequencies in the audible acoustic range and thus requires a long sample (equivalent to the long wavelength). The "pulse-echo" technique depends on a direct measurement of the transit time of a mechanical wave through the specimen and is therefore not accurate for short specimens (very short transit times). McSkimin has proposed two modifications of the basic sonic method, the "Phase Comparison" (221) and "Pulse Superposition" (222) technique, in order to provide more accurate transit time measurements. The phase comparison technique measures the difference in transit time between two pulses which have traveled different numbers of round trips along a specimen. The pulse superposition technique consists

of the superposition of two different waves of similar constant frequency but with a slight phase shift. A "beat" frequency is produced, and the transit time of this beat may be related to the velocity of sound in the sample. Further advancement was made with the development of the "pulse transmission" or "Time of Flight" technique by Birch (223) and the elimination of major instrumentation errors for the same technique by Mattaboni and Schreiber (224).

The pulse transmission method (Figure 19) consists of displaying both a variable "timing frequency" and the initial test pulse, or alternately the final specimen signal, on the same oscilloscope. The variable timing frequency is adjusted (both in frequency and pulse shape) until the time delay between the initial test pulse and the specimen response signal is equal to an integral number of cycles (N) of timing frequency. The time between peaks on the timing frequency display is just $\frac{1}{f}$ and the specimen transit time is

$$t = \frac{1}{f} \times N.$$

The velocity of sound in a sample of length, L, is

$$\vartheta = L/t = L(\frac{f}{N}).$$

In practice, the driver and pickup transducers attached to the specimen may be either x-cut quartz discs for the measurement of the longitudinal wave velocity (ϑ_l), or Y-cut quartz

discs for the measurement of the shear wave velocity (ϑ_s). The shear modulus (G), Young's modulus (E), bulk modulus (K) and Poisson's ratio (σ) are given as:

$$G = \rho \vartheta_s^2$$

$$E = 2\rho\vartheta_s^2 (1 + \sigma)$$

$$K = \rho(\vartheta_l^2 - \frac{4}{3}\vartheta_s^2)$$

$$\sigma = \left[1 - \frac{1}{2}\left(\frac{\vartheta_l}{\vartheta_s}\right)^2\right] \Big/ \left[1 - \left(\frac{\vartheta_l}{\vartheta_s}\right)^2\right], \text{ where}$$

ρ = specimen density

The previous sonic methods suffer, to some degree, from inherent inaccuracies in measuring short transit times, from large end effects caused by specimen geometry, and transducer coupling effects relative to the specimen size. All of these difficulties were eliminated through the development of the "resonant sphere technique" by Fraser and LeCraw (225). The method consists of placing a small sphere of the sample on a single shear wave transducer as in Fraser and LeCraw's original technique, or between two transducers, as in Soga and Anderson's (226) modified method, and of monitoring the resonant frequencies of the sphere.

The major experimental error in this technique is the production of specimens of good sphericity and the measurement of the specimen diameter. Pneumatic sphere grinding

equipment (227) as shown in Figure 20 is used to grind a spherical shape from that of a cube by random tangential abrasion of the cube against the inner wall of the alumina container. A highly polished surface is then obtained by lapping the sphere with successively finer silicon carbide powder and then Linde "B" alumina with counter-rotating lapping pipes (228) as shown in Figure 21.

A schematic representation of the resonant sphere method is shown in Figure 22. The variable frequency signal that excites the specimen is continuously switched on and off by the solid state switch and is monitored on the scope. When the generated frequency causes the sphere to resonate, the sphere continues to vibrate after the signal is switched off and a decay pattern is observed. An RC decay generator with variable capacitance and resistance is used to match the decay pattern, and the "Q" for the circuit (acoustic loss) may be calculated (227) from

$$Q = 2\pi f\tau = 2\pi f(R \cdot C).$$

The modes of vibration of the sphere are either spherical or shear (Figure 23) waves and only the spherical modes are dependent on Poisson's ratio. Fraser and LeCraw (225) have shown that an arbitrary experimental resonant frequency, f, for a sphere of diameter, d, may be related to the resonant frequency of a given specific mode, f_n, by a non-dimensional

normalized or "reduced frequency", f_r, which is not a function of specimen diameter, according to the relation:

$$f_r = \frac{f}{f_n} \times A_n$$

where A_n = mode constant for the nth mode of free-oscillation of a homogeneous elastic sphere.

The constants, A_n, have been determined and tabulated by Sato and Usami (229), and a plot (Figure 24) of reduced frequency versus Poisson's ratio, σ, for each vibrational mode has been given by Fraser and LeCraw (225).

In practice, one of the lower frequency, high intensity modes out of the experimental resonant frequency spectrum is arbitrarily chosen, identified as a specific pure shear mode (therefore not dependent on Poisson's ratio), and a series of reduced frequencies are calculated. A match between the experimental reduced frequencies and the plot of Fraser and LeCraw (225) provides a solution for Poisson's ratio (because the spherical modes <u>are</u> single valued functions of Poisson's ratio); at the same time, each of the vibrational modes is identified. The process may be simplified if the approximate value of Poisson's ratio has been previously determined (as by the "Pulse Transmission" method). If the initial identification of the first pure shear mode was incorrect, the entire process is repeated until a match is found.

The shear velocity may be caluclated (226) for each of the pure shear modes from the relation:

$$v_{shear} = \frac{\pi d f_n}{A_n}$$

The shear velocity and the value of Poisson's ratio are then used to calculate the remaining elastic moduli.

Appendix 3

The Composite Oscillator

The fundamental frequency of free longitudinal vibration of a bar has been found (233) to be related to Young's modulus according to the equation

$$E = \rho f^2(4L^2+2\pi^2\sigma^2r^2) \approx 4\rho f^2L^2 \qquad \text{Eq (A3.1)}$$

where ρ = specimen density

f = frequency of free vibration

L = length

σ = Poisson's ratio

r = radius

If the radius is small compared to the length of the bar, and since $\sigma < 0.5$, the last term may normally be ignored. If a piezoelectric quartz crystal is attached to a rod of given dimensions and if a sinusoidally varying potential difference is applied across the electrode surfaces of the crystal, a stable state of forced vibration is established for the composite system. When the applied frequency is equal to the free vibrational frequency of the composite system, a "resonant" condition is established and the amplitude of the output is at a maximum. If the resonant frequency of the composite can be related to that of the isolated bar,

then the modulus of the bar could be calculated from the above equation. Zacharias (234) first used this method to measure Young's modulus at elevated temperature for thin nickel rods. Fine (235) explained that for materials with high internal friction the capacitance of the crystal distorts the output and the system must be balanced by the use of a second(or "gauge") crystal. If the crystals and specimens are frequency matched then, at resonance, each section is one-half wave length long, the frequency nodes appear at the center of each section, and the stress nodes occur at the cemented joints.

The relation between the resonant frequency of a three part composite oscillator and the natural frequency of each of the components was first given by Rose (236) and then by Cooke (237) as

$$m_1\left[\frac{\tan y_1}{y_1}\right] + m_2\left[\frac{\tan y_2}{y_2}\right] + m_3\left[\frac{\tan y_3}{y_3}\right] - \frac{m_1 m_2 y_3}{y_1 y_2 m_3}\{\tan y_1 \tan y_2 \tan y_3\} = 0$$

where m_i = mass of each section

$$y_i = \pi\left\{\frac{f_x}{f_i}\right\}$$

f_x = resonant frequency of the composite

f_i = resonant frequency of each section.

If the quartz crystals are matched such that $m_1 = m_2 = m_c$,

$y_1 = y_2 = y_c$, and $m_3 = m_s$, $y_3 = y_s$, then this equation may be rewritten in the form

$$(2m_c)f_c \tan\pi\frac{f_x}{f_c} + m_s f_s \tan\pi\frac{f_x}{f_s}\left[1-\left(\frac{m_c^2 f_c^2}{m_s^2 f_s^2}\right)\tan^2\pi\frac{f_x}{f_c}\right] = 0 \qquad \text{Eq(A3.2)}$$

In theory, it is possible to measure the resonant frequency of the crystals alone, and then of the composite, and use equation (A3.2) to calculate the resonant frequency (f_s) of the sample. In practice, the crystals and specimen may be <u>roughly</u> matched such that $f_x \approx f_c \approx f_s$ and the $\tan^2$ term may then be ignored. This results in a simplified expression,

$$M_c f_c \tan\pi\frac{f_x}{f_c} + m_s f_s \tan\pi\frac{f_x}{f_x} = 0 \qquad \text{Eq(A3.3)}$$

where $M_c = 2m_c$ = combined crystal mass.

The tangent terms may be manipulated (238) such that

$$\tan\pi\frac{f_x}{f_i} = \tan\left[\pi + \pi\left\{\frac{f_x}{f_i} - 1\right\}\right] = \tan\pi\left[\frac{f_x}{f_i} - 1\right]$$

since

$$\tan(\alpha+\beta) = (\tan\alpha + \tan\beta)/(1 - \tan\alpha\tan\beta).$$

If $f_x \approx f_i$, then $\frac{f_x}{f_i} \approx 1$, $\left[\frac{f_x}{f_i} - 1\right]$ is small, and $\tan\pi\frac{f_x}{f_i} = \tan\pi\left[\frac{f_x}{f_i} - 1\right] \approx \pi\left[\frac{f_x}{f_i} - 1\right]$. Thus if the crystals are closely matched, equation (A3.3) simplifies into the

linear relation,

$$f_s = f_x + \frac{M_c}{m_s}(f_x - f_c). \qquad \text{Eq(A3.4).}$$

The assumptions inherent in the composite oscillator method may be summarized as,

(1) internal friction for each of the components is small

(2) there is no Poisson's contraction or expansion as the modulus changes (if σ changes then L would change)

(3) there is no length change with temperature (thermal expansion is small)

(4) cement joints are elastic and strain free, and

(5) stress nodes are at or near the joints.

For this investigation, a CDC 6400 computer was used to solve for the frequency of the specimen. Equation (A3.4) provided an initial trial value for f_s and then a Newton-Raphson method was used to solve Equation (A3.2) or (A3.3) for f_s. Young's modulus was then computed from Equation (A3.1) and the modulus was plotted as a function of temperature on a Calcomp Plotter. The final program design and a tabulation of all of the pertinent data (with $\tan^2$ term assumed small) are presented at the end of this appendix.

Marx (239) has shown that the acoustic loss for a composite oscillator such as that described above can be expressed as

$$\delta = K\left\{\frac{V_D}{V_G}\right\}$$

where V_D = input voltage to the driver crystal

V_G = output voltage from the gauge crystal

K = constant depending on the equipment and the material.

A relative measure of δ can be obtained by assuming K = 1 and using the ratio of the input to output voltages.

```
      REAL MS,MC,L
      INTEGER V,VI,VII,VIII
      DIMENSION EASY(100),TEMP(100),ELAS(100),TEM(100)
      DIMENSION E1(100),E2(100),E3(100),E4(100),E5(100)
      DIMENSION T1(100),T2(100),T3(100),T4(100),T5(100)
      DIMENSION E(100),T(100)
      DIMENSION BOX1(100),BOX2(100),BOX3(100),BOX4(100)
      PI=3.14159265
      PRINT 1
    1 FORMAT(1H1,49H     NEWTON-RAPHSON METHOD TO SOLVE THE EQUATION     )
      PRINT 2
    2 FORMAT(55H      MS*FS*TAN(PI*FX/FS)+MC*FC*TAN(PI*FX/FC)=0 ,        )
      PRINT 3
    3 FORMAT(55H      TO CALCULATE YOUNGS MODULUS FROM FS , AND TO        )
      PRINT 4
    4 FORMAT(55H      PLOT THE MODULUS AS A FUNCTION OF TEMPERATURE       )
      READ 21,ITEM
C     NUMBER OF CURVES,MAXIMUM=8,PRINT IN COLUMN 3 OF DATA CARD
      DO 60 MEN=1,ITEM
      PRINT 600
  600 FORMAT(1H1,/////)
      READ 10
  100 FORMAT(66H
     1           )
      PRINT 10
C     SAMPLE IDENTITY,START IN COL.19 OF DATA CARD
      READ 21,I
   21 FORMAT(I3)
C     NUMBER OF DATA POINTS IN EACH RUN,MAXIMUM=100,LAST DIGIT IN COLUMN
C     3
      READ 22,MS,MC,RHO,L
   22 FORMAT(4(F10.4))
C     EXPERIMENTAL CONSTANTS,MASS OF SPECIMEN IN COLUMN 1-10, COMBINED
C     MASS OF CRYSTALS IN COLUMN 11-20,SPECIMEN DENSITY IN COLUMN 21-30,
C     SPECIMEN LENGTH IN COLUMN 31-40,ALL IN CGS SYSTEM OF UNITS
```

```
      PRINT 24,MS,MC,RHO,L
  240 FORMAT(1HX,*MS=*,F10.4,2X,*MC=*,F10.4,2X,*RHO=*,F10.4,2X,
     1*L=*,F9.4)
      DO 52 M=1,1
C     EXPERIMENTAL DATA,FREQUENCY OF CRYSTALS IN COLUMN 1-10,FREQUENCY
C     OF COMPOSITE OSCILLATOR IN COLUMN 11-20,TEMPERATURE IN COLUMN 21-
C     30
      READ 23,FC,FX,T(M)
      BOX3(M)=FX $ BOX4(M)=FC
      K=1
C     FOR VARIABLE TAN SQUARE TERM REPLACE THIS CARD WITH
C     K=1 $ VK=1. $ MIX=1
   23 FORMAT(3(F10.4))
      FS=FX+(MC/MS)*(FX-FC)
      BOX1(M)=FS
      C = 1.
C     FOR VARIABLE TAN SQUARE TERM REPLACE THIS CARD WITH
C     C=1.-(ABS(MC*FC*TAN(PI*FX/FC)/(MS*FS)))**2.
      B=MC*FC*TAN(  PI*FX/FC)
   49 A=MS*FS*TAN(  PI*FX/FS)
      E(M)=((ABS(2.*L*FS))**2.)*RHO    $    ZERO=A*C+B

C     FOR VARIABLE TAN SQUARE TERM REPLACE THIS CARD WITH
C     ZERO1=ZERO
C     ZERO=ABS(A*C)-ABS(B)
C     IF(MIX.EQ.1) GO TO 99
C     IF (ABS(ZERO).GT.ABS(ZERO1))VK=-VK
C  99 MIX=0
C     E(M)=((ABS(2.*L*FS))**2.)*RHO
      BOX2(M)=FS
      IF (ABS(ZERO)-1.E-2)52,52,51
   51 IF(ABS(ZERO).GT.100000.)K=2.
      IF(K.GT.1)GO TO 299
```

```
      FS=FS+(ZERO/(MS*FS*(((ABS(COS(PI*FX/FS)*FS)))**-2.)*PI*FX-(A/FS)))
     1*1./C
C     FOR VARIABLE TAN SQUARE TERM REPLACE THIS CARD WITH
C    1*1./C*VK
      GO TO 49
  299 FS=FS+ZERO*.001
C     FOR VARIABLE TAN SQUARE TERM REPLACE THIS CARD WITH
C 299 FS=FS+ZERO*.01*VK
      GO TO 49
   52 CONTINUE
      PRINT 53
   530FORMAT(//18X,*T,DEGC          E,DYN/SQCM       FSO,CPS       FSF,CPS
     1       FX,CPS        FC,CPS*)
      PRINT 100
  100 FORMAT(1H0)
      DO 60  M=1,I
      PRINT 54,T(M),E(M),BOX1(M),BOX2(M),BOX3(M),BOX4(M)
   54 FORMAT(18X,F6.1,6X,E13.5,4(6X,F7.0))
      IF(MEN.GT.1) GO TO 500
      EASY(M)=E(M)
      TEMP(M)=T(M)
      II=I
      GO TO 60
500   IF(MEN.GT.2) GO TO 501
      ELAS(M)=E(M)
      TEM(M)=T(M)
      III=I
      GO TO 60
  501 IF(MEN.GT.3)GO TO 502
      E1(M)=E(M)
      T1(M)=T(M)
      IV=I
      GO TO 60
  502 IF(MEN.GT.4)GO TO 503
      E2(M)=E(M)
      T2(M)=T(M)
```

```
      V=I
      GO TO 60
  503 IF(MEN.GT.5)GO TO 504
      E3(M)=E(M)
      T3(M)=T(M)
      VI=I
      GO TO 60
  504 IF(MEN.GT.6)GO TO 505
      E4(M)=E(M)
      T4(M)=T(M)
      VII=I
      GO TO 60
  505 IF(MEN.GT.7)GO TO 60
      E5(M)=E(M)
      T5(M)=T(M)
      VIII=I
      GO TO 60
   60 CONTINUE
      CALL NAMPLT
      CALL QIKSET(7.0,0.0,50.0,9.0,8.0E11.2,E11)
     0CALL QIKPLT(TEMP,EASY, II,   19H*TEMPERATURE,DEG C*,
     127H$YOUNGS MODULUS,DYNES/SQCM$,35H*YOUNGS MODULUS VERSUS TEMPERATU
     2RE*)
      CALL PLOT(-8.0,1.0,-3)
      CALL QLINE(TEMP,EASY,-II,0)
      CALL QLINE(TEM,ELAS,-III,-2)
      CALL QLINE(T1,E1,-IV,-3)
      CALL QLINE(T2,E2,-V,-11)
      CALL QLINE(T3,E3,-VI,-1)
      CALL QLINE(T4,E4,-VII,-4)
      CALL QLINE(T5,E5,-VIII,-5)
      CALL QLINE(T,E,-I,-10)
      CALL PLOT(10.0,0.0,-3)
      CALL ENDPLT
      CALL EXIT
      END
```

PURE NIO,RUN 16,118.5 KC XTALS,FRST UP
MS= 5.1881 MC= 4.8352 RHO= 6.7830 L= 1.9000

T,DEGC	E,DYN/SQCM	FS0,CPS	FSF,CPS	FX,CPS	FC,CPS
26.0	9.09720E+11	96259	96374	107350	119251
83.5	9.05293E+11	96019	96139	107208	119214
119.0	9.24039E+11	97033	97129	107716	119179
158.0	9.37089E+11	97731	97813	108048	119118
188.0	9.67268E+11	99320	99375	108841	119057
210.0	1.00947E+12	101490	101520	109938	119003
212.0	1.01389E+12	101714	101742	110051	118997
222.0	1.04923E+12	103484	103500	110952	118965
234.0	1.13095E+12	107452	107455	112989	118930
245.0	1.39093E+12	119167	119167	119037	118897
247.0	1.69374E+12	131484	131501	125410	118893
248.0	1.87626E+12	138326	138405	128950	118890
248.5	2.40049E+12	155779	156551	137984	118890
249.0	2.42918E+12	156645	157484	138431	118888
249.5	2.43282E+12	156754	157602	138487	118887
250.0	2.43508E+12	156821	157675	138521	118885
252.0	2.43539E+12	156830	157685	138522	118878
256.0	2.42996E+12	156666	157509	138433	118869
288.0	2.31300E+12	153075	153671	136527	118771
312.0	2.20481E+12	149622	150034	134708	118705
315.0	2.18443E+12	148958	149339	134359	118695

PURE NIO,RUN 16,118.5 KC XTALS,FRST DWN
MS= 5.1881 MC= 4.8352 RHO= 6.7830 L= 1.9000

T,DEGC	E,DYN/SQCM	FSO,CPS	FSF,CPS	FX,CPS	FC,CPS
23.0	9.21863E+11	96914	97015	107690	119252
88.0	9.29675E+11	97334	97425	107886	119208
119.0	9.41240E+11	97950	98029	108191	119179
157.0	9.68123E+11	99364	99419	108895	119122
189.0	1.00993E+12	101513	101543	109975	119055
199.0	1.02888E+12	102468	102491	110459	119033
205.0	1.04398E+12	103223	103241	110842	119017
212.0	1.06377E+12	104202	104215	111339	118997
222.0	1.09916E+12	105928	105934	112217	118965
236.0	1.20017E+12	110695	110695	114665	118925
245.0	1.42300E+12	120533	120533	119744	118897
248.0	1.79362E+12	135279	135323	127373	118890
250.0	2.43006E+12	156671	157512	138443	118885
252.0	2.43326E+12	156766	157616	138489	118878
262.0	2.41538E+12	156226	157036	138197	118852
268.0	2.40028E+12	155768	156544	137949	118830
272.0	2.38232E+12	155220	155957	137661	118820

PURE NIO,RUN. 16,118.5 KC XTALS,SCND UP
MS= 5.1881 MC= 4.8352 RHO= 6.7830 L= 1.9000

T,DEGC	E,DYN/SQCM	FSO,CPS	FSF,CPS	FX,CPS	FC,CPS
37.0	9.22701E+11	96960	97059	107710	119245
90.0	9.23850E+11	97022	97119	107724	119207
112.0	9.26587E+11	97169	97263	107791	119188
183.0	9.80311E+11	99996	100043	109195	119065
207.0	1.01680E+12	101860	101888	110140	119024
237.0	1.18874E+12	110166	110166	114389	118920
240.0	1.25457E+12	113176	113176	115942	118910
241.0	1.29812E+12	115123	115123	116949	118908
243.0	1.31144E+12	115712	115712	117252	118904
244.0	1.36568E+12	118081	118081	118476	118900
245.0	1.42893E+12	120784	120785	119873	118895
246.0	1.52319E+12	124703	124705	121900	118892
247.5	1.79558E+12	135352	135397	127410	118888
249.5	2.16033E+12	148175	148513	134045	118884
250.0	2.43241E+12	156741	157588	138478	118882
250.0	2.44042E+12	156981	157847	138602	118882
252.0	2.44566E+12	157137	158017	138682	118880
261.0	2.43551E+12	156831	157689	138509	118850
294.0	2.36115E+12	154567	155263	137294	118760

PURE NIO,RUN 16,118.5 KC XTALS,SCND DWN
MS= 5.1881 MC= 4.8352 RHO= 6.7830 L= 1.9000

T,DEGC	E,DYN/SQCM	FS0,CPS	FSF,CPS	FX,CPS	FC,CPS
26.0	9.22531E+11	96950	97050	107710	119255
75.0	9.27281E+11	97206	97300	107823	119215
181.0	1.00318E+12	101169	101203	109804	119069
182.0	1.00418E+12	101220	101254	109830	119068
182.0	1.00707E+12	101367	101399	109906	119068
184.0	1.00751E+12	101389	101421	109916	119065
185.5	1.01034E+12	101533	101564	109989	119062
190.0	1.02314E+12	102180	102205	110318	119050
192.0	1.02326E+12	102186	102211	110321	119050
196.0	1.02850E+12	102449	102473	110455	119045
204.0	1.04422E+12	103235	103253	110852	119025
216.0	1.08531E+12	105256	105265	111879	118985
222.0	1.10693E+12	106303	106308	112411	118965
226.0	1.12462E+12	107151	107154	112845	118955
248.5	1.70123E+12	131772	131791	125558	118890
250.5	2.45383E+12	157381	158281	138809	118882
254.0	2.45072E+12	157288	158180	138759	118878
282.0	2.39699E+12	155665	156437	137879	118795
284.0	2.38890E+12	155418	156172	137749	118790

•12 PCT LI,RUN 22,118.5 KC XTALS,FRST UP
MS= 4.3655 MC= 4.8352 RHO= 6.2513 L= 1.8910

T,DEGC	E,DYN/SQCM	FSO,CPS	FSF,CPS	FX,CPS	FC,CPS
25.0	9.14305E+11	101007	101120	110593	119248
82.0	9.28055E+11	101782	101878	110943	119214
135.0	9.45787E+11	102770	102847	111382	119157
156.0	9.55000E+11	103279	103346	111606	119124
170.0	9.66839E+11	103928	103985	111898	119094
192.0	9.93616E+11	105376	105415	112561	119048
203.5	1.01533E+12	106532	106560	113096	119022
213.0	1.04417E+12	108046	108063	113800	118995
220.0	1.07065E+12	109414	109425	114436	118970
227.5	1.12341E+12	112086	112089	115693	118950
234.0	1.19311E+12	115514	115514	117309	118930
239.0	1.27850E+12	119576	119576	119226	118910
241.5	1.33707E+12	122284	122284	120510	118908
243.5	1.41471E+12	125786	125785	122167	118900
247.0	1.59959E+12	133749	133751	125940	118890
248.0	1.68297E+12	137180	137193	127567	118888
248.5	1.76346E+12	140402	140435	129095	118886
249.0	1.80367E+12	141980	142027	129843	118885
250.5	1.81532E+12	142433	142485	130057	118883
257.0	1.81568E+12	142447	142499	130053	118863
272.0	1.80564E+12	142056	142105	129845	118820

.12 PCT LI,RUN 22,118.5 KC XTALS,FRST DWN
MS= 4.3655 MC= 4.8352 RHO= 6.2513 L= 1.8910

T,DEGC	E,DYN/SQCM	FSO,CPS	FSF,CPS	FX,CPS	FC,CPS
64.0	8.98336E+11	100097	100233	110151	119228
96.5	8.99176E+11	100146	100280	110161	119203
126.0	9.02896E+11	100360	100488	110245	119170
146.0	9.08090E+11	100656	100776	110370	119140
163.0	9.20731E+11	101373	101475	110693	119108
206.0	9.87875E+11	105068	105110	112397	119014
245.0	1.48045E+12	128675	128674	123537	118898
246.5	1.54601E+12	131492	131492	124872	118895
247.0	1.59119E+12	133397	133400	125775	118893
247.5	1.64076E+12	135455	135461	126750	118891
248.0	1.68128E+12	137111	137124	127535	118889
248.0	1.73518E+12	139280	139305	128564	118889
249.0	1.78977E+12	141437	141479	129586	118886
249.5	1.81103E+12	142267	142317	129979	118885
251.0	1.81548E+12	142440	142492	130060	118883
254.0	1.81656E+12	142481	142534	130073	118870
259.0	1.81439E+12	142397	142449	130025	118855

1.96 PCT LI,RUN 25.118.5 KC XTALS,FRST UP
MS= 4.7995 MC= 4.8352 RHO= 6.7200 L= 1.8840

T,DEGC	E,DYN/SQCM	FSO,CPS	FSF,CPS	FX,CPS	FC,CPS
25.5	9.10007E+11	97516	97662	108424	119251
86.0	9.44294E+11	99386	99485	109336	119213
154.0	9.97918E+11	102219	102271	110704	119126
188.0	1.08288E+12	106521	106536	112812	119057
197.0	1.12485E+12	108573	108580	113822	119032
206.0	1.18575E+12	111479	111481	115261	119015
217.0	1.30793E+12	117084	117084	118038	118985
220.5	1.38601E+12	120528	120528	119746	118970
222.0	1.43900E+12	122810	122810	120882	118968
225.0	1.52544E+12	126444	126445	122688	118960
226.0	1.57990E+12	128679	128683	123800	118957
227.0	1.63375E+12	130849	130857	124878	118951
228.0	1.72966E+12	134620	134643	126754	118946
230.0	1.88580E+12	140510	140589	129685	118940
231.5	2.03728E+12	145940	146127	132388	118936
233.0	2.07515E+12	147255	147479	133040	118930
237.5	2.07481E+12	147243	147467	133029	118920
243.0	2.02670E+12	145569	145747	132185	118900

1.96 PCT LI,RUN 25,118.5 KC XTALS,FRST DWN
MS= 4.7995 MC= 4.8352 RHO= 6.7200 L= 1.8840

T,DEGC	E,DYN/SQCM	FSO,CPS	FSF,CPS	FX,CPS	FC,CPS
28.0	9.54093E+11	99910	100000	109614	119246
96.0	1.00586E+12	102630	102677	110948	119205
152.0	1.05473E+12	105118	105142	112150	119130
178.0	1.11661E+12	108174	108182	113646	119078
220.0	1.34533E+12	118746	118746	118859	118971
221.0	1.36300E+12	119523	119523	119245	118969
222.0	1.38963E+12	120685	120685	119822	118965
223.5	1.42235E+12	122098	122098	120524	118962
225.0	1.47293E+12	124250	124250	121595	118960
227.0	1.60319E+12	129623	129628	124267	118951
229.0	1.71287E+12	133969	133988	126428	118943
230.0	2.00227E+12	144709	144866	131777	118940

1.96 PCT LI,RUN 25,118.5 KC. XTALS.SCND UP
MS= 4.7995 MC= 4.8352 RHO= 6.7200 L= 1.8840

T,DEGC	E,DYN/SQCM	FSO,CPS	FSF,CPS	FX,CPS	FC,CPS
110.0	9.90750E+11	101846	101903	110549	119188
131.0	1.05836E+12	105300	105322	112257	119163
145.0	1.03972E+12	104361	104391	111778	119140
150.0	1.05034E+12	104897	104923	112041	119132
153.5	1.07415E+12	106088	106105	112631	119126
178.0	1.08839E+12	106792	106806	112960	119082
190.0	1.13650E+12	109135	109141	114111	119050
204.0	1.20159E+12	112222	112223	115631	119015
213.0	1.26996E+12	115372	115372	117185	118985
220.0	1.37231E+12	119931	119931	119449	118971
222.0	1.40884E+12	121516	121516	120236	118965
227.0	1.61107E+12	129940	129945	124425	118951
229.0	1.70942E+12	133834	133853	126361	118943
229.5	1.77747E+12	136456	136491	127666	118941
231.0	1.89682E+12	140914	141000	129885	118937
232.0	2.02831E+12	145626	145805	132230	118933

1.96 PCT LI,RUN 25,118.5 KC XTALS,SCND DWN
MS= 4.7995 MC= 4.8352 RHO= 6.7200 L= 1.8840

T,DEGC	E,DYN/SQCM	FSO,CPS	FSF,CPS	FX,CPS	FC,CPS
25.0	9.59119E+11	100178	100263	109750	119251
104.0	1.00279E+12	102471	102520	110864	119195
203.0	1.18417E+12	111405	111407	115228	119023
215.0	1.26749E+12	115259	115259	117130	118987
229.0	1.75992E+12	135785	135816	127333	118943
230.0	1.88383E+12	140438	140516	129649	118940
231.0	2.01197E+12	145052	145216	131946	118937
232.0	2.02805E+12	145617	145795	132224	118930
232.5	2.06145E+12	146781	146991	132804	118930
236.0	2.04814E+12	146319	146516	132571	118925
239.0	2.04469E+12	146198	146392	132504	118911

4.97 PCT LI,RUN 26,118.5 KC XTALS,FRST UP
MS= 4.9309 MC= 4.8352 RHO= 6.5850 L= 1.8980

T,DEGC	E,DYN/SQCM	FSO,CPS	FSF,CPS	FX,CPS	FC,CPS
39.0	9.79456E+11	101547	101599	110308	119242
64.0	9.96243E+11	102425	102466	110744	119228
95.0	1.02413E+12	103862	103890	111457	119202
108.0	1.04212E+12	104777	104798	111913	119190
114.0	1.05155E+12	105254	105272	112151	119185
124.0	1.06361E+12	105858	105873	112449	119170
139.0	1.09193E+12	107264	107274	113149	119150
151.0	1.12347E+12	108807	108812	113919	119132
161.0	1.16570E+12	110836	110838	114934	119113
183.5	1.35173E+12	119355	119355	119209	119060
189.0	1.44847E+12	123552	123552	121324	119052
192.0	1.52725E+12	126865	126868	122995	119048
193.5	1.59702E+12	129726	129733	124438	119045
196.0	1.67073E+12	132676	132693	125925	119040
197.0	1.74956E+12	135752	135788	127477	119038
198.0	1.81394E+12	138204	138263	128712	119032
199.0	1.86973E+12	140287	140373	129763	119031
200.0	1.92604E+12	142349	142472	130804	119030
201.0	2.00417E+12	145147	145333	132215	119027
201.5	2.09372E+12	148262	148544	133787	119025
202.0	2.16946E+12	150823	151207	135079	119023
202.5	2.22830E+12	152766	153244	136059	119021
203.0	2.27287E+12	154211	154769	136788	119020
203.5	2.28837E+12	154708	155295	137038	119018
204.0	2.29951E+12	155064	155673	137216	119015
207.0	2.30505E+12	155240	155861	137304	119013
213.0	2.30395E+12	155203	155823	137274	118990
218.0	2.30160E+12	155128	155744	137230	118978
223.0	2.29523E+12	154924	155528	137119	118962

4.97 PCT LI,RUN 26,118.5 KC XTALS,FRST DWN
MS= 4.9309 MC= 4.8352 RHO= 6.5850 L= 1.8980

T,DEGC	E,DYN/SQCM	FSO,CPS	FSF,CPS	FX,CPS	FC,CPS
34.0	9.36869E+11	99279	99365	109164	119245
82.0	9.71583E+11	101133	101190	110084	119212
124.0	1.02862E+12	104092	104117	111557	119170
175.0	1.24544E+12	114566	114566	116801	119080
190.5	1.49372E+12	125466	125467	122290	119051
193.0	1.55825E+12	128145	128149	123640	119046
195.0	1.66592E+12	132486	132502	125830	119042
197.0	1.74273E+12	135489	135522	127344	119038
198.0	1.78595E+12	137145	137193	128177	119032
198.0	1.82405E+12	138584	138648	128904	119032
199.0	1.89339E+12	141158	141259	130203	119031
200.0	1.96395E+12	143716	143867	131494	119030
201.5	2.04340E+12	146524	146748	132909	119025
202.0	2.12049E+12	149176	149491	134247	119023
207.0	2.32543E+12	155886	156548	137630	119013
214.0	2.31701E+12	155618	156264	137486	118995
216.0	2.31274E+12	155482	156120	137415	118990

6.84 PCT LI,RUN 30,118.5 KC XTALS,FRST UP
MS= 4.9643 MC= 4.8352 RHO= 6.5718 L= 1.9060

T,DEGC	E,DYN/SQCM	FSO,CPS	FSF,CPS	FX,CPS	FC,CPS
28.0	9.63270E+11	100369	100434	109684	119248
85.0	1.02292E+12	103467	103497	111236	119212
102.5	1.05010E+12	104843	104862	111926	119198
121.5	1.09546E+12	107094	107103	113056	119177
131.0	1.12607E+12	108584	108589	113805	119165
153.0	1.23177E+12	113571	113571	116313	119128
156.5	1.26486E+12	115087	115087	117077	119120
162.0	1.31534E+12	117361	117361	118224	119110
165.5	1.35456E+12	119098	119098	119099	119100
170.0	1.40717E+12	121389	121389	120256	119093
173.0	1.45534E+12	123449	123449	121296	119086
176.0	1.49993E+12	125325	125326	122245	119083
179.0	1.54406E+12	127154	127156	123166	119072
181.0	1.59226E+12	129120	129125	124161	119070
184.0	1.64127E+12	131087	131098	125155	119065
186.0	1.72054E+12	134201	134226	126730	119060
189.0	1.78433E+12	136647	136692	127965	119051
191.0	1.85763E+12	139395	139471	129356	119049
193.0	1.92748E+12	141951	142069	130649	119045
195.0	1.95261E+12	142856	142992	131105	119040
206.0	1.91591E+12	141531	141642	130424	119020

6.84 PCT LI,RUN 30,118.5 KC XTALS,FRST DWN
MS= 4.9643 MC= 4.8352 RHO= 6.5718 L= 1.9060

T,DEGC	E,DYN/SQCM	FSO,CPS	FSF,CPS	FX,CPS	FC,CPS
63.0	9.77234E+11	101105	101159	110046	119226
98.0	1.03114E+12	103886	103912	111442	119200
121.5	1.09172E+12	106911	106920	112963	119177
134.0	1.13694E+12	109108	109112	114063	119150
169.0	1.40658E+12	121363	121363	120243	119093
182.5	1.66762E+12	132131	132146	125685	119067
184.0	1.71940E+12	134156	134182	126710	119065
185.0	1.73873E+12	134903	134934	127087	119062
186.0	1.78311E+12	136601	136645	127946	119060
187.5	1.82129E+12	138041	138100	128674	119057
188.5	1.84373E+12	138879	138948	129096	119052
189.0	1.88677E+12	140469	140561	129901	119051
190.5	1.91650E+12	141554	141664	130450	119050
191.0	1.97987E+12	143830	143987	131602	119048
192.5	1.99563E+12	144388	144559	131884	119046
197.0	1.99837E+12	144485	144658	131930	119040
203.0	1.96028E+12	143130	143273	131235	119022

8.23 PCT LI,RUN 19,118.5 KC XTALS,FRST UP
MS= 4.6808 MC= 4.8352 RHO= 6.2690 L= 1.8980

T,DEGC	E,DYN/SQCM	FSO,CPS	FSF,CPS	FX,CPS	FC,CPS
26.5	1.32299E+12	121019	121019	120120	119250
85.0	1.44749E+12	126585	126585	122838	119211
100.0	1.48611E+12	128261	128263	123656	119198
114.0	1.53309E+12	130270	130274	124636	119182
125.0	1.57378E+12	131984	131992	125473	119170
130.0	1.59740E+12	132968	132979	125953	119162
137.0	1.63221E+12	134403	134420	126654	119152
143.0	1.66752E+12	135842	135866	127357	119143
151.0	1.72263E+12	138053	138093	128438	119130
155.5	1.76252E+12	139628	139682	129209	119123
158.0	1.78264E+12	140414	140477	129593	119118
160.0	1.80466E+12	141267	141342	130010	119112
162.5	1.82160E+12	141920	142004	130329	119108
165.0	1.85610E+12	143239	143343	130974	119102
167.0	1.87238E+12	143854	143970	131276	119100
169.0	1.89181E+12	144585	144715	131632	119093
170.5	1.90996E+12	145263	145407	131964	119090
173.0	1.94386E+12	146518	146692	132579	119085
176.0	1.97566E+12	147682	147887	133149	119080
182.0	1.99438E+12	148361	148586	133478	119070
189.0	2.00146E+12	148616	148850	133589	119042
198.0	2.00785E+12	148846	149087	133697	119032
230.0	1.99299E+12	148306	148535	133385	118940

8.23 PCT LI,RUN 19,118.5 KC XTALS,FRST DWN
MS= 4.6808 MC= 4.8352 RHO= 6.2690 L= 1.8980

T,DEGC	E,DYN/SQCM	FSO,CPS	FSF,CPS	FX,CPS	FC,CPS
43.0	1.34338E+12	121948	121948	120572	119240
76.0	1.40134E+12	124550	124551	121842	119220
94.0	1.44622E+12	126529	126529	122806	119202
107.0	1.48635E+12	128271	128273	123658	119192
123.0	1.55025E+12	130996	131001	124988	119172
136.0	1.61483E+12	133689	133702	126304	119155
158.0	1.77208E+12	140002	140061	129390	119117
161.0	1.80318E+12	141211	141285	129981	119110
164.0	1.83284E+12	142351	142442	130538	119102
168.0	1.87196E+12	143838	143954	131264	119092
171.0	1.90865E+12	145214	145358	131938	119086
173.5	1.94171E+12	146439	146611	132540	119085
177.0	2.00536E+12	148757	148994	133679	119082
178.0	2.01021E+12	148932	149175	133764	119080
180.5	2.01566E+12	149128	149377	133855	119070
185.5	2.01805E+12	149213	149465	133892	119060
194.0	2.01853E+12	149230	149483	133891	119042
200.0	2.01781E+12	149204	149457	133872	119030
203.5	2.01567E+12	149126	149377	133829	119020
208.0	2.01416E+12	149072	149321	133797	119010
212.0	2.01163E+12	148980	149228	133746	118998
218.0	2.00539E+12	148755	148996	133626	118980
225.0	2.00000E+12	148560	148795	133520	118960

LI-MG-NI ALLOY,RUN 34,118.5 KC XTALS,FRST UP
MS= 3.9474 MC= 4.8352 RHO= 5.6400 L= 1.9120

T,DEGC	E,DYN/SQCM	FSO,CPS	FSF,CPS	FX,CPS	FC,CPS
28.0	8.14699E+11	99159	99390	110219	119248
60.0	8.80257E+11	103208	103311	112029	119230
105.5	9.27204E+11	105978	106030	113254	119194
127.5	1.00010E+12	110105	110119	115094	119167
140.0	1.05613E+12	113158	113162	116457	119150
154.0	1.20520E+12	120885	120885	119916	119125
157.0	1.23963E+12	122600	122599	120684	119120
161.0	1.29343E+12	125233	125231	121865	119115
165.0	1.33107E+12	127045	127041	122672	119102
169.5	1.37772E+12	129255	129248	123662	119096
173.0	1.40532E+12	130545	130536	124236	119085
182.0	1.44836E+12	132533	132520	125121	119070
197.0	1.47275E+12	133646	133631	125602	119035
205.5	1.47652E+12	133817	133802	125668	119015
213.5	1.47735E+12	133855	133840	125674	118995
222.0	1.47727E+12	133851	133836	125658	118969

LI-MG-NI ALLOY,RUN 34,118.5 KC XTALS,FRST DWN
MS= 3.9474 MC= 4.8352 RHO= 5.6400 L= 1.9120

T,DEGC	E,DYN/SQCM	FSO,CPS	FSF,CPS	FX,CPS	FC,CPS
40.0	7.98814E+11	98141	98416	109759	119244
57.0	8.13006E+11	99052	99286	110162	119232
72.0	8.29914E+11	100121	100313	110637	119222
95.0	8.69763E+11	102576	102693	111730	119203
120.0	9.42298E+11	106849	106890	113636	119177
127.0	9.77400E+11	108840	108863	114525	119166
153.0	1.16656E+12	118931	118931	119039	119127
157.0	1.22827E+12	122037	122037	120431	119120
164.0	1.30375E+12	125733	125730	122084	119105
176.0	1.42108E+12	131277	131266	124563	119082
182.0	1.44462E+12	132362	132349	125044	119070
184.5	1.45397E+12	132790	132776	125231	119060
192.0	1.46628E+12	133352	133337	125477	119048
200.0	1.47347E+12	133679	133664	125614	119030
212.0	1.47723E+12	133850	133834	125677	119005

PURE NIO,RUN 16,92.5 KC XTALS,FRST UP
MS= 5.1881 MC= 6.3474 RHO= 6.7830 L= 1.9000

T,DEGC	E,DYN/SQCM	FSO,CPS	FSF,CPS	FX,CPS	FC,CPS
26.5	8.61266E+11	93772	93772	93114	92576
189.0	9.27548E+11	97315	97314	94647	92466
192.0	9.31753E+11	97536	97534	94744	92462
226.0	1.03967E+12	103038	103027	97186	92403
234.0	1.10927E+12	106435	106420	98703	92383
241.0	1.21615E+12	111438	111429	100944	92367
244.0	1.28194E+12	114392	114403	102268	92358
246.0	1.51963E+12	124277	124518	106712	92355
248.0	2.11713E+12	144488	147021	115799	92350
250.0	2.14178E+12	145185	147874	116110	92345
261.0	2.11375E+12	144382	146904	115731	92313
266.0	2.11362E+12	144376	146899	115724	92305
270.0	2.13924E+12	145099	147787	116041	92290
272.0	2.15651E+12	145581	148382	116252	92280
292.0	2.03314E+12	142003	144075	114607	92215
296.0	2.02624E+12	141792	143830	114503	92198

PURE NIO;RUN 16;92.5 KC XTALS;SCND UP
MS= 5.1881 MC= 6.3474 RHO= 6.7830 L= 1.9000

T;DEGC	E;DYN/SQCM	FSO;CPS	FSF;CPS	FX;CPS	FC;CPS
26.5	8.83704E+11	94986	94986	93655	92567
42.0	8.82530E+11	94923	94923	93631	92575
59.0	8.82102E+11	94900	94900	93619	92572
72.0	8.82400E+11	94916	94916	93624	92568
86.0	8.83611E+11	94981	94981	93650	92562
105.0	8.86861E+11	95156	95155	93723	92552
140.0	9.08089E+11	96288	96287	94217	92524
158.0	9.14485E+11	96627	96626	94360	92507
194.0	9.54645E+11	98728	98725	95278	92458
219.0	1.02009E+12	102062	102053	96747	92403
232.0	1.10345E+12	106156	106141	98575	92379
243.0	1.32038E+12	116076	116106	103027	92361
247.0	1.91596E+12	138410	139862	113067	92353
249.0	2.15669E+12	145604	148388	116300	92348
250.0	2.15780E+12	145635	148426	116312	92345
252.0	2.15624E+12	145589	148373	116289	92340
256.0	2.15163E+12	145458	148214	116225	92331
280.0	2.09673E+12	143878	146311	115472	92254
292.0	2.08564E+12	143548	145923	115302	92215
308.0	2.06658E+12	142978	145255	115014	92157

PURE NIO,RUN 16,92.5 KC XTALS,SCND DWN
MS= 5.1881 MC= 6.3474 RHO= 6.7830 L= 1.9000

T,DEGC	E,DYN/SQCM	FSO,CPS	FSF,CPS	FX,CPS	FC,CPS
26.5	8.91831E+11	95422	95422	93856	92576
46.0	8.93078E+11	95489	95488	93886	92576
51.0	8.94174E+11	95547	95547	93914	92579
66.0	8.95586E+11	95623	95622	93943	92570
90.0	9.03139E+11	96025	96025	94118	92559
108.0	9.09315E+11	96353	96352	94260	92549
136.0	9.25174E+11	97191	97189	94625	92528
156.0	9.45390E+11	98249	98245	95090	92509
172.0	9.63558E+11	99188	99185	95501	92487
187.0	9.86618E+11	100370	100364	96022	92468
210.0	1.04075E+12	103091	103081	97225	92430
234.0	1.17748E+12	109657	109643	100152	92383
240.0	1.25331E+12	113118	113119	101701	92369
242.0	1.31653E+12	115909	115937	102953	92363
245.0	1.50317E+12	123666	123882	106440	92360
249.0	2.17478E+12	146107	149009	116526	92348
250.0	2.17663E+12	146157	149073	116547	92345
252.0	2.17553E+12	146125	149035	116530	92340
254.0	2.16761E+12	145905	148763	116428	92335
258.0	2.16241E+12	145759	148585	116359	92329
276.0	2.13365E+12	144937	147593	115958	92272
268.0	2.14649E+12	145304	148037	116136	92295
284.0	2.11860E+12	144504	147072	115750	92248
291.0	2.06799E+12	143034	145305	115072	92217
302.0	2.06758E+12	143011	145290	115037	92172

REFERENCES

1. "Conductivity in Semiconductors" K. Lark-Horovitz, Electrical Engineering 68, 1047-56 (1949)

2. "Oxides Which Show a Metal-to-Insulator Transition at the Néel Temperature" F.J. Morin, Phys. Rev. Let. 3, 34-36 (1959)

3. "On the Electrical Resistivity of Metal Oxides with Vacant Lattice Sites in Their Crystal Lattice" E.J.W. Verwey, P.W. Haayman, F.C. Romeyn, Chemisch Weekblad 44, 705-708 (1948)

4. "Controlled-Valency Semiconductors" E.J.W. Verwey, P.W. Haayman, F.C. Romeyn, G.W. van Oosterhout, Philips Res. Repts. 5, 173-187 (1950)

5. "Effect of Added Oxides on p-Conducting Nickel Oxide" G.M. Schwab, H. Schmid. J.A.P., Suppl. 33 (1) 426-8 (1962)

6. "Mechanism of Conduction in Lithium Substituted Transition Metal Oxides" R.R. Heikes, W.D. Johnston, J.Chem. Phys. 26, 582-587 (1957)

7. "Transport Properties of Transition Metal Compounds" R. Heikes, p. 1-15 in Transition Metal Compounds - Transport and Magnetic Properties - Informal Proc. BUHL Int'l. Conf. on Materials, Pittsburgh, Pa. (1963) E.R. Schatz, ed.,Gordon & Breach (1964).

8. "On Electronic Current in NiO" J. Yamashita, T. Kurosawa, J. Phys. Chem. Solids 5, 34-43 (1958)

9. "Model of Thermally Activated Hopping Motion in Solids" G.L. Sewell, Phys. Rev. 129, 597-608 (1963)

10. "Studies of Polaron Motion. Part II. The "Small" Polaron" T. Holstien, Annals of Physics 8, 343-389 (1959)

11. "Self-Trapping of an Electron by the Acoustical Mode of Lattice Vibration. I." Y. Toyozawa, Prog. Theo. Phys. 26, 29-44 (1961)

12. "Self-Trapping of an Electron by the Acoustic Mode of

Lattice Vibration" Y. Toyozawa, p. 211-232 in Polarons and Exitons C.G. Kuper, G.D. Whitfield, ed., Plenum Press (1962)

13. "Polaronic Impurity Hopping Conduction" J. Schnackenberg, Phys. Stat. Solidi 28, 623-633 (1968)

14. "Insulating and Metallic States in Transition Metal Oxides" D. Adler, Solid State Physics, 21, 1-116 (1968)

15. "Polarons" J. Appel, Solid State Physics, 21, 193-393 (1968)

16. "Non-Stoichiometric Compounds" S.J. Anderson, Ann. Repts. Prog. Chem., Chem. Soc. London, 104-120 (1946)

17. "Semiconducting Properties of Some Oxides and Sulfides" A.R. Hutson, p. 541-99 in Semiconductors, N.B. Hannay ed., Reinhold (1959)

18. "Recrystallization Temperature, Electrical Resistance at Low Temperature, and Mechanical and Magnetic Properties of Nickel-Influence of Purity" B. Dubois, O. Dimitrov, Mem. Sci. Rev. Met. 61, 605-621 (1964)

19. "Separation of Copper and Gold During Zone Refining of Nickel in a Chilled Copper Boat" L. Kuchow, O. Dimitrov, Compt. Rend. Ser C, 262, 718-721 (1964)

20. "Pressure Sintering of Ceramics" T. Vasilos, R.M. Spriggs, Prog. Cer. Sci. 4, 95-132 (1966) Pergamon Press

21. "Mechanisms of Densification, Deformation and Strengthening in Alloyed, Thermomechanically Worked MgO" L. Atteraas, Ph.D. Thesis, Lehigh Univ., May 15, 1967

22. "Die Design for Pressure Sintering" H.I. Moss, W.P. Stoller, American Ceramic Society Bulletin, 45, 792-793 (1966)

23. "The Mechanisms of Pressure Sintering Densification of Yttrium Oxide" W.J. McDonough, M.S. Thesis, Lehigh University, 1968

24. Flame Photometry, J.A. Dean, p. 155-160, McGraw-Hill (1960)

25. "NiO-Li_2O Solid Solutions T. Takeuchi, Nagoya Kogyo Gijitsu Shikenjo Hokoku (Rep. Govt. Ind. Res. Inst. Nagoya) 6, 719-722 (1957)

26. "Piezoelectric Crystals and Their Application to Ultrasonics" W.P. Mason, D. Van Nostrand Book Co. (1950)

27. "Charge Carrier Mobility in SiC" H. Van Daal, Philips. Res. Repts., Suppl. No 3, 8-21 (1965)

28. "Apparatus for Measuring the Hall Effect of Low-Mobility Samples at High Temperatures" N.Z. Lupu, N.M. Tallen, D.S. Tannhauser, Rev. Sci. Inst. 38, 1658-1661 (1967)

29. "State Diagram of the System Ni-O_2 and Physicochemical Nature of the Solid Phases in That System" D.P. Bogatskii, Zhur. Obschei. Khim. 21, 3-10 (1951)

30. "Preparation of Pure Nickel Monoxide" M. LeBlanc, H. Sachse, Z. Elektrochem. 32, 58-62 (1926)

31. "Black Nickel Oxide - The Behavior of Nickel Oxide Towards Oxygen Between -182°C and +350°C" M. LeBlanc, H. Sachse, Z. Elektrochem. 32, 204-210 (1926)

32. "The Existence and Preparation of Certain Oxides of the Platinum Metals" G. Lunde, Z. Anorg. Allgem. Chem. 163, 345-354 (1927)

33. "Black Nickel Oxide" M. LeBlanc, H. Sachse, Z. Anorg. Allgem. Chem. 168, 15-16 (1927)

34. "Black Nickel Oxide" G. Lunde, Z.Anorg. Allgem. Chem. 169, 405-406 (1928)

35. "Experimental Studies on the Direct Oxidation at Elevated Pressures of the Oxides of Sr, Ba, Pb, Mn and Co" C.B. Holtermann, Ann. Chim. (Paris), 11th Series, 14, 121-206 (1940)

36. "On Nickel Oxides of High Oxygen Content" Y. Shimomura, I. Tsubokawa, M. Kojima, J. Phys. Soc. Jap. 9, 521-524 (1954)

37. "A Physicochemical Study of Metal Oxides and Hydroxides" E. Ya. Rode, J. Inorg. Chem. USSR 1, 326-336 (1956)

38. "A New Type of End-Point in Electrometric Titration and its Application to Iodimetry" C.W. Foulk, A.T. Bowden, J. Am. Chem. Soc. 48, 2045 (1926)

39. "The Nickel Oxide Electrode. Part 3" G.W.D. Briggs, W.F.K. Wynne-Jones, Trans.Faraday Soc. 52, 1272-1281 (1956)

40. "Fine Structures of X-ray K Absorption Spectra of Nickel in Oxides of Nickel" K. Tsutsumi, J. Phys. Soc. Jap. 13, 586-590 (1958)

41. "A New Superstructure of Nickel Oxide " G.I. Finch, K.P. Sinha, Trans. Faraday Soc. 53, 623-627 (1957)

42. "Physicochemical Study of the Structure and the Properties of the Oxygen Compounds of Nickel" D.P. Bogatskii, I.A. Mineeva, J. Gen. Chem. USSR. 29, 1358-1365 (1959)

43. "The Preparation and Electrochemical Properties of Higher Nickel Oxides" J. Labat, J. Chim. Phys. 60, 1253-1263 (1963)

44. "The Forming Process in Nickel Positive Electrodes" D. Tuomi, J. Electrochem. Soc. 112, 1-12 (1965)

45. "Marked Increase in Conductivity of Nickel Oxide in the Absorption of Oxygen" M. LeBlanc, H. Sachse, Ber. Verhandlsachs Akad. Leipzig Math.-Phys. Klasse 82, 133-140 (1930)

46. "The Electron Conductivity of Solid Oxides with Different Valences" M. LeBlanc, H. Sachse, Phys. Z. 32, 887-890 (1931)

47. "Magnetochemical Investigations IX. Contribution to the Knowledge of Nickel Oxide" W. Klemm, K. Hass, Z. Anorg. Allgem. Chem. 219, 82-86 (1934)

48. "Electrical Conduction of Nickel Oxide" H.H. Baumbach, C. Wagner, Z. Phys. Chem. B24, 59-67 (1934)

49. "Nickel Catalysts I. The Effect of the Temperature of Preparation on the Crystal Size and Composition of Nickel Oxide" M.C. Boswell, R.K. Iler, J. Am. Chem. Soc. 58, 924-928 (1936)

50. "Antiferromagnetic Behavior of the System Nickel Oxide-Oxygen" N. Perakis, J. Phys. Radium. 23, 96-104 (1962)

51. "Decomposition of Nickel Oxide by Irradiation With Neutrons" A. Blaise, P. Lefevre, Compt. Rend. Acad. Sci. (Paris) 258, 2320-2323 (1964)

52. "Structure of Energy States of Nickel (II) Oxide with Various Contents of Lithium and Stoichiometric Excess Oxygen" A.E. Cherkashin, F.I. Vilesov, Akad. Nauk. SSSR,

Sibirskoe Otdelenii Inst. Katalysis, Metody Issledovaniya Katalizatorov Katalicheskikh Reaktsii 1, 192-211 (1965)

53. "Determination of Non-Stoichiometry in Nickel Oxide" P.C. Gravelle, G. El Shobaky, H. Urbain, Compt. Rend. Acad. Sci. (Paris), Ser. C., 262, 549-552 (1966)

54. "Covalency Parameters in MnO, α-MnS, and NiO" B.E.F. Fender, A.J. Jacobson, F.A. Wedgwood, J. Chem. Phys. 48, 990-994 (1968)

55. "The Problem of Excess Oxygen in Nickel Oxide. I. Experimental Results" H. Gossel, Z. Elektrochem. 65, 98-102 (1961)

56. "Superstoichiometric Oxygen in Nickel Oxide.II. Further Experimental Data and Evaluation of the Results" H. Gossel, Deutsche Bunsengesellschaft f. Phys. Chem. Berichte. 69, 736-741 (1965)

57. "Surface and Bulk Electronic Properties of Lithium-Doped Nickel Oxide" J. Deren, J. Nowotny, J. Ziolkowski, Bull. Acad. Pol. Sci., Ser. Sci. Chim. 16, 45-50 (1968)

58. "Study of the Incorporation, Under Vacuum at Low Temperatures of Impurity Ions (Li^{+1} or Ga^{+3}) in Powdered Nickel Oxide.
Part I. Influence of Preparation Temperature of the Oxide on the Incorporation of Impurities (p. 3244-3251)
Part II. Incorporation Mechanism (p. 3251-3656)
Part III. Influence of Oxygen (p. 3670-3677)"
G. El Shobaky, P.C. Gravelle, S.J. Teichner, Bull. Soc. Chim. Fr. 1967

59. "Chemisorption on Metal Oxides - Part 1. - Nickel Oxide" H.B. Charman, R.M. Dell, S.S. Teale, Trans. Faraday Soc. 59, 453-469 (1963)

60. "Electronic Phenomina in Semiconductor Catalysis - Investigation of the Effect of Admixtures Dissolved in Nickel Oxide Sublattice upon Catalytic Activity" N.P. Keier, S.Z. Roginskii, I.S. Sazanova, Doklady Akad. Nauk SSSR 106, 859-861 (1956)

61. "Reflectance Spectroscopy as a Tool for Investigating Dispersed Solids and Their Surfaces" K. Klier, Catalysis Reviews 1, 207-232 (1967)

62. "Theory of Arranged Mixed Phases" W. Schottky, C. Wagner, Z. Phys. Chem. B11, 163-210 (1930)

63. "Dissarrangements in Crystallized Polar Compounds as the Basis of Electronic and Ionic Conduction" C. Wagner, Z. Elektrochem. 39, 543-544 (1933)

64. Electronic Processes in Ionic Crystals, N.F. Mott, R.W. Gurney, Oxford University Press (1940)

65. "Oxygen Pressure Dependence of the Electrical Conductivity of Some Mixed Oxides" K. Hauffe, J. Block, Z. Phys. Chem. 196, 438-446 (1951)

66. "Relations Between the Concentrations of Imperfections in Crystalline Solids" F.A. Kroger, H.J. Vink, Progress in Solid State Physics 3, 307-435 (1956)

67. "Electrical Conductivity and Thermodynamic Equilibrium in Nickel Oxide" S.P. Mitoff, J. Chem. Phys. 35, 882-889 (1961)

68. "Electrical Conductivity and Thermogravimetric Studies on CoO, NiO, and MnO" N.G. Eror, Ph.D. Thesis, Northwestern University, Evanston, Illinois (1965)

69. "Chemical Diffusion in Single Crystals of CoO and NiO" J.B. Price, Master's Thesis, Northwestern University, Evanston, Illinois (1965)

70. "Determination of the Chemical Diffusion Coefficients in Single Crystals of CoO and NiO" J.B. Price, J.B. Wagner, Z. Phys. Chem (N.F.) 49, 257-270 (1966)

71. "Coulometric Titration with Solid Metal Oxide Electrolytes" H.G. Sockel, H. Schmalzried, Deutsche Bunsengesellschaft f. Phys. Chem. Berichte. 72, 745-754 (1968)

72. "Maximum Concentration of Vacancies in Binary Compounds" B.F. Ormont, Doklady Akad. Nauk SSSR 166, 1393-1396 (1966)

73. "An Examination of the Decrease of Surface-Activity Method of Measuring Self-Diffusion Coefficients in Wüstite and Cobaltous Oxide" R.E. Carter, F.D. Richardson, Journal of Metals. 6, 1244-1257 (1954) [Trans. AIME. 200, 1244-1257 (1954)]

74. "Electrical Properties of Cobalt Monoxide" B. Fisher, D.S. Tannhauser, J. Chem. Phys. 44, 1663-1672 (1966)

75. "The Non-Stoichiometry of Manganous Oxide" M.W. Davies, F.D. Richardson, Trans. Faraday Soc. 55, 604-610 (1959)

76. "The System Iron-Oxygen. I. The Wüstite Field and Related Equilibria" L.S. Darken, R.W. Gurry, J.Am. Chem. Soc. 67, 1398-1412 (1945)

77. "The System Iron-Oxygen. II. Equilibrium and Thermodynamics of Liquid Oxide and Other Phases" L.S. Darken, R.W. Gurry, J. Am. Chem. Soc. 68, 798-816 (1946)

78. "An X-Ray Study of the Wüstite (FeO) Solid Solutions" E.R. Jette, F. Foote, J. Chem. Phys. 1, 29-36 (1933)

79. "High Temperature Defect Structure of Ferrous Oxide" I. Bransky, D.S. Tannhauser, Trans. A.I.M.E. 239, 75-80 (1967)

80. "Electrical Conduction in Li-Doped MnO Single Crystals" M. Ali, M. Fridman, M. Denayer, P. Nagels, Phys. Stat. Solidi. 28, 193-206 (1968)

81. "High Temperature Electrical Properties of Manganese Monoxide" A. Z. Hed, D.S. Tannhauser, J. Chem. Phys. 47, 2090-2103 (1967)

82. "n-Type Hall Effect In MnO" H.J. DeWitt, C. Crevecoeur, Phys. Let. 25A, 393-394 (1967)

83. "The Nature of Defects of the Oxides MnO and CoO as a Function of Oxygen Partial Pressure at High Temperature" H. LeBrusq, J.J. Oehlig, F. Marion, Compt. Rend. Acad. Sci. (Paris) 266, 965-968 (1968)

84. "Effects of the Oxygen Pressure on the Electrical Conductivity of a Semiconductor, NiO" S. Takeuchi, K. Igaki, J. Japan Inst. Metals. 14B, 16-21 (1950)

85. "The Electrical and Magnetic Properties of Nickel Oxide" K. Igaki, Bull. Naniwa Univ. A3, 113-123 (1955)

86. "The Semiconductor Behavior of Nickel Oxide" G. Schlosser, Z. Elektrochem. 65, 453-462 (1961)

87. "Lithium and Gallium Doped Nickel Oxide" H. P. Rooksby, M. W. Vernon, Brit. Jour. Appl. Phys. 17, 1227-1228 (1966)

88. "Magnetic and Physicochemical Study of Powdered Nickel Oxide, Pure and Doped" G. El Shobaky, P.C. Gravelle, S.

J. Teichner, Y. Trambouze, P. Turlier, J. Chim. Phys. 64, 310-319 (1967)

89. "Hopping Conduction in NiO" D. P. Snowden, H. Saltsburg Phys. Rev. Let. 14, 497-499 (1965)

90. "High-Temperature Defect Structure and Electrical Properties of NiO" I. Bransky, N.M. Tallen, J. Chem. Phys. 49, 1243-1249 (1968)

91. "High Temperature Defect Structure and Electrical Properties of NiO" I. Bransky, N.M. Tallen, p. 147-148 in Mass Transport In Oxides, N. B. S. Special Publication #296 (1968)

92. "Hall Effect Between 300°K and 1100°K In NiO" A. J. Bosman, H.J. Van Daal, G.F. Knuvers, Phys. Let. 19, 372-373 (1965)

93. "Hall Effect in CoO, NiO, and α-Fe_2O_3" H. J. Van Daal, A. J. Bosman, Phys. Rev. 158, 736-747 (1967)

94. "The Hall Mobility of NiO at Elevated Temperatures" N. M. Tallen, D.S. Tannhauser, Phys. Let. 26A, 131-132 (1968)

95. "Experimental Evidence for Highly Mobile Electrons in MnO and NiO at High Temperature" D. S. Tannhauser, N. M. Tallen, M. Gvishi, p. 145-146 in Mass Transport in Oxides, N. B. S. Special Publication #296 (1968)

96. The Nature of the Chemical Bond, L. Pauling, p. 518, Cornell Univ. Press (1960)

97. "Alkali Metal-Nickel Oxides of the Type $MNiO_2$" L.D. Dyer, B.S. Borie, G.P. Smith, J. Am. Chem. Soc. 76, 1199-1503 (1954)

98. "The Effects of Magnesium Additions on the Electrical Resistivity Behavior of Lithium - Doped Cobalt Oxide (CoO)" J. D. Oakey, M.S. Thesis, Lehigh Univ. (1967)

99. The Structure of Metals and Alloys, W. Hume-Rothery, G. V. Raynor,p. 97-110, Inst. Metals (1954)

100. "Structure of Solid Solutions" T. B. Massalski,p. 149-211, in Physical Metallurgy, R. W. Cahn, ed., J. Wiley (1965)

101. "Solid Solutions of CuO with Oxides of Bivalent Metals.

The Systems CuO-NiO, CuO-MgO, CuO-ZnO" R. Rigamonti, Atti Accademia Nazionale dei Lincei, Rome, Classe Sci. Fis., Mat., e Nat., 2, 446-451 (1947)

102. "Solid Solutions of ZnO with Oxides of Bivalent Metals" R. Rigamonti, Gazz. Chim. Ital. 76, 474-484 (1946)

103. "X-ray Diffraction Studies of the Solid-State Reaction in the NiO-ZnO System" H. Kedesdy, A. Drukolsky, J. Am. Chem. Soc. 76, 5941-5946 (1954)

104. "Oxidic Semiconductors" E. J. W. Verwey, p. 151-161 in Semiconducting Materials, T. J. Gray, ed., Butterworths (1951)

105. "Thin Films of NiO with Lithium Impurity, Part I. Preparation, Part II. Electrical Properties" T. R. Kohler, N. C. Jamison, Phys. Rev. 81, 322 (1951)

106. "A Study of Several Systems of the Type $Li_x[Co_yNi_{(1-y)}]_{(1-x)}O$" W. D. Johnston, R. C. Miller, R. Mazelsky, J. Phys. Chem. 63, 198-202 (1959)

107. "Induced Ferromagnetism due to the Addition of Lithium Ions in Nickel Oxide" N. Perakis, A. Serres, G. Parravano, J. Wucher, C. R. Acad. Sci. (Paris) 242, 1275-1277 (1956)

108. "Thermomagnetic Remanence in Nickel Oxides and the Alloys Pd_3Mn_2 and CrSb" N. Perakis, J. Wucher, G. Parravano, R. Wendling, C. R. Acad. Sci. (Paris) 247, 3037-3040 (1958)

109. "Magnetic Properties of the System $Ni_{(1-x)}Li_xO$ Between 80 and 300°K" N. Perakis, J. Wucher, G. Parravano, C. R. Acad. Sci. (Paris) 248, 2306-2308 (1959)

110. "Solid Solutions of Lithium Oxide in Nickel Oxide" P. J. Fensham, J. Am. Chem. Soc. 76, 969-971 (1954)

111. "Reinvestigation of Reported Ferromagnetism in $Li_xNi_{(1-x)}O$" T. P. Janusz, R. R. Heikes, W. D. Johnston, J. Chem. Phys. 26, 973-974 (1957)

112. "The Preparation, Crystallography, and Magnetic Properties of the $Li_xCo_{(1-x)}O$ System." W. D. Johnston, R. R. Heikes, D. Sestrich, J. Phys. Chem. Solids 7, 1-13 (1958)

113. "Some Ferrimagnetic Properties of the System $Li_xNi_{1-x}O$" J. B. Goodenough, D. G. Wickham, W. J. Croft, J.A.P., 29, 382-383 (1958)

114. "Some Magnetic and Crystallographic Properties of the System $Li^{+}_{x}Ni^{++}_{1-2x}Ni^{+++}_{x}O$" J. B. Goodenough, D. G. Wickham, W. J. Croft, J. Phys. Chem. Solids 5, 107-116 (1958)

115. "The Lattice Parameter of Nickel Oxide as a Function of Lithium Oxide Dissolved" Y. Iida, J. Am. Cer. Soc. 43, 225 (1960)

116. "A Note on the Solid Chemistry of the NiO-Li_2O Solid Solution" Y. Iida, N. Hayashi, Bull. Chem. Soc. Jap. 37, 659-662 (1964)

117. "On the NiO-Li_2O Solid Solution" N. Hayashi, Y. Iida, Nagoya Kogyo Gijitsu Shikenjo Hokoku, 14, 291-294 (1965)

118. "On the Variation of Lattice Parameters of Some Semiconducting Oxides " L. D. Brownlee, E. W. J. Mitchell, Proc. Phys. Soc. (London) B65, 710-716 (1952)

119. "Electron Diffraction Determination of Lattice Parameters of Polycrystalline Specimens Giving Broad Diffraction Peaks II. A Study of NiO" G. G. Libowitz, S. H. Bauer, J. Phys. Chem. 59, 214-217 (1955)

120. "The Influence of Doping NiO Catalysts with Altervalent Metal Additives I. Composition and Defect Concentration in Lithium Doped NiO" A. Bielanski, K. Dyrek, Z. Kluz, J. Sloczynski, T. Tobiasz, Bull. Acad. Polon. Sci., Ser. Sci. Chim. 12, 657-661 (1964)

121. "Effect of Lithium Additives on Néel Temperature and Lattice Parameter of NiO" D. Mehandjeev, I. Tsolovski, B. Piperov, B. Anghelov, Comptes Rendus Academie Bulgare Sciences 19, 1167-1170 (1966)

122. "Electrical Properties of $Li_xNi_{(1-x)}O$ Single Crystals" S. Koide, J. Phys. Soc. Jap. 20, 123-132 (1965)

123. "Investigation of the Carrier Mobility in NiO with Lithium Impurity" Y. M. Ksendzov, L. N. Anselm, L.L. Vasileva, V. M. Latysheva, Soviet Phys. Solid State 5, 1116-1123 (1963)

124. "Niccolates of the Alkali Metals" W. Bronger, H. Bade, W. Klemm, Z. Anorg. Allgem. Chem. 333, 188-200 (1964)

125. "Behavior of Nickel Oxide Towards Alkali Metal Oxides Heated in a Current of Oxygen" H. Bade, W. Bronger, W. Klemm, Bull. Soc. Chim. France, 1124-1129 (1965)

126. "Formation of NiO-Li_2O Solid Solutions by Solid State Reaction" Y. Iida, S. Ozaki, K. Shimada, Nagoya Kogyo Gijitsu Shikenjo Hokoku 9, 266-270 (1960)

127. "Time Dependence of NiO-Li_2O Solid Solution Formation" Y. Iida, J. Am. Cer. Soc. 43, 117-118 (1960)

128. "Evaporation of Lithium Oxide from Solid Solution of Lithium Oxide in Nickel Oxide" Y. Iida, J. Am. Cer. Soc. 43, 171-172 (1960)

129. "Temperature Dependence of the Formation of NiO-Li_2O Solid Solution" Y. Iida, S. Ozaki, K. Shimada, Bull. Chem. Soc. Jap. 33, 656-657 (1960)

130. "Solid Solutions, Isomorphism, and Symmorphism Among Oxides of the Bivalent Metals II. The Systems CoO-NiO, CoO-MgO, CoO-MnO, CoO-CdO, NiO-MgO, NiO-MnO, NiO-CdO" L. Passerini, Gazz. Chim. Ital. 59, 144-154 (1929)

131. "X-Ray Examination of a System of Mixed Crystals with Monoxide Components" S. Holgersson, A. Karlsson, Z. Anorg. Allgem. Chem. 182, 255-271 (1929)

132. "Melting Point Diagrams of Highly Refractory Oxides V. Systems with Magnesia" H. von Wartenberg, E. Prophet, Z. Anorg. Allgem. Chem. 208, 369-379 (1932)

133. "Activity Measurements in Oxide Solid Solutions: The System NiO-MgO and NiO-MnO in the Temperature Interval 1100 - 1300°C" W. C. Hahn, A. Muan, J. Phys. Chem. Solids 19, 338-348 (1961)

134. "Thermodynamic Properties of the Oxides of Fe, Ni, Pb, Cu, and Mn, by EMF Measurements" G. G. Charette, S. N. Flengas, J. Electrochem. Soc. 115, 796-804 (1968)

135. "Thermodynamics of the Vaporization of Nickel Oxide" R. T. Grimley, R. P. Burns, M. G. Inghram, J. Chem. Phys. 35, 551-554 (1961)

136. "Measurements on Galvanic Cells Involving Solid Electrolytes" K. Kiukkola, C. Wagner, J. Electrochem. Soc.

104, 379-387 (1957)

137. "Contributions to the Data on Theoretical Metallurgy XII. Heats and Free Energies of Formation of Inorganic Oxides" J.P. Coughlin, U.S. Bureau of Mines Bull. No. 542 (1954)

138. "Vapor Pressures of Nickel and of Nickel Oxide" H.L. Johnson, A.L. Marshall, J. Am. Chem. Soc. 62, 1382-1390 (1940)

139. R. E. Bickelhaupt, Private Communication, Southern Research Institute, Birmingham, Alabama, February 21, 1969

140. "Diffusional Prestressing of Ceramics" R. E. Bickelhaupt, Summary Report 9222-2000-XII, August 1968, Southern Research Institute, Birmingham, Alabama for Naval Air Systems Command

141. Scott's Standard Methods of Chemical Analysis, N.H. Furman, ed., 5th Ed., 675 (1939)

142. "Transport Phenomena in Pure and Doped MgO" M. O. Davies, J. Chem. Phys. 38, 2047-2055 (1963)

145. "Oxygen Chemisorption and Catalysis of N_2O Decomposition on NiO-MgO and Related Solid Solutions " A. Cimeno, M. Schiavello, F. S. Stone, Trans. Faraday Soc. 35, 350-361 (1966)

144. "The Adsorption of Gases on Nickel Oxide" S. J. Teichner, J. A. Morrison, Trans. Faraday Soc. 51, 961-967 (1955)

145. "Adsorption of Gas by Powdered Oxides I. Nickel Oxide" S. J. Teichner, R. P. Marcellini, P. Rue, Adv. Catal. 9, 458-471 (1957)

146. "Oxidation Reaction Catalyzed by Doped Nickel Oxide" M. E. Dry, F. S. Stone, Disc. Faraday Soc. 28, 192-216 (1959)

147. "Depletive Adsorption of Hydrogen and Carbon Monoxide on Nickel Oxide" J. D. Cotton, P. J. Fensham, Trans. Faraday Soc. 59, 1444-1457 (1963)

148. "Thermal Decomposition of Nickel Oxide" T. Imoto, Y. Harano, Y. Nishi, Nippon Kagaku Zasshi 86, 694-696 (1965)

149. "Decomposition of Nickel Oxide" F. P. Larkens, P. J. Fensham, Nature 215, 1268-1269 (1967)

150. "Energies and Grooving Kinetics of [001] Tilt Boundaries in Nickel Oxide" D. W. Readey, R. E. Jech, J. Am. Cer. Soc. 51, 201-208 (1968)

151. "The p-T-x Phase Diagram of the Lead-Sulphur System" J. Bloem, F. A. Kroger, Z. Phys. Chem. (N.S.) 7, 1-14 (1956)

152. Metallurgical Thermochemistry, O. Kubachewski, E. L. Evans, p. 38, Pergamon Press (1958)

153. "Composition Stability Limits of Binary Semiconductor Compounds" R. F. Brebrick, J. Phys. Chem. Solids 18, 116 - 128 (1961)

154. "Statistical Mechanics of Dilute Solid Solutions" R. F. Brebrick, J.A.P., Suppl. 33 (1) 422 - 425

155. R. F. Brebrick, Private Communications, Sept. 1968 and March 1969

156. "Semiconduction in $Li_xNi_{(1-x)}O$" S. Van Houton, J. Phys. Chem. Solids, 17, 7 - 17 (1960)

157. "Oxides of the 3-d Transition Metals" F. J. Morin, Chapter 14, p. 600 - 633, in Semiconductors, N. B. Hannay, ed., Reinhold (1959)

158. "Point Defects and Phase Stability of Transition Metal Oxides" F. A. Kroger, J. Phys. Chem. Solids, 29, 1889-1899 (1968)

159. "Non-Stoichiometry in Binary Semiconductor Compounds, $M_{1/2-\delta}N_{1/2+\delta}(C)$" Prog. S.S. Chem. 3, 213-264 (1967)

160. Massanalyse, G. Jander, K. F. Jahr, 1, 89 (1940) Berlin

161. A Textbook of Quantitative Inorganic Analysis, A. I. Vogel, 2nd Ed., 345 (1951) Longmans, Green and Co., London

162. "Surface Chemistry of Chromic Oxide" S. W. Weller, S. E. Voltz, J. Am. Chem. Soc. 76, 4695-4701 (1954)

163. "Radiation Induced Chemisorption of Oxygen on Chromia"

M. Nachman, I. Maxim, T. Braun, J. Phys. Chem. Solids 20, 307-314 (1961)

164. "The Determination of Stoichiometric Composition of NiO by the Modified Bunsen-Rupp Method" J. Deren, J. Haber, J. Sloczynski, Chemia Analityczna 6, 659-662 (1961)

165. "Physico-chemical Properties of Alkali-and Iron-Doped Nickel Oxide" A. Bielanski, J. Deren, J. Haber, J. Sloczynski, Trans. Faraday Soc. 58, 166-175 (1962)

166. Private Communication, P. Ch. Gravelle, January 17, 1968

167. "The Measurement of Surface Excess Oxygen of Nickel Oxide Catalysts by Reduction with Hydrazine" T. Uchijima, M. Takahashi, Y. Yoneda, Bull. Chem. Soc. Jap. 40, 2767-2772 (1967)

168. "A Critical Examination of Methods Used for the Determination of Available Oxygen in Higher Metal Oxides" D. A. Panthony, A. Siddiqi, Talanta 9, 811-821 (1962)

169. "Sintering of High-Purity Nickel Oxide" Y. Iida, J. Am. Cer. Soc. 41, 397-406 (1958)

170. "Sintering of High-Purity Nickel Oxide, II" Y. Iida, S. Ozaki, J. Am. Cer. Soc. 42, 219-228 (1959)

171. "Lattice Defects and the Sintering of Oxides" L. C. F. Blackman, Industrial Chemist, A58, 620-626 (1962)

172. "Sintering in Active Nickel Oxide" R.A. Brown, J. Am. Cer. Soc. 48, 627-630 (1965)

173. "Sintering Studies of NiO Compacts by the Electrical Resistivity Method" F. Y. Wang, J. A. P. 37, 929-930 (1966)

174. "Sintering Crystalline Solids. I. Intermediate and Final State Diffusion Models" R. L. Coble, J.A.P. 32, 787-792 (1961)

175. "Sintering of Nickel Oxides" R. M. Jodlowski, G. C. Kuczynski, Sintering and Related Phenomena, p. 553-563, G. C. Kuczynski, ed., Gordon and Breach (1967)

176. "Diffusion of Nickel In Single Crystals of Nickel Oxide" J.S. Choi, W. J. Moore, J. Phys. Chem. 66, 1308-1311 (1962)

177. "Diffusion of Oxygen In Single Crystals of Nickel Oxide" M. O'Keeffe, W. J. Moore, J. Phys. Chem. 65, 1438-1439 (1961)

178. "Observations on the Mechanical Properties of Nickel Oxide Scales" I. A. Menzies, K. N. Strafford, J. Mat'l. Sci. 2, 358-364 (1967)

179. "New Method of Obtaining Volume, Grain Boundary and Surface Diffusion Coefficients from Sintering Data" D. L. Johnson, J.A.P. 40, 192-200 (1969)

180. "Mechanical Properties of Polycrystalline Ceramics" N. B. Harrison, Quarterly Status Report No. VI (1962), Army Research Office, Durham, N.C.

181. "The Mechanical Properties of Polycrystalline NiO" R. J. Herbst, Chief Investigators Conference, Coordinated Basic Research on the Military Theme: Ceramics for Structural Use (1962)

182. "Mechanical Characteristics of Polycrystalline NiO" R. J. Herbst, A. L. Friedberg, Final Report AD-423663 (1963)

183. "The Mechanical Behavior of Polycrystalline Ceramics" W. B. Harrison, Chief Investigators Conference, Coordinated Basic Research on the Military Theme: Ceramics for Structural Use (1962)

184. "Pressure- Sintered Nickel Oxide" R. M. Spriggs, L. A. Brissette, T. Vasilos, Am. Cer. Soc. Bull. 43, 572-577 (1964)

185. "The Hot Pressing of Ceramics" T. Vasilos, R. M. Spriggs, Proc. Brit. Cer. Soc., No. 3, 195-221 (1965)

186. "Effect of Electronic Structure of Nickel Oxide on Oxygen Exchange" N. P. Keier, Kinetics and Catalysis 1, 200-206 (1960)

187. "The Mechanism of Oxygen Self-Diffusion in Nickel and Cobalt Oxides" M. Hoch, R. Szwarc, Tech. Rept. No. AFML-TR-67-331 (1967)

188. "The Mechanism of Oxygen Self-Diffusion in Nickel and Cobalt Oxides" M. Hoch, R. Szwarc, p. 143, Mass Transport in Oxides, N.B.S. Special Publication No. 296 (1968)

189. "Diffusion of Oxygen in Magnesium Oxide" L. H. Rovner, Cornell Univ., Dept. Eng. Phys., Rept. No 10. March 1, 1966.

190. "Effect of Grain Boundaries on Diffusion-Controlled Processes in Aluminum Oxide" A. E. Paladino, R. L. Coble, J. Am. Cer. Soc. 46, 133-136 (1963)

191. "Oxygen -18 Diffusion in Surface Defects on MgO as Revealed by Proton Activation" J. B. Holt, R. H. Condit, p. 13-29, Materials Science Research, Volume 3 (1966)

192. "Oxygen Diffusion in CoO as Measured by Proton Activation of ^{18}O" J. B. Holt, Proc. Brit. Cer. Soc., No. 9, 157-170 (1967)

193. Results of G. Goodman, Reported by J. E. Burke in Discussion of "Ceramic Problems for the Consideration of the Solid State Physicist" W. R. Buessem, p. 14-29, Physics and Chemistry of Ceramics, C. Klingsberg, ed., Gordon and Breach (1963)

194. "Electrical Properties of NiO" F. J. Morin, Phys. Rev. 93, 1199-1204 (1954)

195. "Electrical Properties of Non-Stoichiometric Nickel Oxide" M. Nachman, L. N. Cojocaru, L. V. Ribco, Phys. Stat. Solidi 8, 773-783 (1965)

196. "Mechanism of the Electrical Conduction in Li-Doped NiO" A. J. Bosman, C. Crevecoeur, Phys. Rev. 144, 763-770 (1966)

197. "High Frequency Conductivity of NiO" S. Kabashima, T. Kawakubo, J. Phys. Soc. Japan 24, 493-497 (1968)

198. "Effect of Grain Boundaries on the Electrical Conductivity of NiO" H. R. Thornton, Ph. D. Thesis,U. Ill. (1963)

199. "Grain Boundary Diffusion in MgO" B. J. Wuensch, T. Vasilos, J. Am. Cer. Soc. 47, 63-68 (1964)

200. "Self Diffusion of Oxygen in Single Crystal and Polycrystalline Aluminum Oxide" Y. Oishi, W. D. Kingery, J. Chem. Phys. 33, 480-486 (1960)

201. "A Model for Boundary Diffusion Controlled Creep in Polycrystalline Materials" R. L. Coble, J.A.P. 34, 1679-1682 (1963)

202. "Anomalous Variation of Young's Modulus of Antiferromagnets at the Néel Point" R. Street, B. Lewis, Nature 168, 1036-1037 (1951)

203. "On a Type of Transformation Common to the Monoxides of Manganese, Iron, Cobalt and Nickel" M. Foex, Compt. Rend. 227, 193-194 (1948)

204. "Antiferromagnetism of Nickel Oxide" M. Foex, C. H. LaBlanchetais, Compt. Rend. 228, 1579-1580 (1949)

205. "Contribution to the Study of Antiferromagnetism - Thermomagnetic Study of the Monoxides of Cobalt and Nickel" H. LaBlanchetais, J. Phys. Rad. 12, 765-771 (1951)

206. "Antiferromagnetism of Nickel and Cobalt Monoxides" M. Trombe, J. Phys. Rad. 12, 170-171 (1951)

207. "Magnetic Properties of Colloidal Nickelous Oxide" J. T. Richardson, W. O. Milligan, Phys. Rev. 102, 1289-1294 (1955)

208. "Magnetic Susceptibility of NiO and CoO Single Crystals" J. R. Singer, Phys. Rev. 104, 929-932 (1956)

209. "Some Magnetic Properties of Mixed Metal Oxides with Ordered Perovskite Structure" G. Blasse, Philips Res. Repts. 20, 327-336 (1965)

210. "Magnetic Anisotropy Measurements of NiO Single Crystal" H. Kondoh, E. Uchida, Y. Nakazumi, T. Nagamiya J. Phys. Soc. Jap. 13, 579-586 (1958)

211. "Multispin Axis Structures for Antiferromagnets" W. L. Roth, Phys. Rev. 111, 772-781 (1958)

212. "Fe^{57} Mossbauer Effect in Nickel Oxide" V. G. Bhide, G. K. Skenoy, Phys. Rev. 143, 309-315 (1966)

213. "Some Physical Properties of Nickel Oxides" Y. Shimomura, I. Tsubokawa, J. Phys. Soc. Jap. 9, 19-21 (1954)

214. "The High Temperature Heat Content of Nickel Oxide" J. R. Tomlinson, L. Domash, R. G. Hay, C. W. Montgomery, J. Am. Chem. Soc., 77, 909-910 (1955)

215. "Heat Contents above 298.15°K of Oxides of Cobalt and Nickel" E. G. King, A. U. Christensen, J. Am. Chem. Soc. 80, 1800-1801 (1958)

216. "Determining the Curie and Néel Points by the Thermographic Method" V. K. Maksimov, Ind. Lab. 7, 976-977 (1967)

217. "Modulus Anomaly in Antiferromagnets" K. P. Belov, R. Z. Levitin, p. 78-82, Ferrity, Izv. Akad. Nauk. Bel. S.S.R., Minsk (1960)

218. "Magnetostriction of Antiferromagnetic Nickel Monoxide" K. P. Belov, R. Z. Levitin, Sov. Phys. JETP 37, 400-401 (1959)

219. "A Method for Determining the Mechanical Resonance Frequencies and for Calculating Elastic Moduli from these Frequencies" S. Spinner, W. E. Tefft, Am. Soc. Testing Mater. Proc., 61, 1221-1238 (1961)

220. "Ultrasonic Methods for Measuring the Mechanical Properties of Liquids and Solids" H. J. McSkimin, Chap. 4 in Physical Acoustics, Vol. 1, W. P. Mason, ed., Academic Press (1964)

221. "Ultrasonic Measurement Techniques Applicable to Small Solid Specimens" H. J. McSkimin, J. Acoustic Soc. Am. 22, 413-421 (1950)

222. "Pulse Superposition Method for Measuring Ultrasonic Wave Velocities in Solids," J. Acoustic Soc. Am. 33, 12-16 (1961)

223. "The Velocity of Compressional Waves in Rocks to 10 Kilobars" F. Birch, J. Geophys. Res. 65, 1083-1102 (1960)

224. "Method of Pulse Transmission Measurements for Determining Sound Velocities" P. Mattaboni, E. Schreiber, J. Geophys. Res. 72, 5160-5163 (1967)

225. "Novel Method of Measuring Elastic and Anelastic Properties of Solids" D. B. Fraser, R. C. LeCraw, Rev. Sci. Inst. 35, 1113-1115 (1964)

226. "Elastic Properties of Tektites Measured by Resonant Sphere Technique" N. Soga, O. L. Anderson, J. Geophys. Res. 72, 1733-1739

227. "Elastic Constants of Small Sintered Ceramic Specimens" E. Schreiber, O. L. Anderson, Air Force Materials Laboratory Rept. No. AFML-TR-65-202 Part III (1968)

228. "Making Spheres of Crystals with Anisotropy of Hardness" J. Durand, Rev. Sci. Inst. 30, 840-841 (1959)

229. "Basic Study on the Oscillation of a Homogeneous Elastic Sphere. I. Frequency of Free Oscillations" Y. Sato, T. Usami, Geophysical Mag. (Japan) 31, 15-24 (1962)

230. Private Communication, J. B. Wachtman, Jr., National Bureau of Standards, July, 1968

231. Private Communication, E. P. Papadakis, Bell Telephone Laboratories, June, 1968

232. Private Communication, O. L. Anderson, Lamont Geological Observatory, August, 1968

233. The Theory of Sound, Lord Rayleigh, Vol. 1, p. 252, Second Ed., (1896)

234. "The Temperature Dependence of Young's Modulus for Nickel" J. Zacharias, Phys. Rev. 44, 116-122 (1933)

235. "Dynamic Methods For Determining the Elastic Constants and Their Temperature Variation in Metals" M. E. Fine, p. 43-67, in "Symposium on Determination of Elastic Constants" A.S.T.M. Special Publication No. 129 (1952)

236. "The Variation of the Adiabatic Elastic Moduli of Rocksalt with Temperature Between 80°K and 270°K"F. C. Rose, Phys. Rev. 49,50-54 (1936)

237. "The Variation of the Internal Friction and Elastic Constants with Magnetization in Iron. Part I" W. T. Cooke, Phys. Rev. 50, 1158-1164 (1936)

238. "The Internal Friction of Single Metal Crystals" T. A. Read, Phys. Rev. 58, 371-380 (1940)

239. "Use of the Piezoelectric Gauge for Internal Friction Measurements" J. Marx, Rev. Sci. Inst. 22, 503-509 (1951)

240. "A Study of the Magnetoelastic Properties of Some Ferromagnetic and Antiferromagnetic Materials" B. Lewis, Thesis, p. 161, University of Nottingham (1954)

241. G. A. Slack, Footnote (9) in "Sublattice Magnetization and Lattice Distortions in MnO and NiO" D. S. Rodbell, J. Owen, J.A.P. Suppl. to 35 (3) Part 2, 1002-1003 (1964)

242. "The Effect of Pressure on the Lattice Parameters. Part I. PbS and PbTe, Part II. Gd, NiO, and α-MnS" I. Wakabayashi, H. Kobayashi, H. Nagasaki, S. Minomura, J. Phys. Soc. Jap. 25, 227-233 (1968)

243. "Elastic Constants of Small Sintered Ceramic Specimens" O. L. Anderson, N. Soga, Air Force Materials Laboratory Rept. No. AFML-TR-65-202 (1965)

244. "The Heat Capacity of Nickel Oxide from 68-298°K and the Thermodynamic Properties of the Oxide" H. Seltz, B. J. DeWitt, H. J. McDonald, J. Am. Chem. Soc. 62, 88-89 (1940)

245. "Thermochemical Calculations" R. R. Wenner, p. 146, McGraw-Hill (1941)

246. "Compressibility and Absorption Frequency of Ionic Crystals" B. Szigeti, Proc. Royal Soc. (London) 204, 51-62 (1950)

247. "Optical Properties of Transition Metal Oxides" R. Marshall, S. S. Mitra, P. J. Giellisse, J. N. Plendl, Proc. 7th Int. Conf. (Paris 1964) Physics of Semiconductors, p. 1101-1106, Dunod Press, Paris (1964)

248. "The Elasticity and Antiferromagnetism of Cr_2O_3" R. Street, B. Lewis, Phil. Mag. 1, 663-668 (1956)

249. "Evidence for Domain Structure in Antiferromagnetic CoO from Elasticity Measurements" M. E. Fine, Phys. Rev. 87, 1143 (1952)

250. "Magnetomechanical Effects in an Antiferromagnet, CoO" M. E. Fine, Rev. Mod. Phys. 25, 158 (1953)

251. "Crystallography and Domain Walls in Antiferromagnetic NiO Crystals" G. A. Slack, J.A.P. 31, 1571-1582 (1960)

252. "Anomalies in the Modulus of Elasticity in Shear of

the Antiferromagnetic Materials MnO, CoO, and Cr_2O_3" L. A. Yevtushchenko, R. A. Levitin, Metals and Metallography 12, 139-140 (1961)

253. "Internal Friction Anomalies in Ferromagnets and Antiferromagnets near the Curie Point" K. P. Belov, G. I. Katayev, R. Z. Levitin, J.A.P. Suppl. 31, 153S-156S (1960)

254. "Structure of Nickel Oxide" H. P. Rooksby, Nature 152, 304 (1943)

255. "A Note on the Structure of Nickel Oxide at Subnormal and Elevated Temperatures" H. P. Rooksby, Acta. Cryst. 1, 226 (1948)

256. "Deformations in the Crystal Structures of Antiferromagnetic Compounds" S. Greenwald, J. S. Smart, Nature 166, 523-524 (1950)

257. "Structure of Nickel Oxide Containing Alumina" E. Gillam, J. P. Holden, J. Am. Cer. Soc. 46, 601-604 (1963)

258. "Anomalies in the Electrical Conductivity of Nickel Oxide Above Room Temperature" M. W. Vernon, M. C. Lovell, J. Phys. Chem. Solids 27, 1125-1131 (1966)

259. "The Rhombohedral Distortion in NiO" A. J. Springthorpe, Phys. Stat. Solidi 24, K3 (1967)

260. "Effect of Doping Nickel Oxide Catalysts with Altervalent Metal Additives. II. Magnetic Properties of Lithium-and Chrome-Doped Nickel Oxide" A. Bielanski, K. Dyrek, Z. Kluz, Bull. Acad. Pol. Sci., Ser. Sci. Chim. 13, 285-290 (1965)

261. "Electrical Conduction and Paramagnetic Susceptibility of NiO" M. Akiyama, J. Phys. Soc. Japan 20, 182-183 (1965)

262. M. Akiyama, K. Uchicho, S. Nakaya, Epitome of the Autumn Meeting of the Physics Society of Japan. 1963 Part I, p. 280

263. "Recent Developments in the Theory of Antifferomagnetism" J. H. Van Vleck, J. Phys. Rad. 12, 262-274 (1951)

264. "Spin Configuration in Antiferromagnetic Domain Walls of the NiO-Type Crystals" T. Yamada, J. Phys. Soc. Jap. 21, 650-664 (1966)

265. Ferrites, J. Smit, H. P. J. Wijn, p. 20, J. Wiley (1959)

266. "Antiferromagnetic Superexchange Effect" R. K. Nesbet Phys. Rev. 119, 658-662 (1960)

267. "Hopping Conduction in $Li_xNi_{1-x}O$ Crystals at Low Temperatures" A.J. Springthorpe, I. G. Austin, B. A. Austin, Sol. St. Comm. 3, 143-146 (1965)

268. "Polarons in Transition - Metal Oxides" N. F. Mott, Comments on Solid State Physics 1, 105-111 (1968)

269. "Band Structure and Electrical Conductivity of NiO" J. Feinleib, Phys. Rev. Let. 21, 1010-1013 (1968)

270. "Optical Absorption in the Divalent Oxides of Cobalt and Nickel" W. P. Doyle, G. A. Lonergan, Disc. Faraday Soc. 26, 27-33 (1958)

271. "Paramagnetic and Optical Spectra of Divalent Nickel in Cubic Crystalline Fields" W. Low, Phys. Rev. 109, 247-255 (1958)

272. "Optical Properties of Nickel Oxide" R. Newman, R. M. Chrenko, Phys. Rev. 114, 1507-1513 (1959)

273. "Photoemission and Optical Studies of the Electronic Structure of NiO, CoO, and V_2O_4" R. J. Powell, AD835266 (1967)

274. "Optical Absorption of Small Polarons in Semiconducting NiO and CoO in the Near and Far Infra-Red" I. G. Austin, B. D. Clay, C. E. Turner, Proc. Phys. Soc. (London) Ser. 2, 1, 1418-1434 (1968)

275. "Polaron Mechanism of Light Absorption in Rutile Crystals (TiO_2)" V. N. Bogomolov, E. K. Kudinov, D. N. Mirlin, Yu. A. Firsov, Sov. Phys. Sol. St. 9, 1630-1639 (1968)

276. "Polaron Nature of the Current Carriers in Rutile (TiO_2)" V. N. Bogomolov, E. K. Kudinov, Yu. A. Firsov, Sov. Phys. Sol. St. 9, 2502-2513 (1968)

Table 1

IMPURITY CONCENTRATION OF STARTING MATERIALS

(parts per million)

Material Identification / Impurity	NiO Johnson-Matthey Specpure Grade I Lot. No. S6616	NiO Atomergic Sub-Micron Lot No. C1435	NiO Baker Reagent Lot. No. 2796	Fisher MgO "Electronic Grade"			Fisher Li_2CO_3 Lot. No. 764296
Ag	<1						
Al	<1	20			150	75	
B				10	40	3	
Ca	<1			50	1000	150	100
Cl			50	27	180	285	30
Co		200	2000			10	
Cr		10			10	5	
Cu	<1	150	200	3	1		
F					140	110	
Fe	10	200	100	100	200	85	10
K							100
Mg	<1	30					
Mn					70	2	
N			50			100	2
Na					180	100	100
Ni	-	-	-		5	10	
P					7	130	
Pb			50				10
S			100	50	50	510	1000
Si	3	300		300	1000	2400	
Ti					50	10	
Zn						5	
Other, as Insolubles (in HCl)			2000				
Approx. Particle Size, Micron	2-5	0.015	0.1	.05	.05	-	
Source of Analysis, Note No.	1	1	1	2	2	3	1

Notes: 1. Supplier Analysis

2. Jet Propulsion Lab. Tech. Rept. No. 32-736, M.H. Leipold, T. H. Nielsen

3. "Impurity Distribution in MgO" M.H. Leipold, J.Am. Cer. Soc. 49, 498 (1966)

Table 2

Survey of Stoichiometry Range Reported

For Pure Nickel Oxide

Stoichiometry Range	Nature of Sample	Year (and Reference)
$NiO_{1.05}$ (Max.)	Powder	1931 (46)
$NiO_{1.025}$ (Max.)	Powder Calcined from $NiCO_3$	1934 (47)
$NiO_{1.0005}$-$NiO_{1.005}$	Oxidized Nickel Foil	1934 (48)
NiO - $NiO_{1.006}$	Porous Sintered Specimen	1936 (49)
NiO - $NiO_{1.07}$	Powder, 300 Atm. Pressure	1940 (35)
$NiO_{1.02}$ - $NiO_{1.2}$	Powder, Calcined $Ni(NO_3)_2$	1954 (36)
$NiO_{1.0007}$- $NiO_{1.0196}$	Powder, Calcined $Ni(NO_3)_2$	1962 (50)
$NiO_{1.00098}$	"Commercial" Nickel Oxide	1964 (51)
$NiO_{1.00013}$ - $NiO_{1.0224}$	Powder, Calcined $NiCO_3$	1965 (52)
NiO - $NiO_{1.00016}$	Thermal Dehydration $Ni(OH)_2$	1966 (53)
$NiO_{1.000 \pm 0.002}$	"Specpure" Nickel Oxide	1968 (54)

Table 3

Calculated Values of $[V_{Ni}]$ at 25°C and 1200°C and P_{O_2} = 0.209 atm, (vacancies per ion pair)

Source	$[V_{Ni}]$ at 25°C	$[V_{Ni}]$ at 1200°C
Mitoff (67)	3.6×10^{-11}	1.83×10^{-4}
Price (69, 70)	3.6×10^{-11}	1.83×10^{-4}
Eror (68)	-	2.47×10^{-4}
Sockel, Schmalzried (71)	-	3.1×10^{-4}
Ormont (72)	2×10^{-11}	-

Table 4

Ni^{+3} and Li^{+1} Chemical Analyses

Description	pH	Powder Analysis, at% Ni^{+3}	Powder Analysis, at % Li^{+1}	Sample Analysis, at % Ni^{+3}	Sample Analysis, at % Li^{+1}
"Blank"	-	0	-	-	-
99.999% NiO, as rec'd.	-	0	-	-	-
99.999% NiO, 1000°C airfire	-	0	-	-	-
5%Li(Nom), unwashed	Basic	5.2413 ±0.297	5.31	5.0731 ±0.0491	5.29
				5.3364	5.63
0.1%Li(Nom), washed	Neutral	0.1180±0.0003	0.12	0.117	
0.5%Li(Nom), washed	Neutral	0.4920 ±0.0003			
1%Li(Nom), washed	Neutral	0.9449 ±0.0041			
2%Li(Nom), washed	Neutral	1.9586 ±0.0452			
5%Li(Nom), washed	Neutral	4.9684 ±0.0010	4.98		
20%Li(Nom), washed	Neutral	6.8389 ±0.0205			
20%Li(Nom), washed	Neutral	6.9585 ±0.1211			
10%Li(Nom), washed	Neutral	8.2320 ±0.1337	8.277	8.2230 ±0.1345	
30%Li(Nom), washed	Neutral	9.9745 ±0.0292			
25%Li(Nom), washed	Neutral	12.278 $\pm^{.300}_{.150}$			

Table 5

Periodic Table of the Elements Demonstrating the Extent of Solubility and Compound Formation in NiO-M_xO_y Phase Systems.

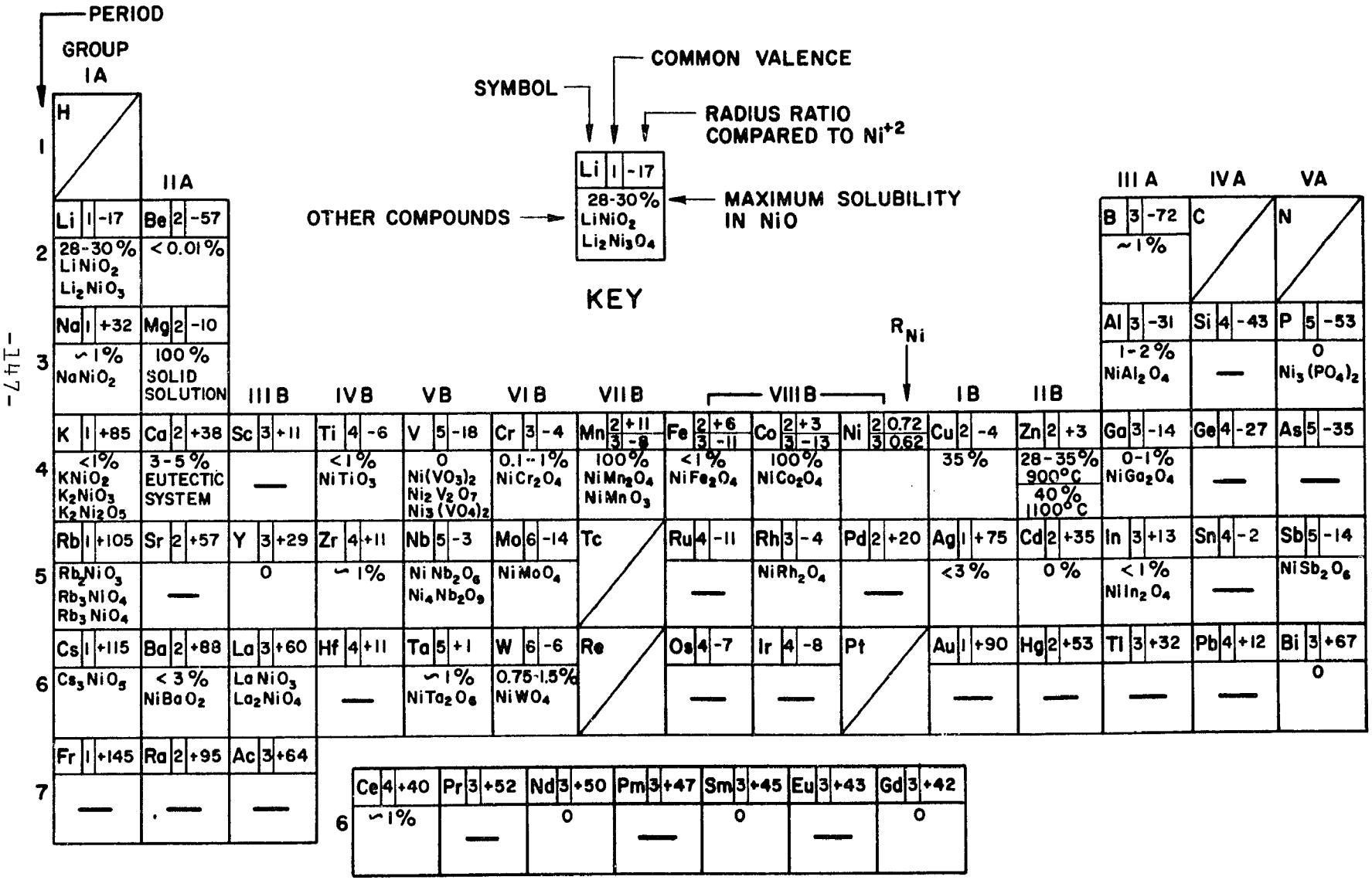
PERIOD
GROUP
IA
IIA
IIIB
IVB
VB
VIB
VIIB
VIIIB
IB
IIB
IIIA
IVA
VA
SYMBOL
COMMON VALENCE
RADIUS RATIO COMPARED TO Ni+2
MAXIMUM SOLUBILITY IN NiO
OTHER COMPOUNDS
KEY
R_{Ni}
H
Li 1 -17
28-30% $LiNiO_2$ Li_2NiO_3
Be 2 -57
< 0.01%
Na 1 +32
Mg 2 -10
~1% $NaNiO_2$
100% SOLID SOLUTION
B 3 -72
~1%
C
N
Al 3 -31
1-2% $NiAl_2O_4$
Si 4 -43
P 5 -53
0 $Ni_3(PO_4)_2$
K 1 +85
Ca 2 +38
3-5% EUTECTIC SYSTEM
Sc 3 +11
Ti 4 -6
<1% $NiTiO_3$
V 5 -18
0 $Ni(VO_3)_2$ $Ni_2V_2O_7$ $Ni_3(VO_4)_2$
Cr 3 -4
0.1-1% $NiCr_2O_4$
Mn 2 +11 / 3 -8
100% $NiMn_2O_4$ $NiMnO_3$
Fe 2 +6 / 3 -11
<1% $NiFe_2O_4$
Co 2 +3 / 3 -13
100% $NiCo_2O_4$
Ni 2 0.72 / 3 0.62
Cu 2 -4
35%
Zn 2 +3
28-35% 900°C 40% 1100°C
Ga 3 -14
0-1% $NiGa_2O_4$
Ge 4 -27
As 5 -35
Rb 1 +105
Sr 2 +57
Y 3 +29
Zr 4 +11
Nb 5 -3
Mo 6 -14
Tc
Ru 4 -11
Rh 3 -4
Pd 2 +20
Ag 1 +75
Cd 2 +35
In 3 +13
Sn 4 -2
Sb 5 -14
Rb_2NiO_3 Rb_3NiO_4 Rb_3NiO_4
0
~1% $NiNb_2O_6$ $Ni_4Nb_2O_9$
$NiMoO_4$
$NiRh_2O_4$
<3%
0%
<1% $NiIn_2O_4$
$NiSb_2O_6$
Cs 1 +115
Ba 2 +88
La 3 +60
Hf 4 +11
Ta 5 +1
W 6 -6
Re
Os 4 -7
Ir 4 -8
Pt
Au 1 +90
Hg 2 +53
Tl 3 +32
Pb 4 +12
Bi 3 +67
Cs_3NiO_5
< 3% $NiBaO_2$
$LaNiO_3$ La_2NiO_4
~1% $NiTa_2O_6$
0.75-1.5% $NiWO_4$
0
Fr 1 +145
Ra 2 +95
Ac 3 +64
6
Ce 4 +40
Pr 3 +52
Nd 3 +50
Pm 3 +47
Sm 3 +45
Eu 3 +43
Gd 3 +42
~1%
0
0
0

Table 6

Final Grain Size Range for Pressure Sintered

Lithium-Nickel Oxide Alloys

Atomic Percent Lithium	Run No.	Grain Size Range, microns
Pure NiO	16	1-2
Pure NiO	16, airfired	15-20
.12	22	3-4
.49	27	10-15
.95	29	15-20
.95	31	15-20
1.96	25	40
4.97	26	35-50
6.84	30	30-60
8.23	19	8-10

Table 7.

Experimental Values of Néel Temperature for Nickel Oxide

Néel Temperature	Measurement Method	Author	Reference No.
525	Dilatometric	Foex	(203)
525	Magnetic Susceptibility	Perakis	(50)
604	" "	Perakis and coworkers	(107)
623	" "	Perakis and coworkers	(108)
607	" "	Foex and coworkers	(204)
647	" "	LaBlanchetais	(205)
647	" "	Trombe	(206)
523	" "	Richardson and coworkers	(207)
523(640)	" "	Singer	(208)
523	" "	Blasse	(209)
523	Magnetic Torque	Kondoh and coworkers	(210)
533	Magnetic Scattering	Roth	(211)
520	Mossbauer Effect	Bhide and coworkers	(212)
518	Specific Heat	Shimomura and coworkers	(213)
523	" "	Tomlinson and coworkers	(214)
525	" "	King and coworkers	(215)
513	" "	Maksimov	(216)
507	Modulus	Street and Lewis	(202)
510	Modulus	Belov and Levitin	(217)
524	Magnetostriction	Belov and Levitin	(218)

Table 8

Resonant Sphere Method Data Analysis - Pure NiO Run #12

Intensity	f, Observed Frequency cps	f_r, Reduced Frequency (*)	Mode Identification (**)	A_n, (#) Shear Wave Mode Constant	ϑ_s, Shear Velocity (###) cm/sec	R, ohms	C, micro-farads	Q^{-1}, Inverse Acoustic Loss (##)
Weak	19,830	Background and Equipment Resonance	------	-----	------	---	---	----
Weak	43,240		------	-----	------	---	---	----
Weak	136,000		------	-----	------	---	---	----
Weak	141,000		------	-----	------	---	---	----
Very weak	204,000		------	-----	------	---	---	----
Weak	256,000		------	-----	------	---	---	----
Very strong	274,500	2.501	$_1T_2$	2.501	2.255×10^5	22,000	.01	2.74×10^{-3}
Very weak	279,000	2.540	Unidentified Split Peaks	-----	-----	---	---	----
Weak	290,000	2.640		-----	-----	---	---	----
Medium	307,000	2.796	$_1S_2$	-----	-----	---	---	----
Very strong	407,870	3.715	$_2S_1$	-----	-----	18,000	.01	2.17×10^{-3}
Medium	419,460	3.820	$_1T_3$	3.865	2.225×10^5	---	---	----
Medium	543,830	4.953	$_1T_4$	5.095	2.200×10^5	---	---	
Medium	679,840	6.193	$_1S_5$	-----	-----	---	---	
Medium	684,840	6.238	$_1T_5$	6.266	2.250×10^5	---	---	
Weak	776,500	7.073	$_2T_2$	7.136	2.240×10^5	---	---	
Weak	805,000	7.333	$_3S_1$	-----	-----	---	---	
Very strong	856,200	7.798	$_1S_0$	-----	-----	31,000	.01	5.96×10^{-4}
			Average Shear Velocity =		2.231×10^5			

(*) based on the tentative assumption that the peak at f = 274,000 = f_n is a $_1T_2$ shear mode with $A_n = 2.501$ and $f_r = f\left(\frac{An}{f_n}\right) = f\left[\frac{2.501}{274,000}\right]$

(**) based on match between experimental reduced frequencies and the curve of f_r versus Poisson's ratio given by Fraser and LeCraw(225) at σ=0.416

(#) from Sato and Usami (229)

(##) from $Q = 2\pi f_n(RC)$

(###) from $\vartheta_s = \pi d\frac{f_n}{An}$ where d = 0.6549 cm.

Table 9

Compilation of Experimental Data and Elastic Moduli for Pure and Doped Nickel Oxide Using Different Measurement Techniques

	Sample Identity and Measurement Method						
	Pure NiO Run 12 Pulse Transmission Longitudinal Wave Measurement	Pure NiO Run 12 Pulse Transmission Shear Wave Measurement	Pure NiO Run 12 Resonant Sphere Method (#)	Pure NiO Run 12 Composite Oscillation Method	8.23% Li Alloy Run 19 Pulse Transmission Longitudinal Wave Measurement	8.23% Li Alloy Run 19 Pulse Transmission Shear Wave Measurement	8.23% Li Alloy Run 19 Composite Oscillator Method
Specimen Length, cm	0.6934	0.6934	-	1.90	0.6797	0.6797	1.898
Specimen Diameter, cm	-	-	0.6549	-	-	-	-
Matched timing frequency, cps	2,641,000	1,129,789	-	-	2,719,236	2,595,700	-
Integer frequency number	3	4	-	-	3	6	-
Resonant frequency, cps	-	-	-	98,600(*)	-	-	121,019(**)
Velocity, cm/ sec	$6.137 \times 10^5 (\vartheta_l)$	$1.959 \times 10^5 (\vartheta_s)$	2.231×10^5	-	$6.161 \times 10^5 (\vartheta_l)$	$2.94 \times 10^5 (\vartheta_s)$	-
Shear modulus, d/cm^2	2.61×10^{11}		3.38×10^{11}	-	5.41×10^{11}		-
Young's modulus, d/cm^2	7.50×10^{11}		9.58×10^{11}	9.56×10^{11}	14.66×10^{11}		13.23×10^{11}
Bulk modulus, d/cm^2	22.0×10^{11}		19.0×10^{11}	-	16.62×10^{11}		-
Poisson's ratio	0.443		0.416	-	0.35		-
Density, g/cm^3	6.801		6.801	6.801	6.269		6.269

(*) Measurement was made using quartz crystals with an average frequency of 92,550 cps, a total crystal mass of 6.34 grams, and a specimen mass of 5.26 grams. "Silastic" cement was used.

(**) Measurement was made using quartz crystals with an average frequency of 119,250 cps, a total crystal mass of 4.84 grams, and a specimen mass of 4.68 grams. "GA-60" cement was used.

(#) See Table 8 for Resonant Sphere Data Analysis.

Table 10

Experimental and Derived Values of Mean Sound Velocity and Bulk Modulus for Pure Nickel Oxide at Room Temperature

Source	K, dyne/cm^2	υ_m, cm/sec
Sphere Resonance	19.0×10^{11}	2.55×10^5
Pulse Transmission	22.0×10^{11}	2.2×10^5
Compressibility Data	18.5×10^{11}	2.49×10^5
Szigeti Relation	20.2×10^{11}	2.59×10^5
Debye Analysis	25.0×10^{11}	2.9×10^5

Table II

Comparison of Modulus Values Obtained for Pure Nickel Oxide Using Equation (A3.3) and Equation (A3.2)

			Equation (A3.3)			Equation (A3.2)		
T, °C	f_x, cps	fs(o), cps	C_1(*)	fs(f) cps	E, dyne/cm^2	C_2(#)	fs(f), cps	E, dyne/cm^2
26	107,710	96,950	1.0	97,050	9.2×10^{11}	0.871	95,631	8.96×10^{11}
250.5	138,809	157,381	1.0	158,281	25.5×10^{11}	0.833	161,781	25.6×10^{11}

Note: (*) $C_1 \equiv 1.0$

(#) $$C_2 = 1 - \frac{M_c^2 f_c^2}{m_s^2 f_s^2} \tan^2 \pi \frac{f_x}{f_c}$$

Figure 1

Vacuum Pressure Sintering Furnace. The Water-Cooled Base and the Induction Heating Coil can be seen in the Foreground. A Similar System is Shown Inside the Chamber. The 1¼ Inch Diameter "T.Z.M." Plungers are Attached to the Upper and Lower Rams.

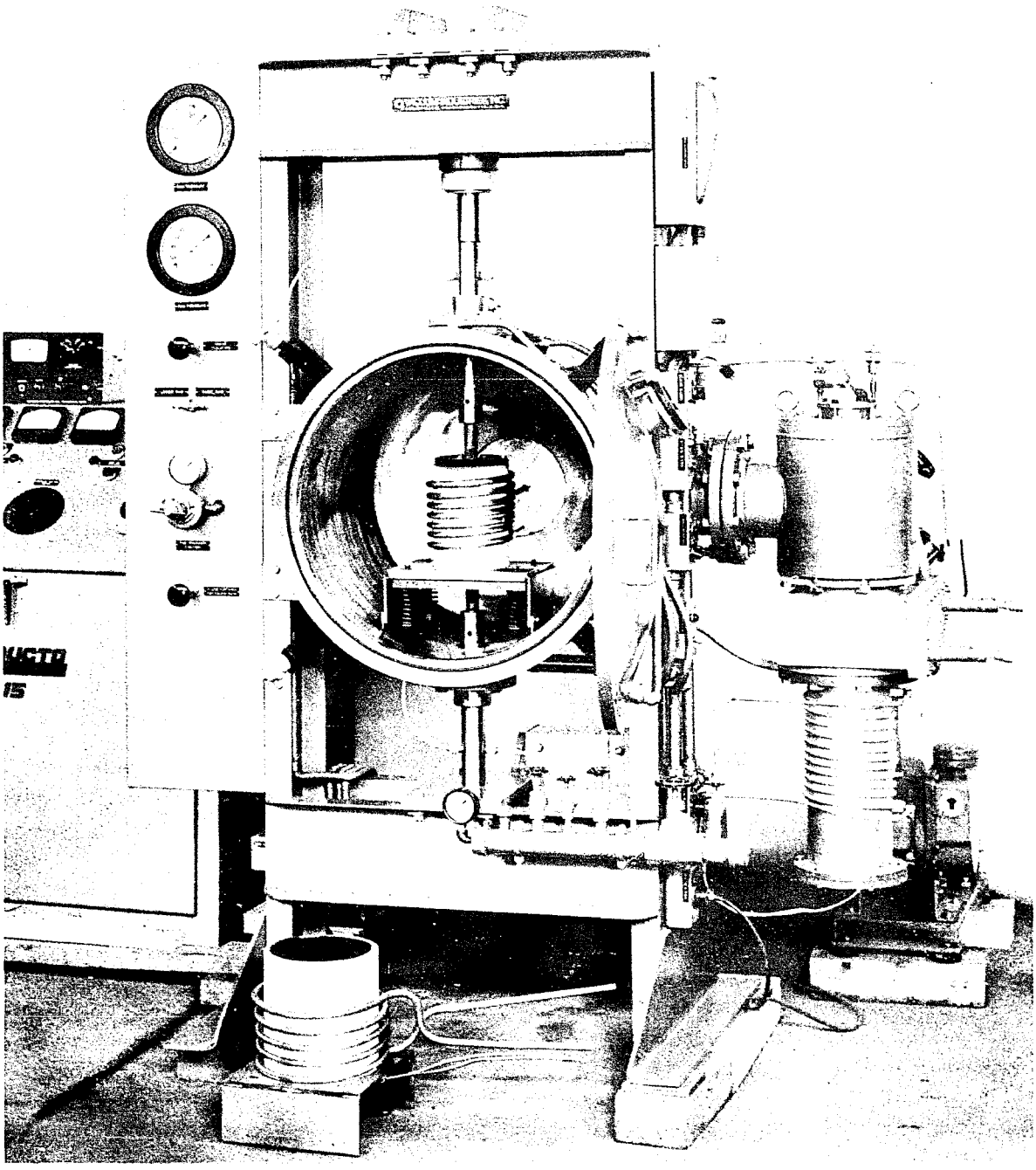

Figure 2

Schematic Drawing of Pressure-Sintering Die System. Graphite Susceptors Extend Over the Entire Length of the Silica Liner for Uniform Heating.

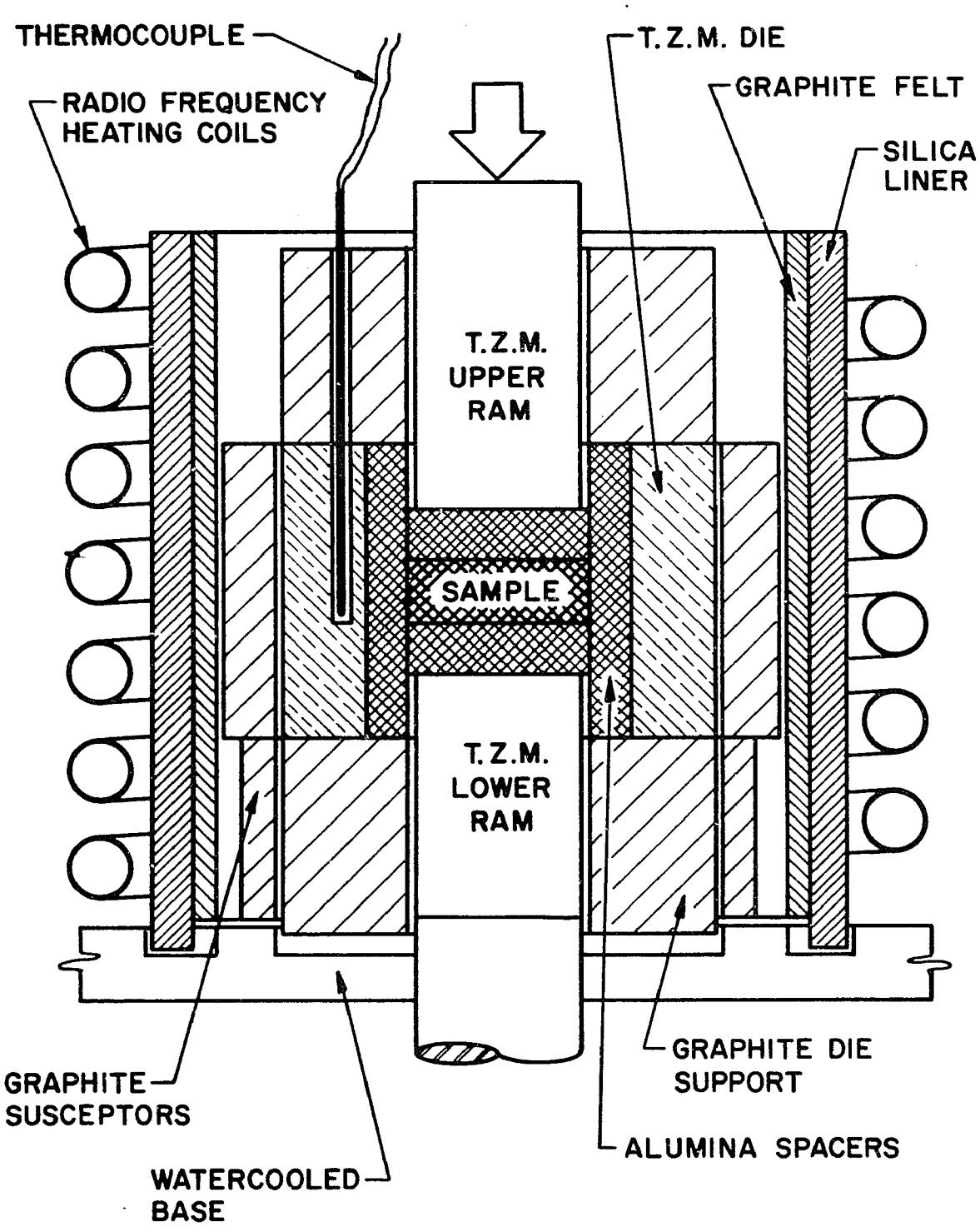
THERMOCOUPLE
RADIO FREQUENCY HEATING COILS
T.Z.M. DIE
GRAPHITE FELT
SILICA LINER
T.Z.M. UPPER RAM
SAMPLE
T.Z.M. LOWER RAM
GRAPHITE SUSCEPTORS
WATERCOOLED BASE
GRAPHITE DIE SUPPORT
ALUMINA SPACERS

Figure 3

Chemical Apparatus for the Dissolution of Powdered Samples in Hydrochloric Acid for the Iodometric Titration Analysis of Ni^{+3}

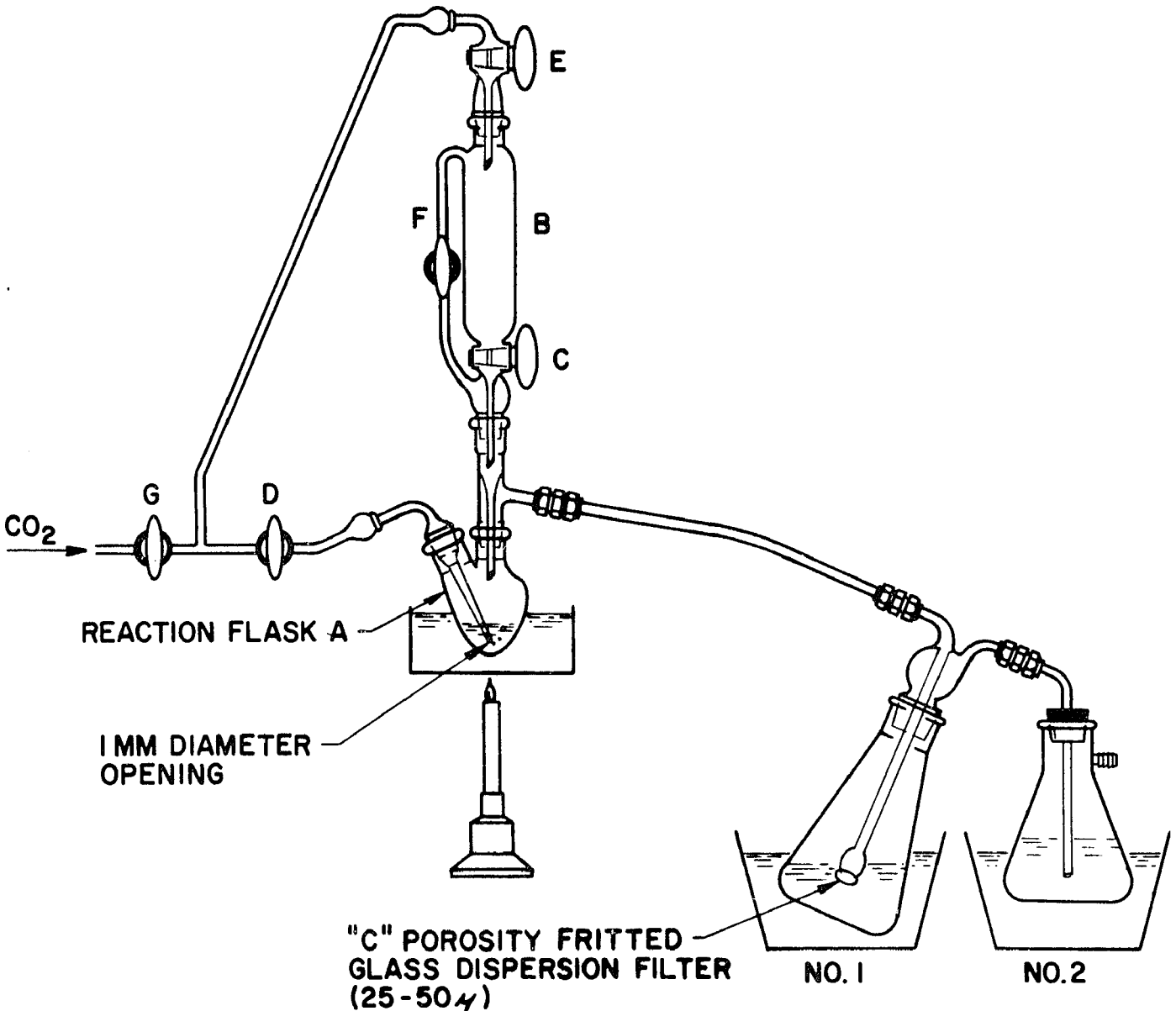
E
F
B
C
G
D
CO_2
REACTION FLASK A
1 MM DIAMETER OPENING
"C" POROSITY FRITTED GLASS DISPERSION FILTER (25-50μ)
NO. 1
NO. 2

Figure 4

Schematic Representation of the Composite Oscillator Method for the Determination of Young's Modulus.

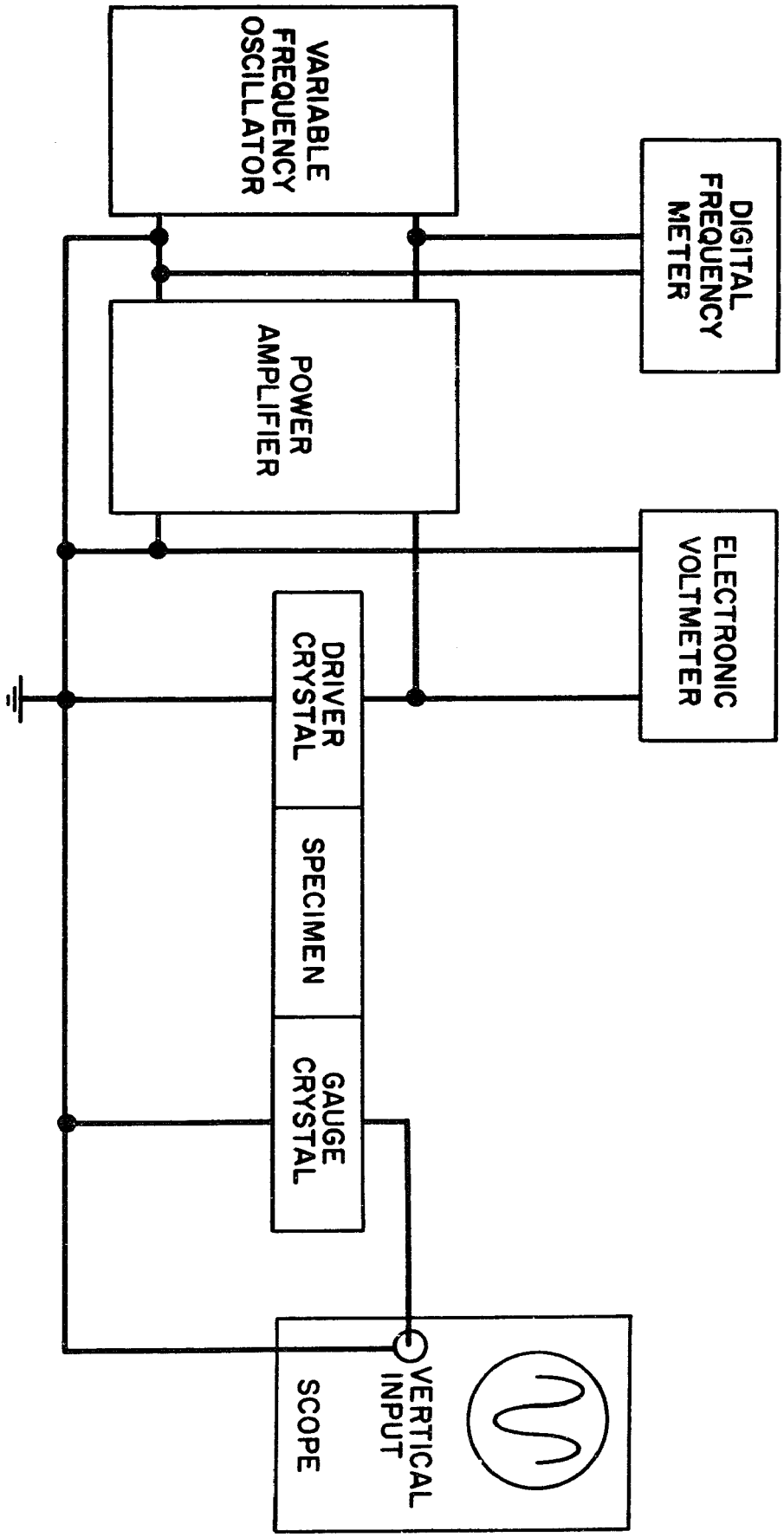
VARIABLE FREQUENCY OSCILLATOR
DIGITAL FREQUENCY METER
POWER AMPLIFIER
ELECTRONIC VOLTMETER
DRIVER CRYSTAL
SPECIMEN
GAUGE CRYSTAL
VERTICAL INPUT
SCOPE

Figure 5

Schematic Representation of the Equipment Used for the Four Point Resistivity Measurements.

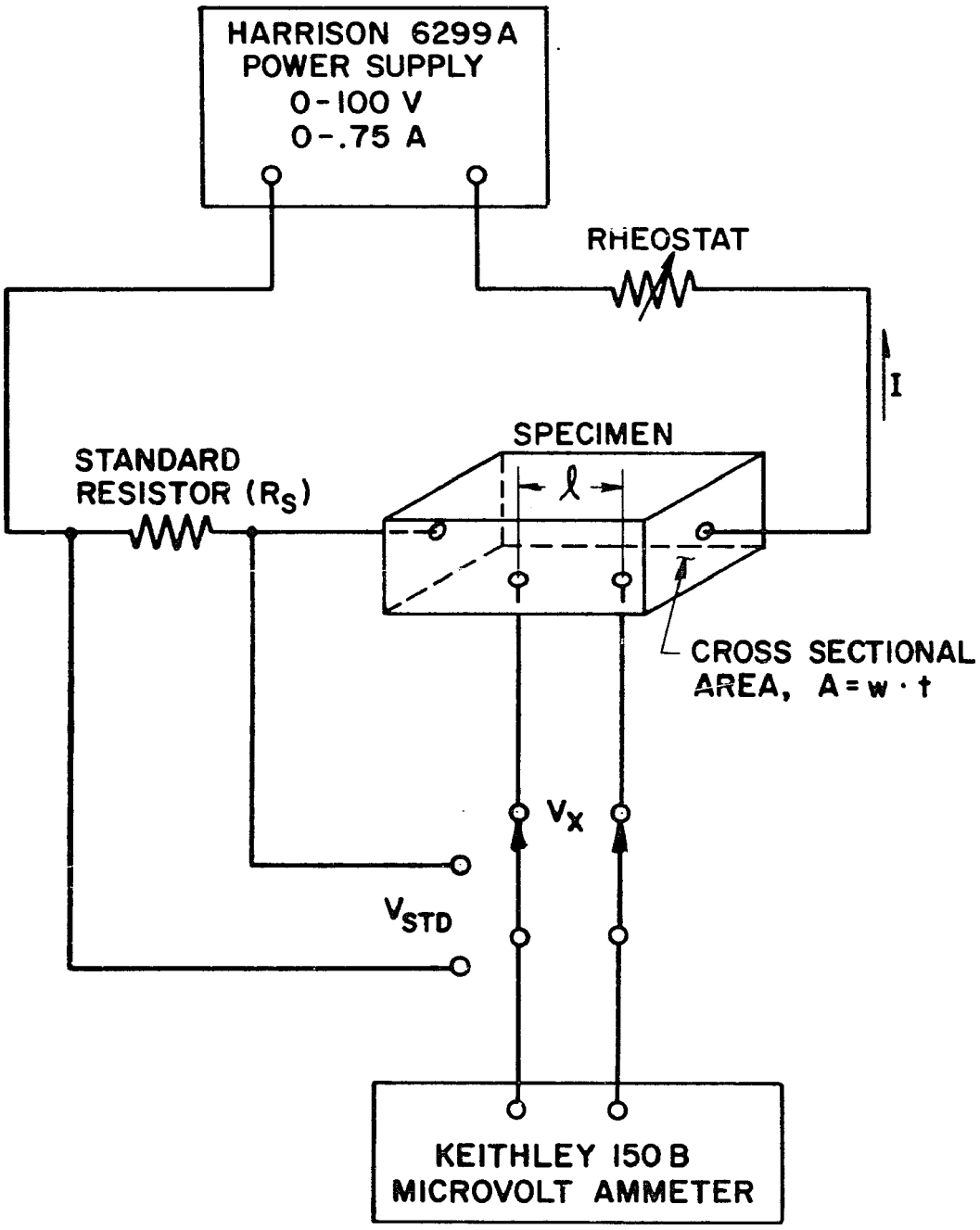

$$\rho = \frac{wt}{\ell} \cdot \frac{V_X}{V_{STD}} \cdot R_{STD}$$

Figure 6

Phase Diagram for the Ni-O System (After Bogatskii (29)).

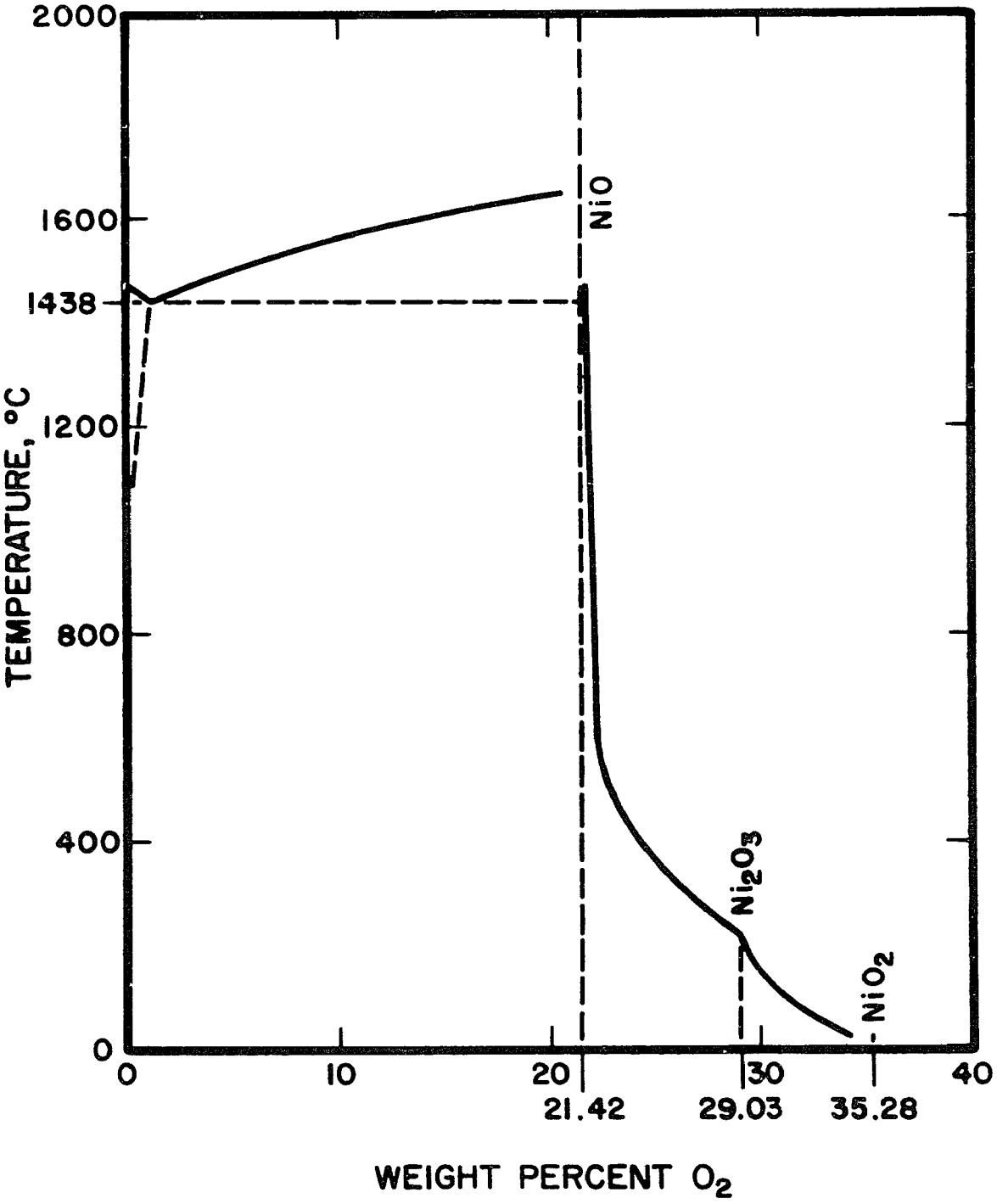
2000
1600
1438
1200
800
400
0
TEMPERATURE, °C
NiO
Ni_2O_3
NiO_2
0
10
20
30
40
21.42
29.03
35.28
WEIGHT PERCENT O_2

Figure 7

Standard Free Energy of Formation (Kilocalories per Half Mole Oxygen) as a Function of Temperature. The Upper Shaded Area is the Stable Phase Field for Pure NiO and the Cross-Hatched Area is the Stable Phase Field for Pure FeO.

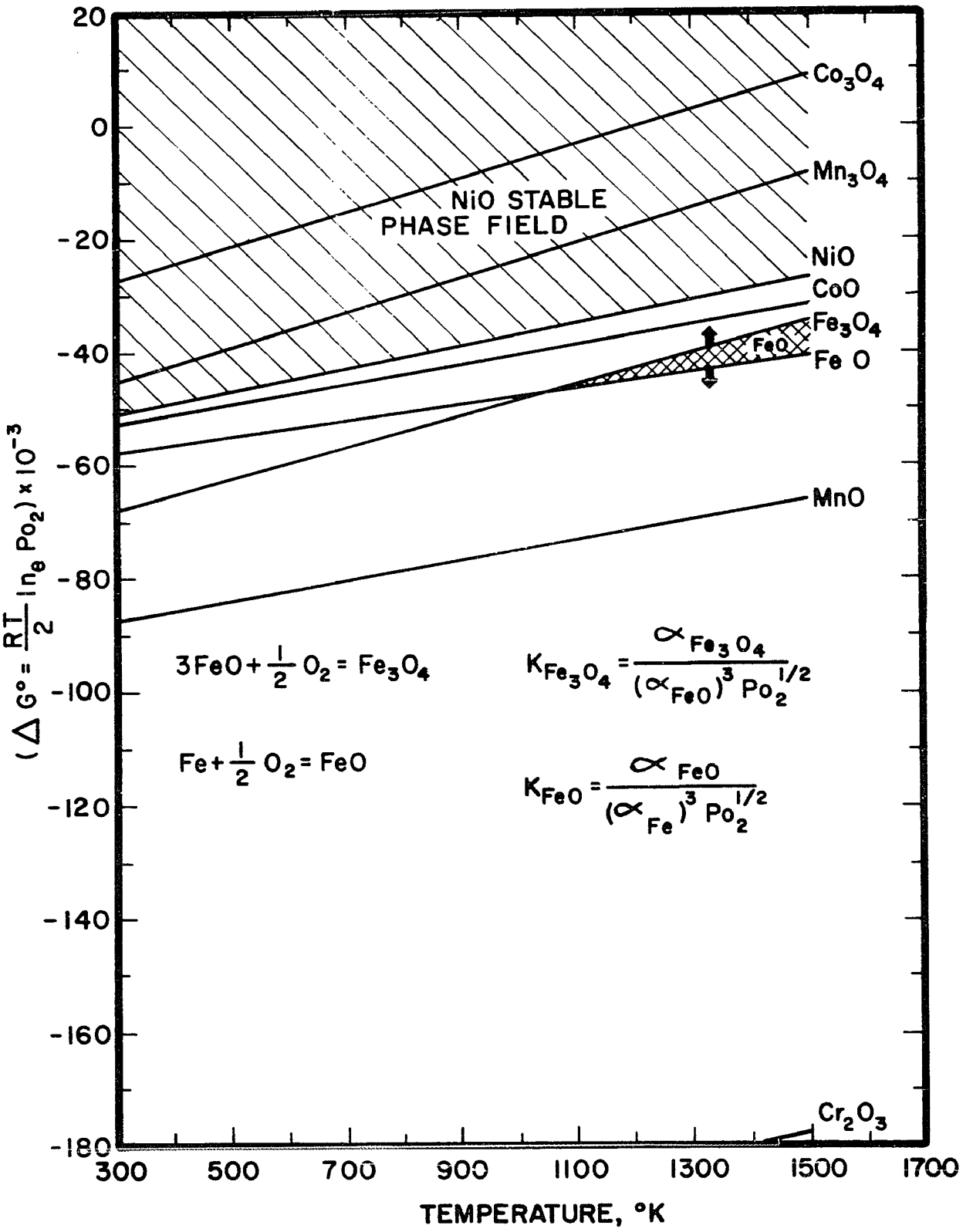
20
0
-20
-40
-60
-80
-100
-120
-140
-160
-180
$(\Delta G^\circ = \frac{RT}{2} \ln_e Po_2) \times 10^{-3}$
Co_3O_4
Mn_3O_4
NiO STABLE
PHASE FIELD
NiO
CoO
Fe_3O_4
FeO
Fe O
MnO
Cr_2O_3
$3FeO + \frac{1}{2} O_2 = Fe_3O_4$
$K_{Fe_3O_4} = \frac{\propto_{Fe_3O_4}}{(\propto_{FeO})^3 Po_2^{1/2}}$
$Fe + \frac{1}{2} O_2 = FeO$
$K_{FeO} = \frac{\propto_{FeO}}{(\propto_{Fe})^3 Po_2^{1/2}}$
300
500
700
900
1100
1300
1500
1700
TEMPERATURE, °K

Figure 8

Lattice Parameter (in Terms of Unit Cell Volume) as a Function of Mole Percent Lithium in Nickel Oxide.

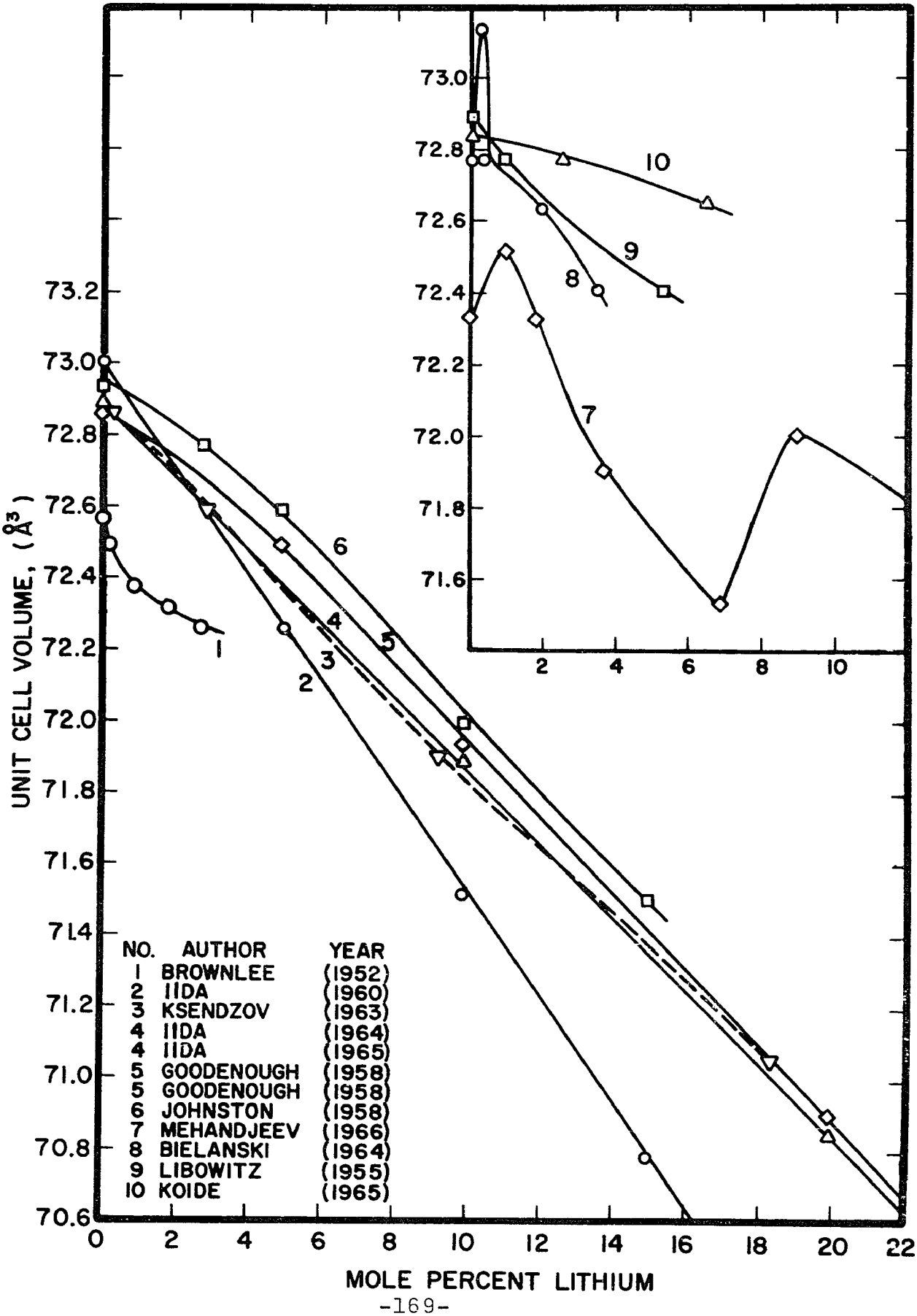
UNIT CELL VOLUME, (Å³)
MOLE PERCENT LITHIUM
NO. AUTHOR YEAR
1 BROWNLEE (1952)
2 IIDA (1960)
3 KSENDZOV (1963)
4 IIDA (1964)
4 IIDA (1965)
5 GOODENOUGH (1958)
5 GOODENOUGH (1958)
6 JOHNSTON (1958)
7 MEHANDJEEV (1966)
8 BIELANSKI (1964)
9 LIBOWITZ (1955)
10 KOIDE (1965)

Figure 9

A P-T Diagram Showing Published Data on the Ni/NiO Phase Boundary. The Vertical Line Between the Two Open Circles Represents the Ambient Pressure Range During Sintering in the Present Investigation.

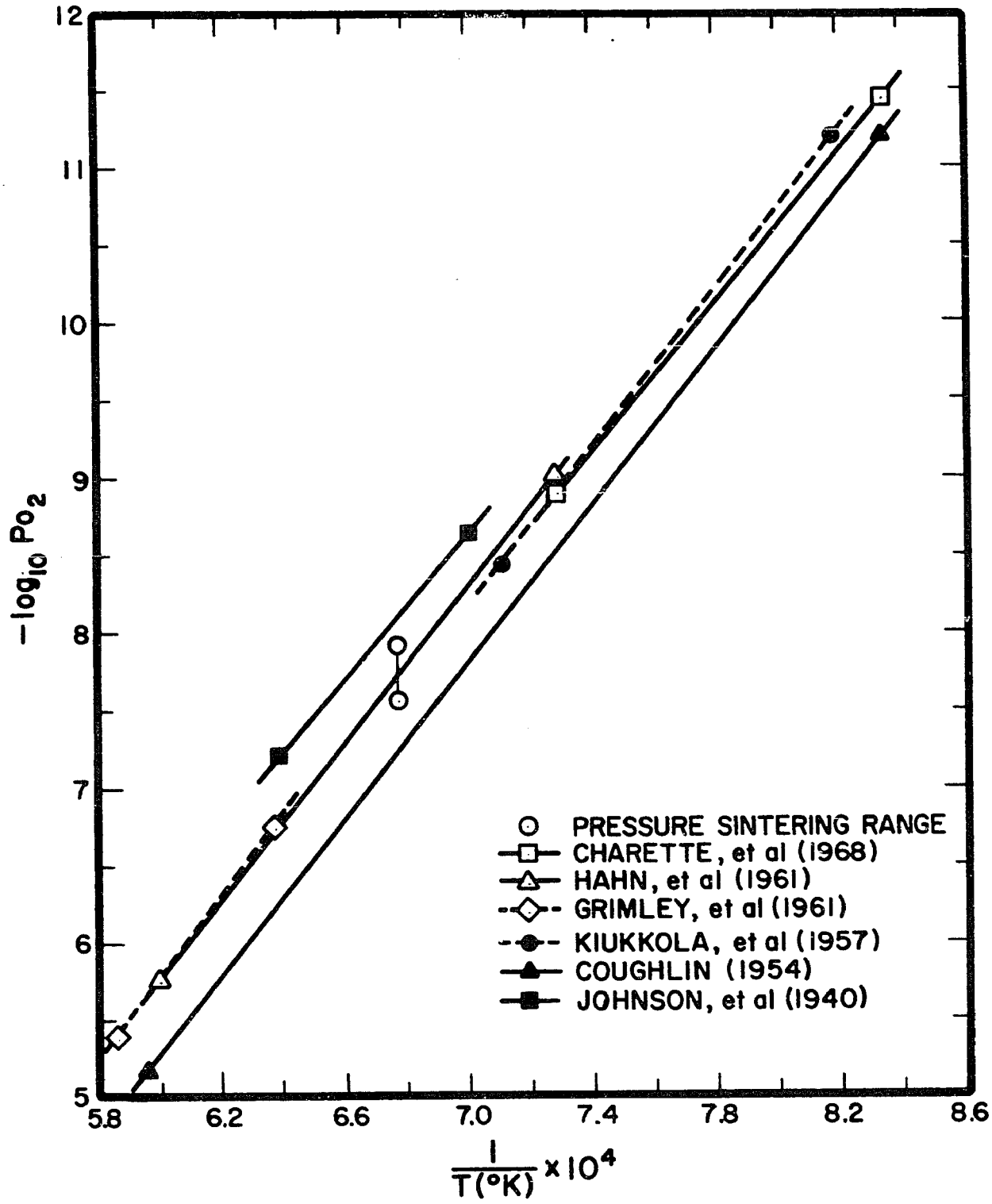
12
11
10
9
8
7
6
5
$-\log_{10} Po_2$
5.8
6.2
6.6
7.0
7.4
7.8
8.2
8.6
$\frac{1}{T(°K)} \times 10^4$
PRESSURE SINTERING RANGE
CHARETTE, et al (1968)
HAHN, et al (1961)
GRIMLEY, et al (1961)
KIUKKOLA, et al (1957)
COUGHLIN (1954)
JOHNSON, et al (1940)

Figure 10

Relative Density as a Function of Atomic Percent Lithium for Specimens Pressure-Sintered at 1100°C for 90 Minutes. The Pure Nickel Oxide Sample was Fired at 1350°C for 24 Hours After Vacuum Pressure-Sintering.

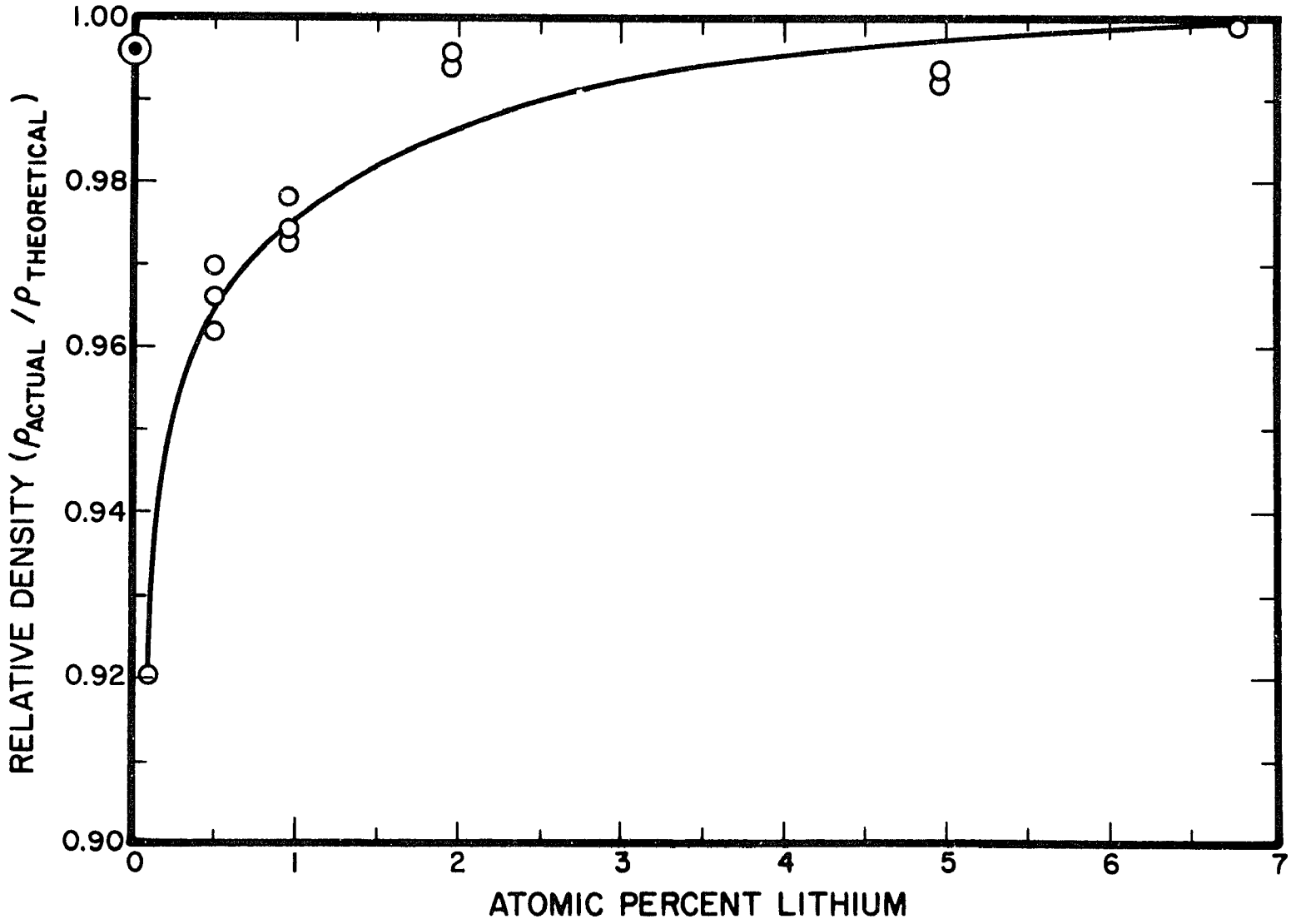
1.00
0.98
0.96
0.94
0.92
0.90
RELATIVE DENSITY (ρ_{ACTUAL} / $\rho_{THEORETICAL}$)
0
1
2
3
4
5
6
7
ATOMIC PERCENT LITHIUM

Figure 11

Electron Photomicrographs of Representative Pure- and Alloy-Starting Powders.

A. STARTING POWDER. PURE NICKEL OXIDE. 2300X. ONE INCH EQUALS 11μ.

B. STARTING ALLOY POWDER. 0.12 ATOMIC PERCENT LITHIUM ALLOY. 2357X. ONE INCH EQUALS 10μ.

C. STARTING ALLOY POWDER. 1.96 ATOMIC PERCENT LITHIUM ALLOY. 2357X. ONE INCH EQUALS 10μ.

D. STARTING ALLOY POWDER. 8.23 ATOMIC PERCENT LITHIUM ALLOY. 2357X. ONE INCH EQUALS 10μ.

Figure 12

Carbon-Chrome Electron Microscope Replicas of Representative Pure and Alloy Pressure-Sintered Samples.

A. CARBON-CHROME REPLICA OF PURE NICKEL OXIDE AFTER 1350°C AIR FIRE. 5100X. ONE INCH EQUALS 5.5μ.

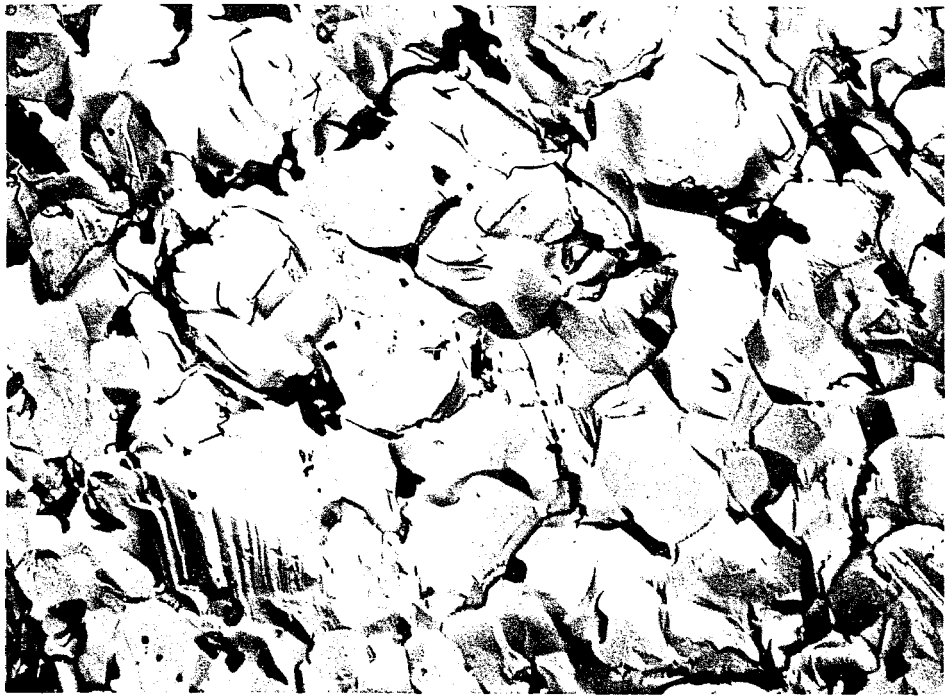

B. CARBON-CHROME REPLICA OF 0.12 ATOMIC PERCENT LITHIUM ALLOY. 3674X. ONE INCH EQUALS 7.1μ.

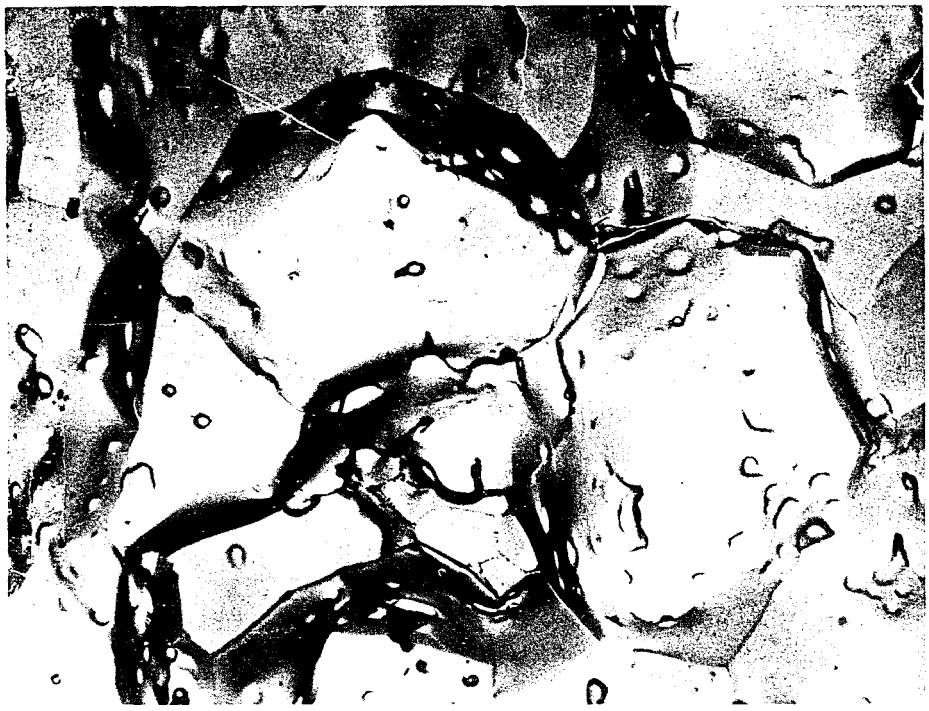

C. CARBON-CHROME REPLICA OF 1.96 ATOMIC PERCENT LITHIUM ALLOY. 2839 X. ONE INCH EQUALS 10μ.

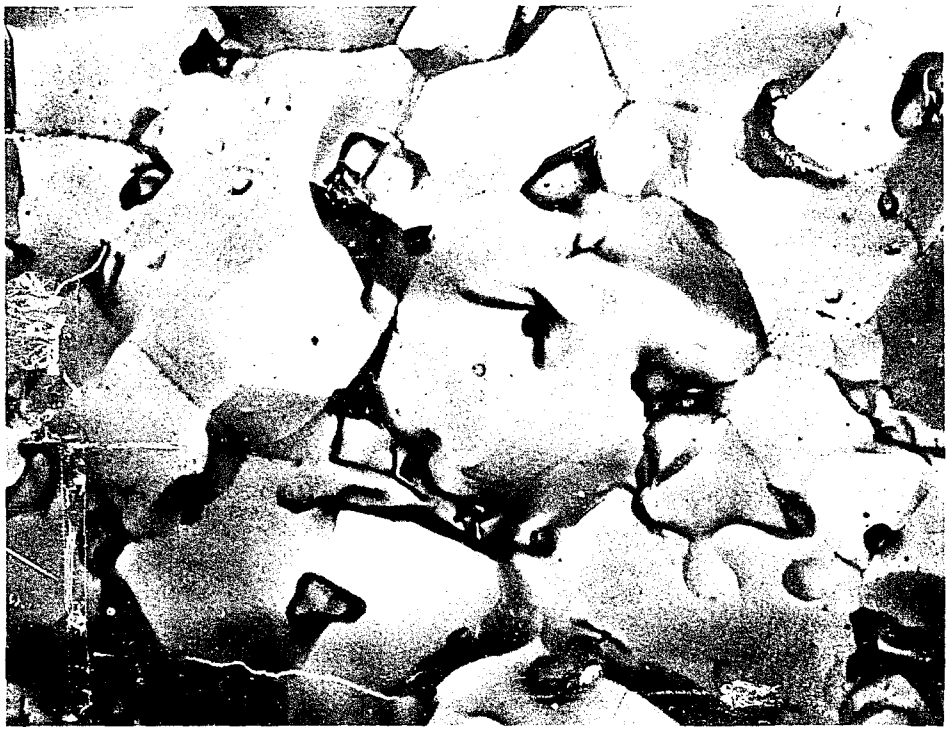

D. CARBON-CHROME REPLICA OF 8.23 ATOMIC PERCENT LITHIUM ALLOY. 2839 X. ONE INCH EQUALS 10μ.

Figure 13

Photomicrographs Showing Microprobe Trace (A) Before Etching and Same Area (B) After Etching of Pure Nickel Oxide Specimen. These Photographs are the Mirror Image of the Microprobe Scans Shown in Figures 14, 15 and 16. The Pore at the Right-Center Position in Each Photograph (Left-Center Position in Each Probe Scan) may be Used as a Reference.

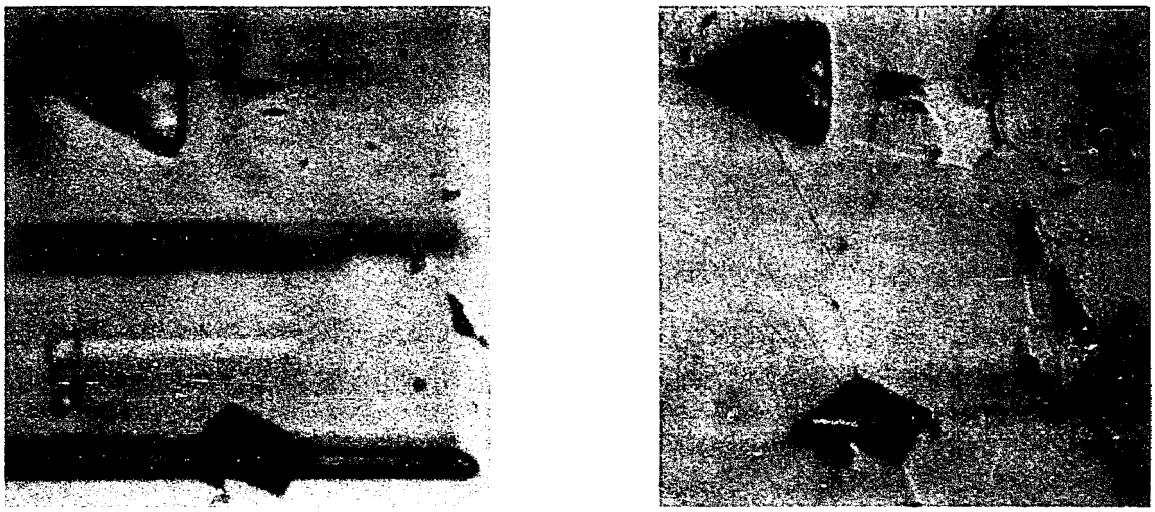

A B

PHOTOMICROGRAPHS OF PURE NICKEL OXIDE SPECIMEN. 1000X.

A. SHOWING TRACE FROM MICROPROBE SCAN BEFORE ETCHING.

B. SAME AREA ETCHED FOR 10 MINUTES IN BOILING CONCENTRATED HCl. NOTE POSITION OF GRAIN BOUNDARIES.

Figure 14

Electron Microprobe Specimen Current Image (A) and Line Scan (B) for Pure Nickel Oxide.

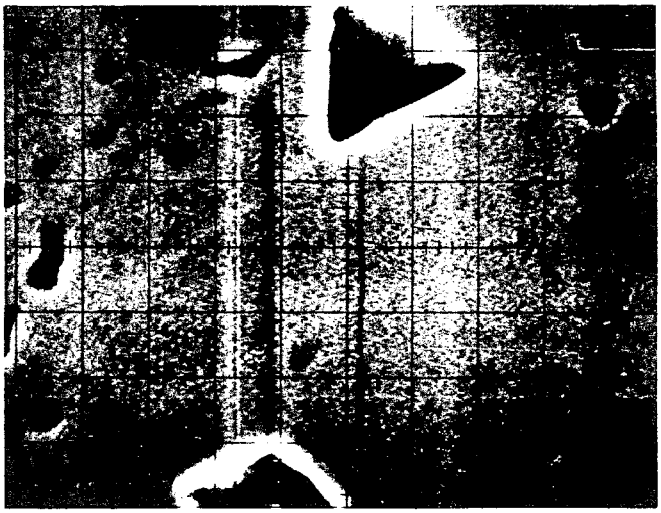

A

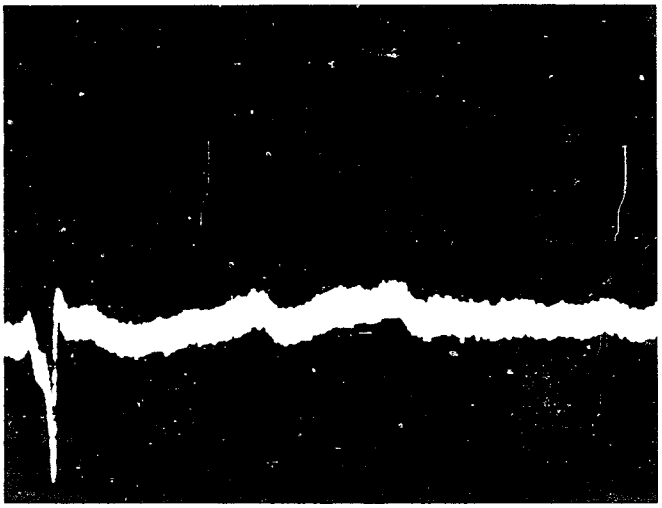

B

SPECIMEN CURRENT IMAGE (A) AND LINE SCAN (B) AT 1000X. PURE NICKEL OXIDE. PEAK HEIGHT IS 0.0004μAMPS. ABOVE BASE LINE. BASE LINE CURRENT IS 0.01 μAMPS.

Figure 15

Electron Microprobe Secondary Electron Image (A) and Line Scan (B) for Pure Nickel Oxide.

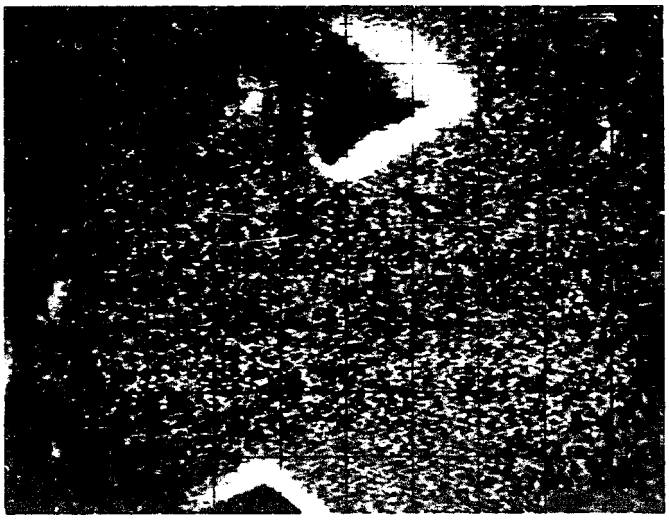

A

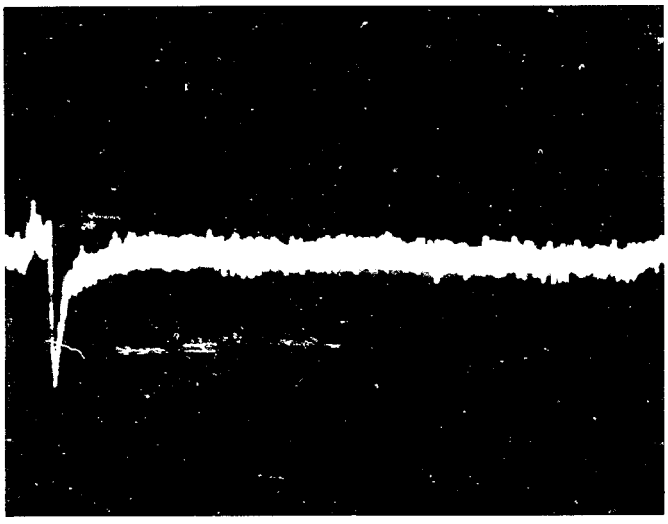

B

SECONDARY ELECTRON IMAGE (A) AND LINE SCAN (B) AT 1000X. PURE NICKEL OXIDE.

Figure 16

Electron Microprobe Back Scattered Electron Image (A) and Line Scan (B) for Pure Nickel Oxide. The Line Scan (B) is Flipped 180° on the Horizontal Axis so That the Trace at the Pore Conforms With Figures 14 and 15.

A

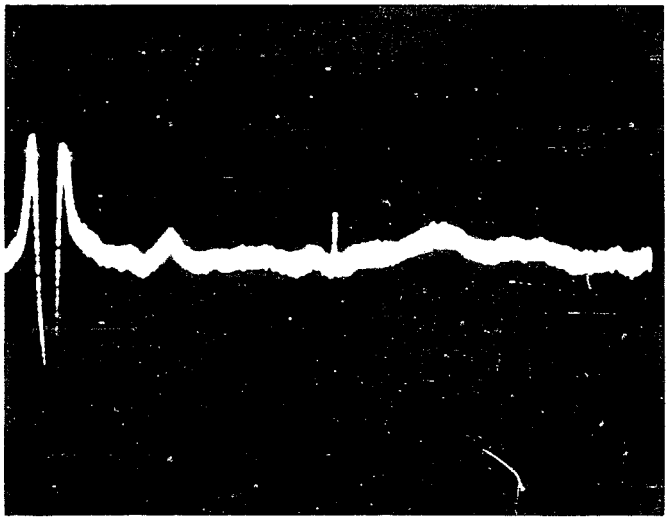

B

BACK SCATTERED ELECTRON IMAGE (A) AND LINE SCAN (B) AT 1000X. PURE NICKEL OXIDE.

Figure 17

Electron Microprobe Specimen Current Image (A) and Line Scan (B) for 8.23 Atomic Percent Lithium Alloy.

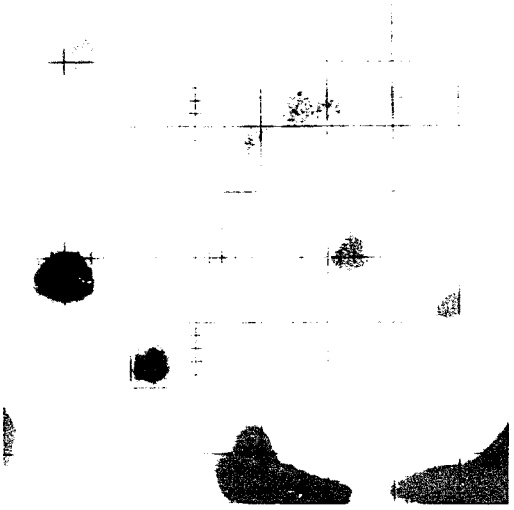

A

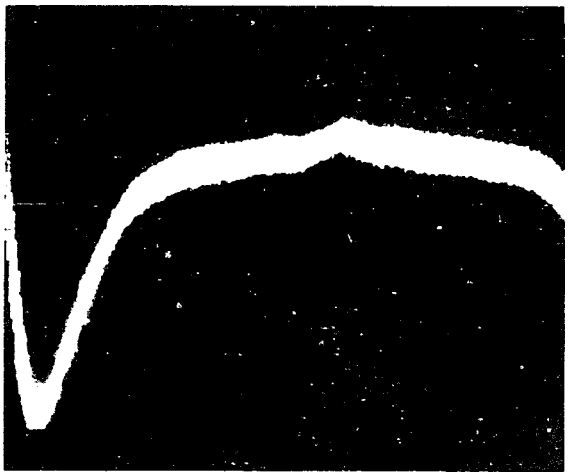

B

SPECIMEN CURRENT IMAGE (A) AT 1000X AND LINE SCAN (B) AT 2000X. 8.23 ATOMIC PERCENT LITHIUM ALLOY. PORE PEAK HEIGHT IS 0.0017 μ AMPS. BELOW BASE LINE. BASE LINE CURRENT IS 0.0112 μ AMPS.

Figure 18

Ni-Kα Scan for 8.23 Atomic Percent Lithium-Nickel Oxide Alloy (A) and Mg-Kα Scan for 5 Atomic Percent Lithium-Magnesium Oxide Alloy (B).

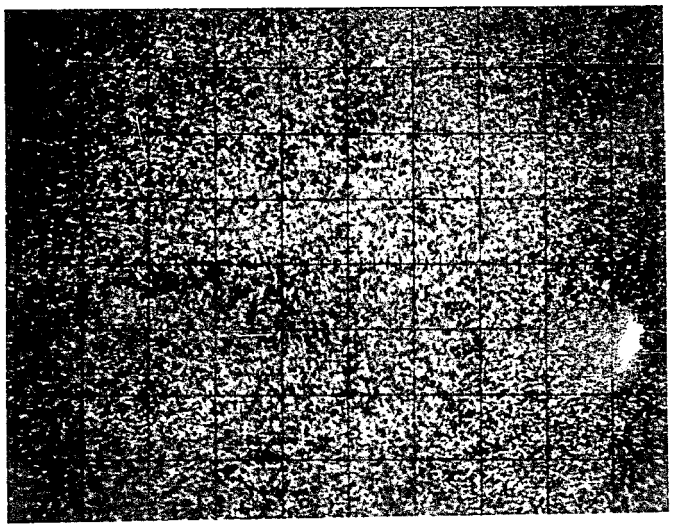

A

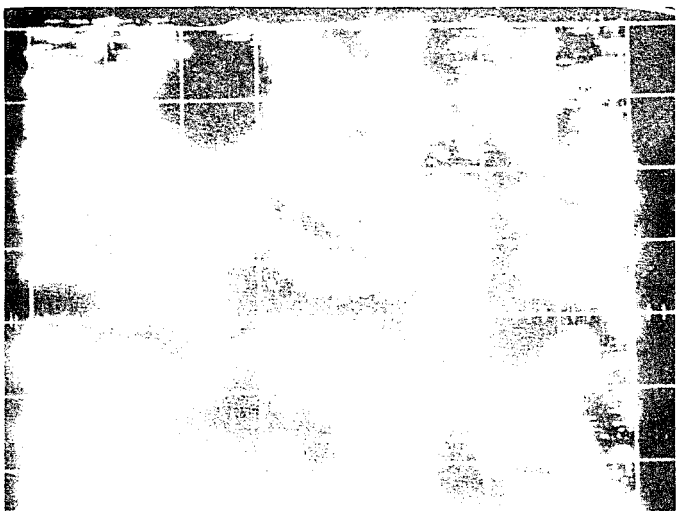

B

A. Ni-Kα SCAN FOR 8.23 ATOMIC PERCENT LITHIUM-NICKEL OXIDE ALLOY. 1000X. (PRESENT STUDY).

B. Mg-Kα SCAN FOR 5 ATOMIC PERCENT LITHIUM-MAGNESIUM OXIDE ALLOY. (AFTER BICKELHAUPT).

Figure 19

Schematic Representation of the Pulse Transmission Method for Modulus Measurements

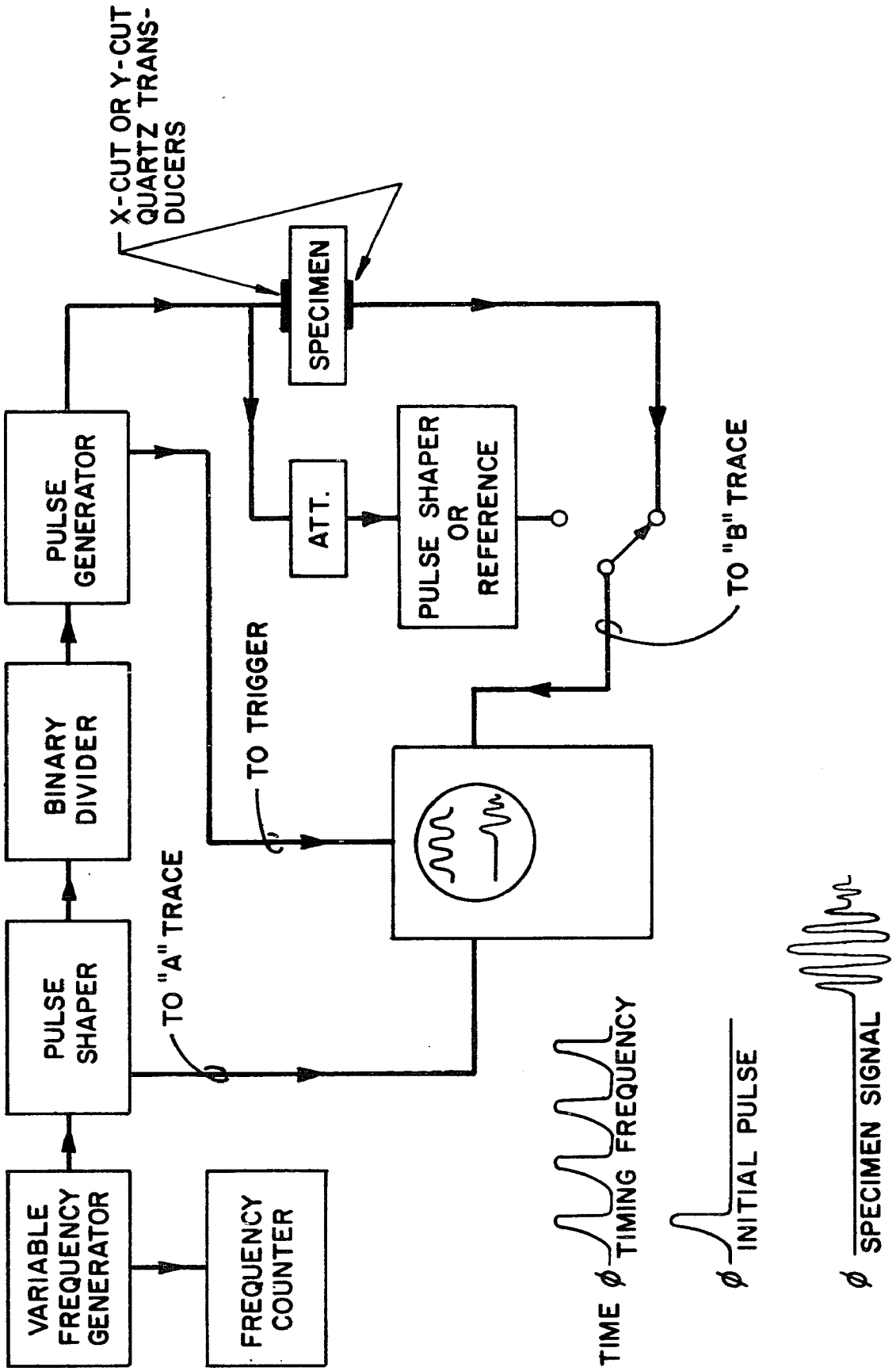
X-CUT OR Y-CUT QUARTZ TRANS-DUCERS
SPECIMEN
PULSE GENERATOR
ATT.
PULSE SHAPER OR REFERENCE
TO "B" TRACE
BINARY DIVIDER
TO TRIGGER
PULSE SHAPER
TO "A" TRACE
VARIABLE FREQUENCY GENERATOR
FREQUENCY COUNTER
TIME
TIMING FREQUENCY
INITIAL PULSE
SPECIMEN SIGNAL

Figure 20

Schematic Representation of the Pneumatic Sphere Grinder.

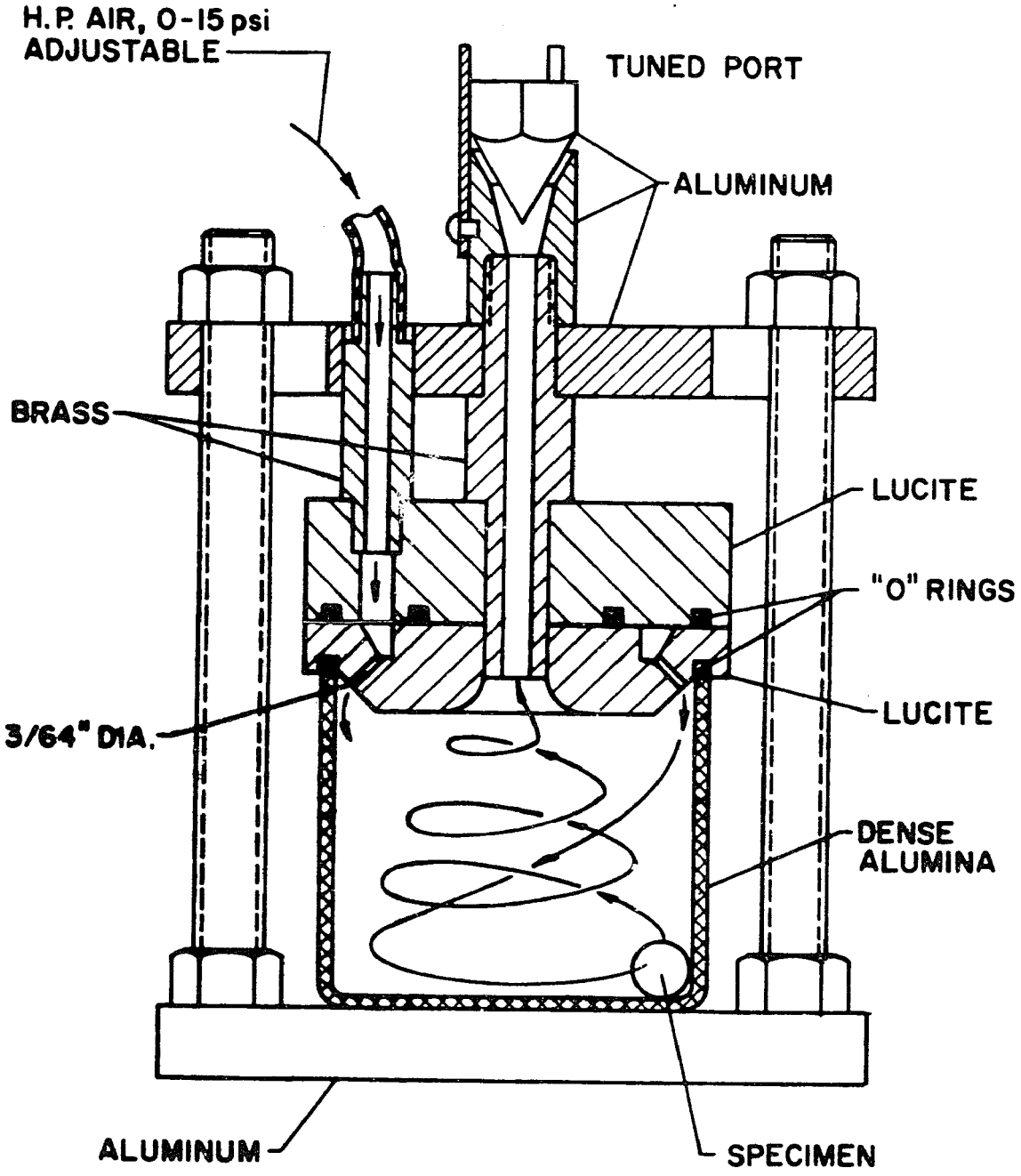
H.P. AIR, 0-15 psi
ADJUSTABLE
TUNED PORT
ALUMINUM
BRASS
LUCITE
"O" RINGS
3/64" DIA.
LUCITE
DENSE
ALUMINA
ALUMINUM
SPECIMEN

Figure 21

Schematic Representation of the Contra-Rotating Sphere Lapping and Polishing System.

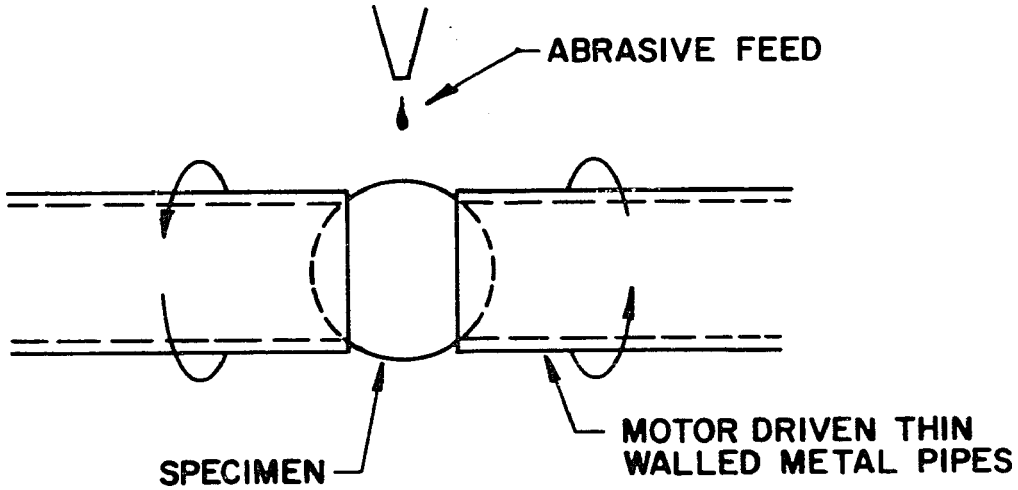
ABRASIVE FEED
SPECIMEN
MOTOR DRIVEN THIN
WALLED METAL PIPES

Figure 22

Schematic Representation of the Sphere Resonance Method for Modulus Measurements.

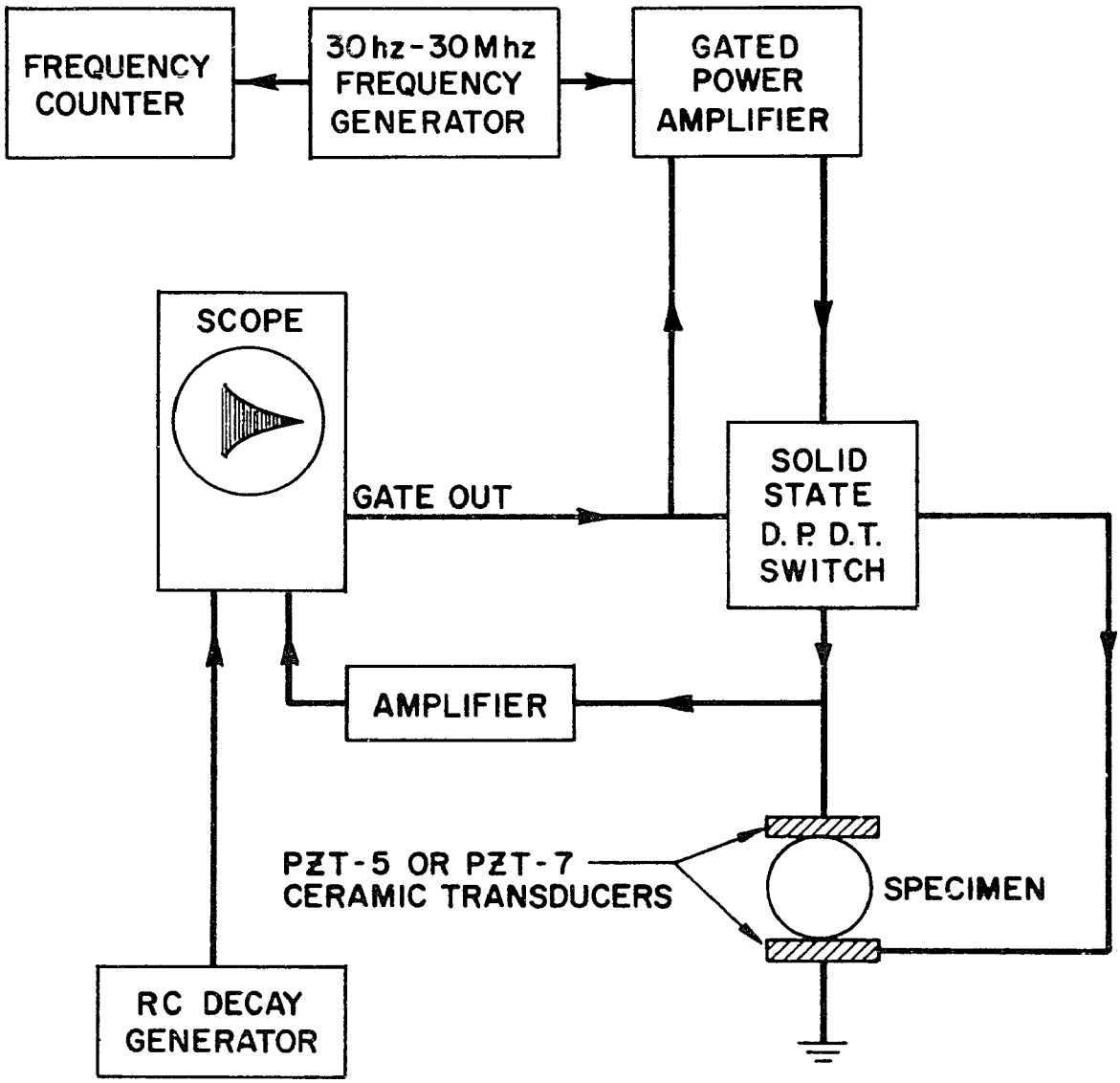
FREQUENCY COUNTER
30hz-30Mhz FREQUENCY GENERATOR
GATED POWER AMPLIFIER
SCOPE
GATE OUT
SOLID STATE D. P. D.T. SWITCH
AMPLIFIER
PZT-5 OR PZT-7 CERAMIC TRANSDUCERS
SPECIMEN
RC DECAY GENERATOR

Figure 23

Schematic Representation of the First Three Shear Vibration Modes of a Sphere.

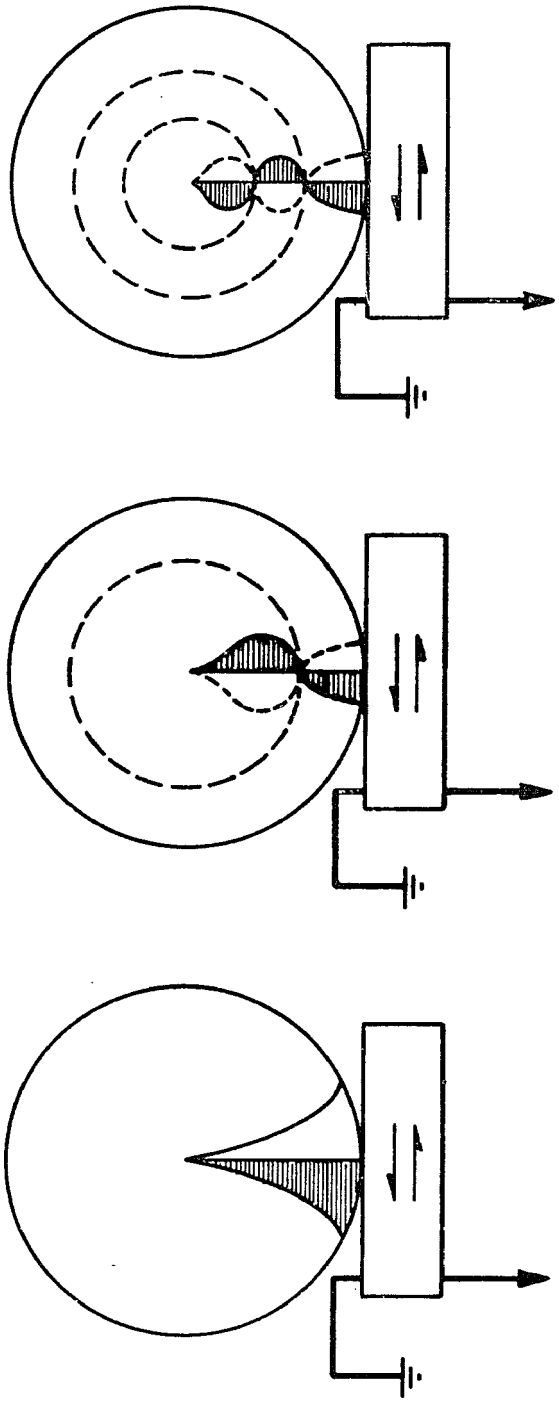

Figure 24

Normalized Resonant Sphere Frequency, f_r, Versus Poison's Ratio. Note That Only the Spherical Modes, ${}_iS_j$, are a Function of Poisson's Ratio. The Data for Pure Nickel Oxide are Shown and a Best Fit is Found at $\sigma = 0.416$.

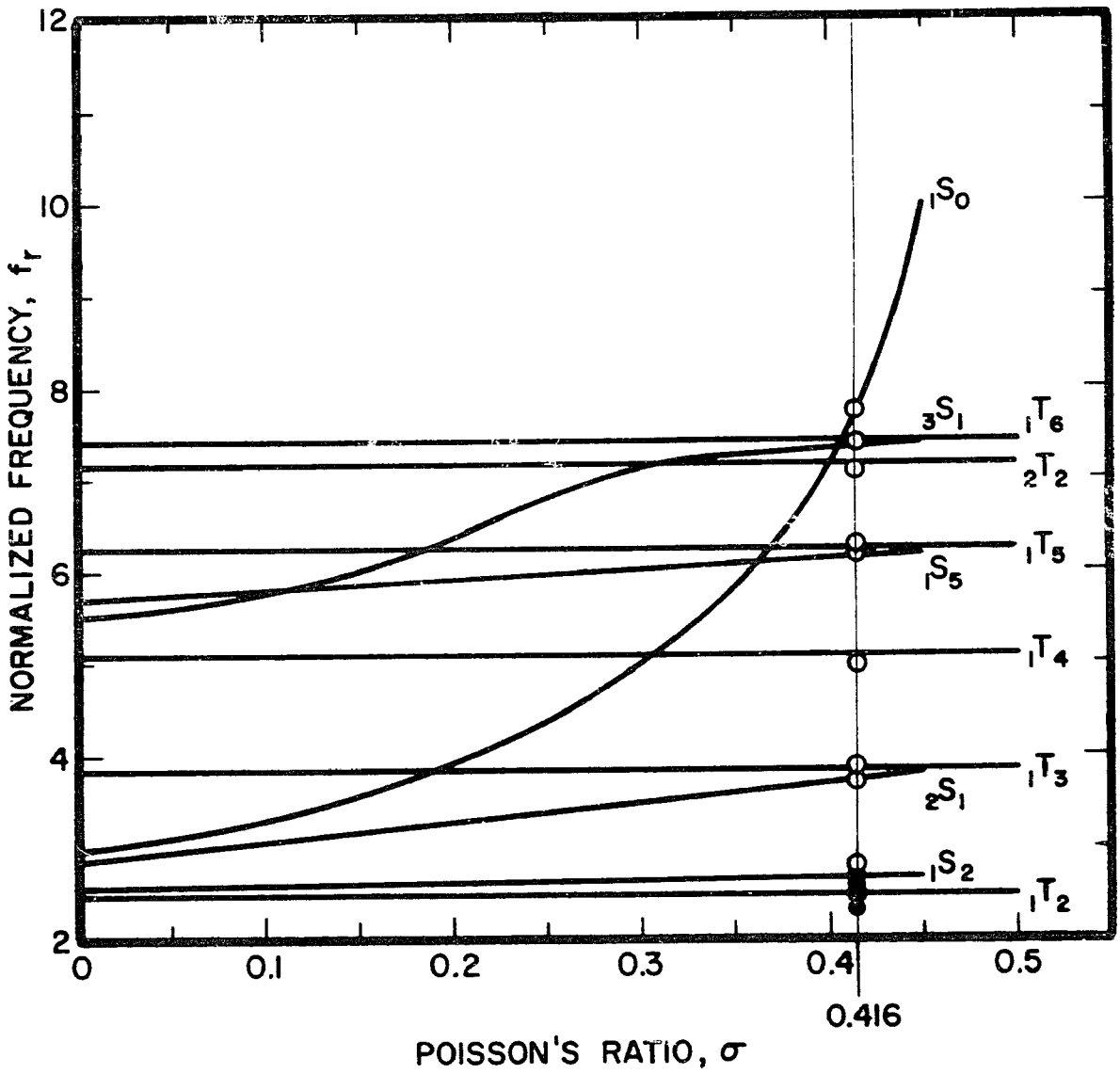
12
10
8
6
4
2
NORMALIZED FREQUENCY, f_r
0
0.1
0.2
0.3
0.4
0.5
0.416
POISSON'S RATIO, σ
$_1S_0$
$_3S_1$
$_1T_6$
$_2T_2$
$_1T_5$
$_1S_5$
$_1T_4$
$_1T_3$
$_2S_1$
$_1S_2$
$_1T_2$

Figure 25

Young's Modulus as a Function of Temperature for the Same Pure Nickel Oxide Specimen Using Two Different Sets of Matched Crystals. Open Circles are 92.5 KC Measurements, Closed Circles are 118.5 KC Measurements.

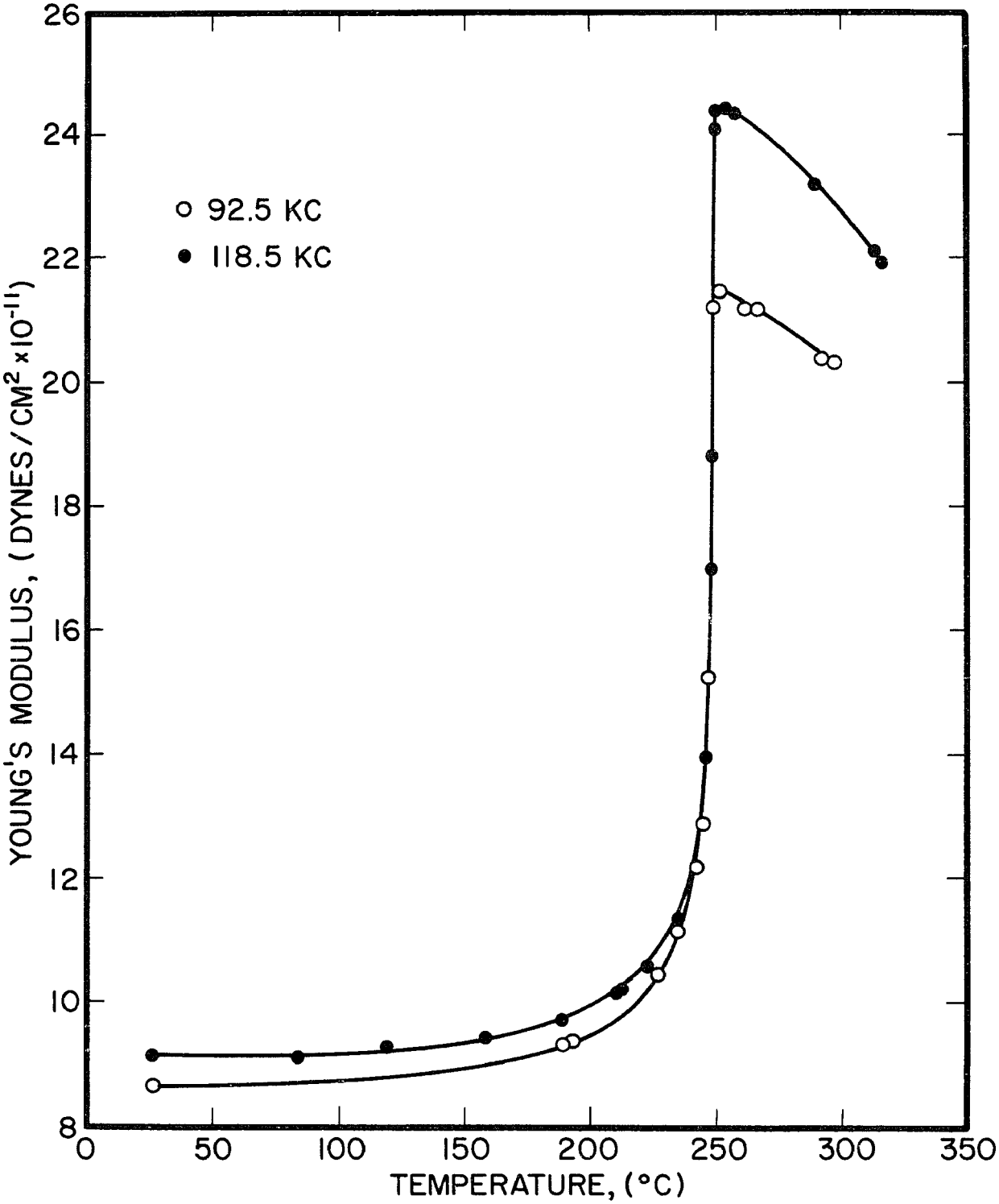
26
24
22
20
18
16
14
12
10
8
0
50
100
150
200
250
300
350
○ 92.5 KC
● 118.5 KC
YOUNG'S MODULUS, (DYNES/CM² x10⁻¹¹)
TEMPERATURE, (°C)

Figure 26

Young's Modulus as a Function of Temperature for Pure Nickel Oxide Measured with 118.5 KC Crystals. Open Circles are Values Obtained From Equation A3.2 ($\tan^2$ Term Variable) and Closed Circles are Values Obtained From Equation A3.3 ($\tan^2 \equiv 0$).

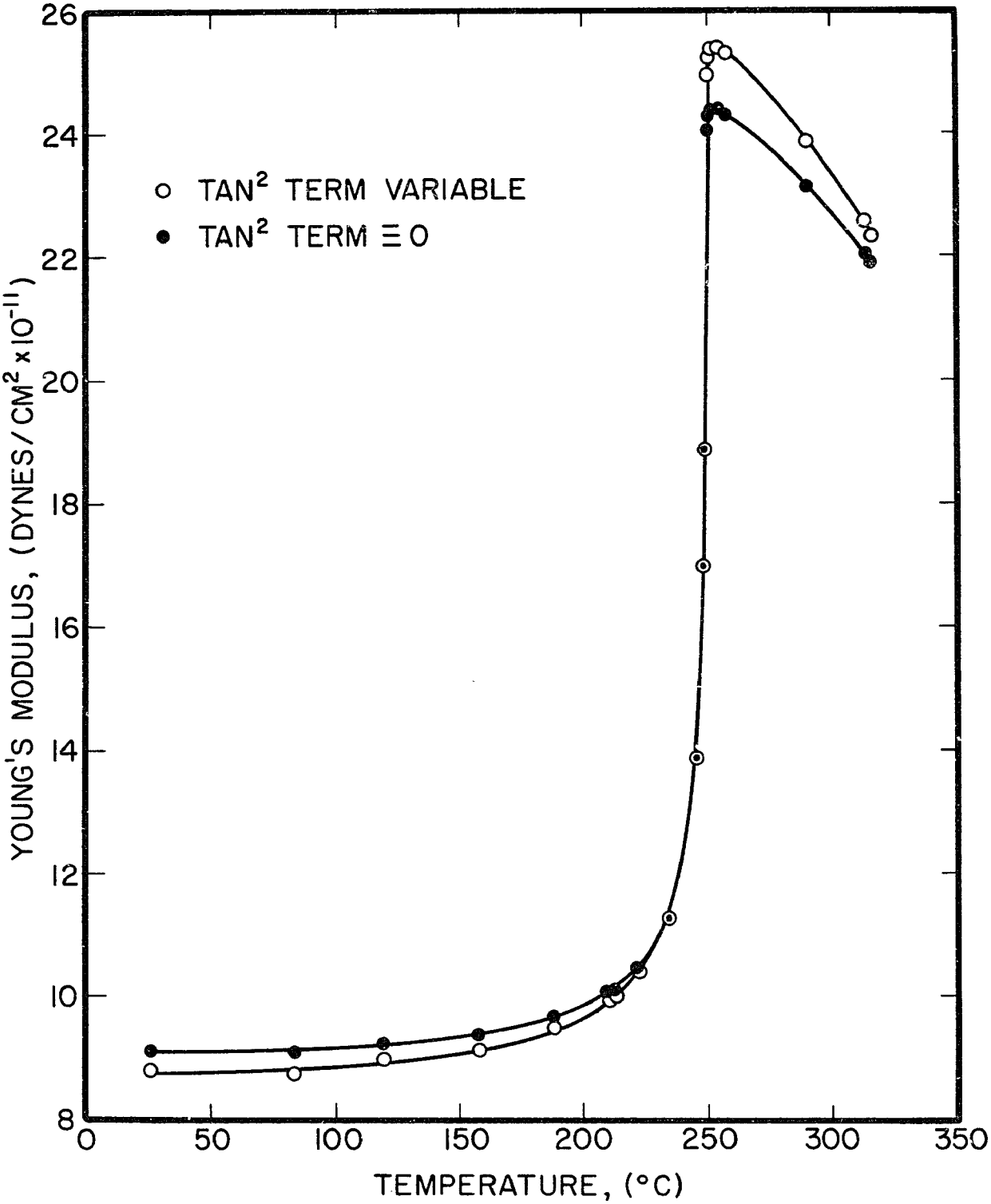
26
24
22
20
18
16
14
12
10
8
0
50
100
150
200
250
300
350
TAN² TERM VARIABLE
TAN² TERM ≡ 0
YOUNG'S MODULUS, (DYNES/CM² x 10⁻¹¹)
TEMPERATURE, (°C)

Figure 27

Young's Modulus as a Function of Temperature for Each of the Lithium-Nickel Oxide Alloys Investigated. Each Curve is Identified by the Lithium Content (Atomic Percent) of the Sample, Measurements Taken With 118.5 KC Crystals (Increasing Temperature).

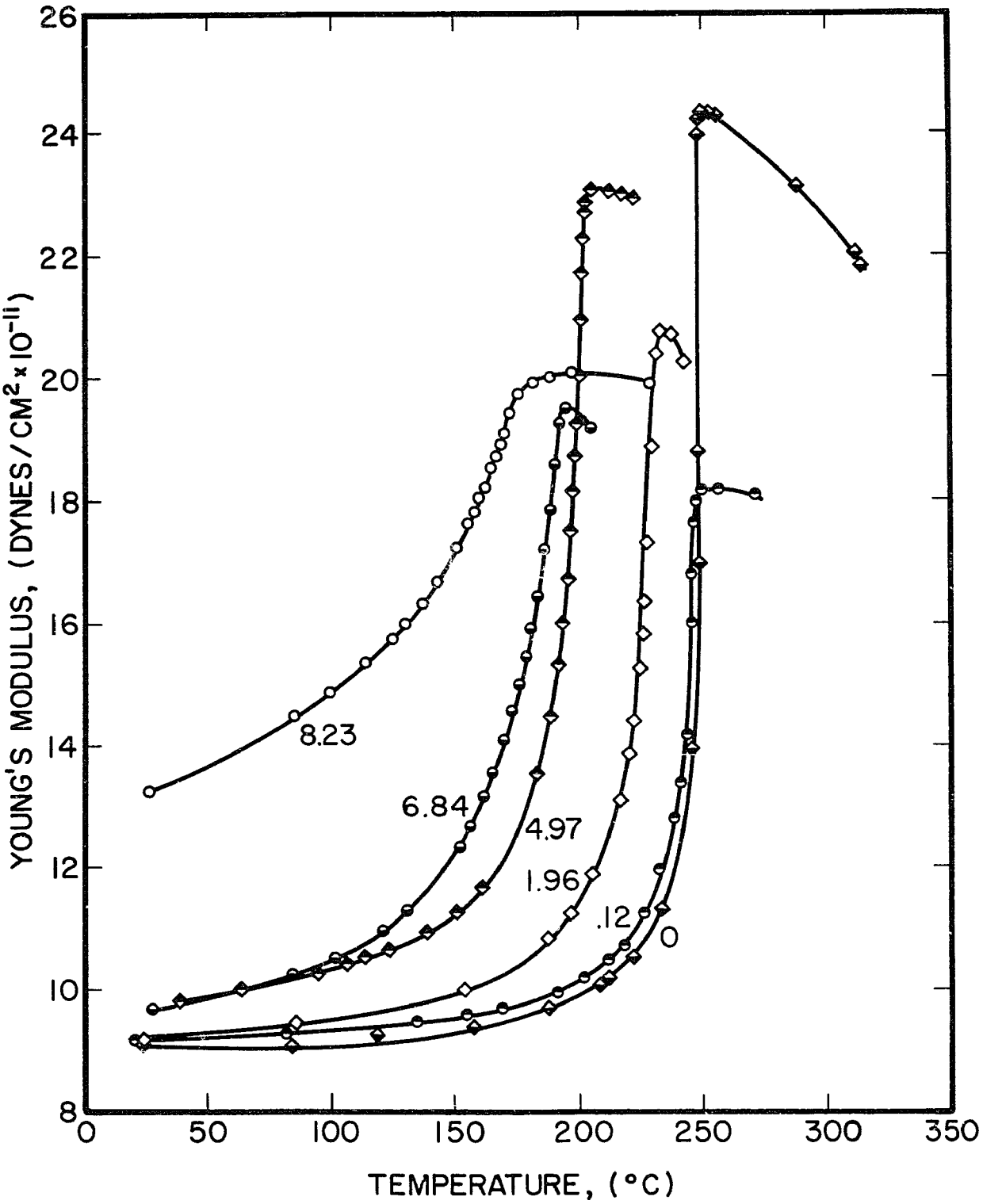
YOUNG'S MODULUS, (DYNES/CM^2 x 10^{-11})
TEMPERATURE, (°C)
26
24
22
20
18
16
14
12
10
8
0
50
100
150
200
250
300
350
8.23
6.84
4.97
1.96
.12
0

Figure 28

Young's Modulus as a Function of Temperature for Each of the Lithium-Nickel Oxide Alloys Investigated. Each Curve is Identified by the Lithium Content (Atomic Percent) of the Sample. Measurements Taken With 118.5 KC Crystals (Decreasing Temperature).

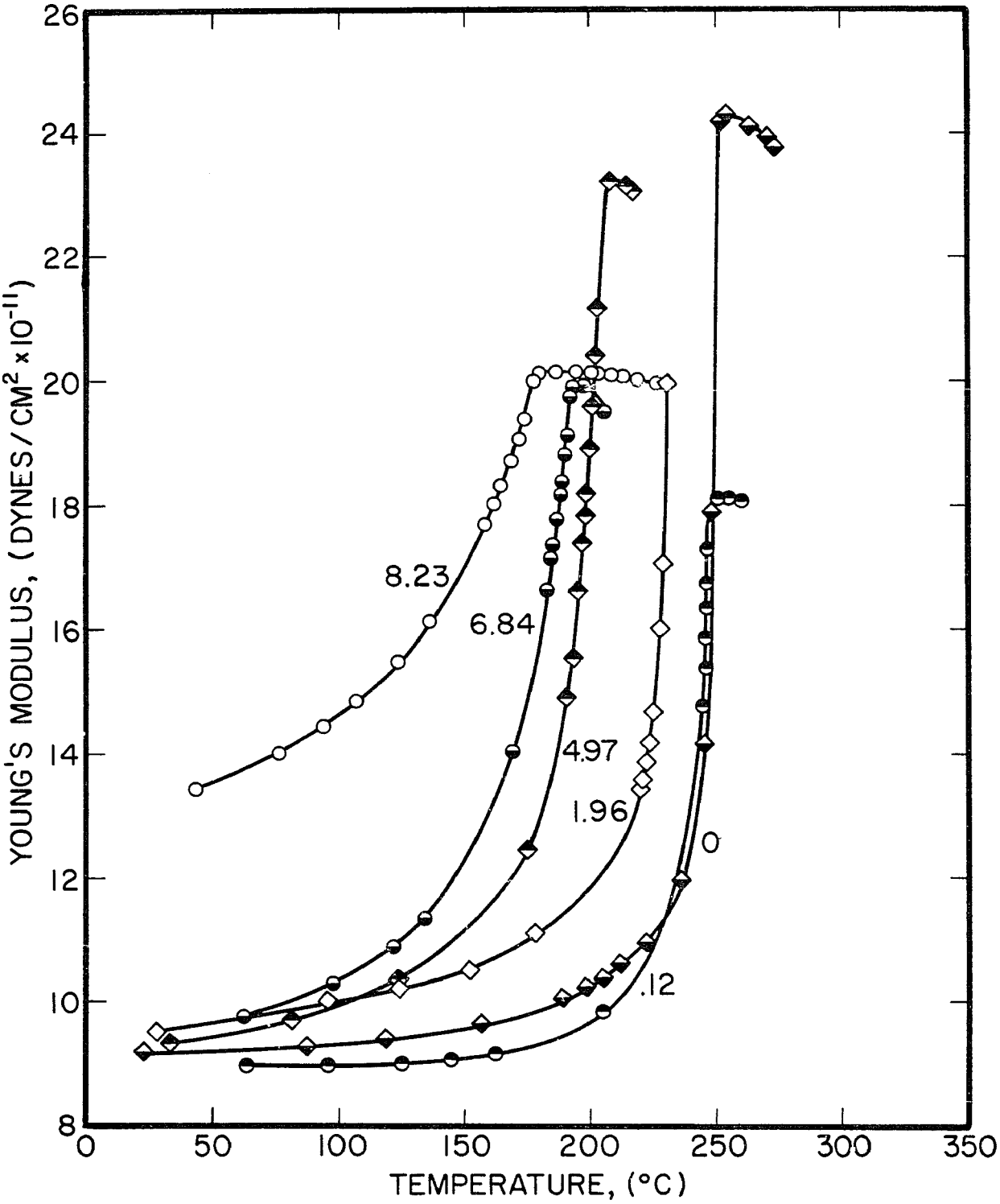
YOUNG'S MODULUS, (DYNES/CM² x 10⁻¹¹)
TEMPERATURE, (°C)
8.23
6.84
4.97
1.96
0
.12

Figure 29

Relative Acoustic Loss as a Function of Temperature for Each of the Lithium-Nickel Oxide Alloys Investigated. Each Curve is Identified by the Lithium Content (Atomic Percent) of the Sample. Measurements Taken With 118.5 KC Crystals (Increasing Temperature). The Flat Response of the 1.96, 6.84 and 8.23 Atomic Percent Lithium Alloys is Caused by the Peak Amplitude at Resonance Going to Zero Above the Néel Temperature.

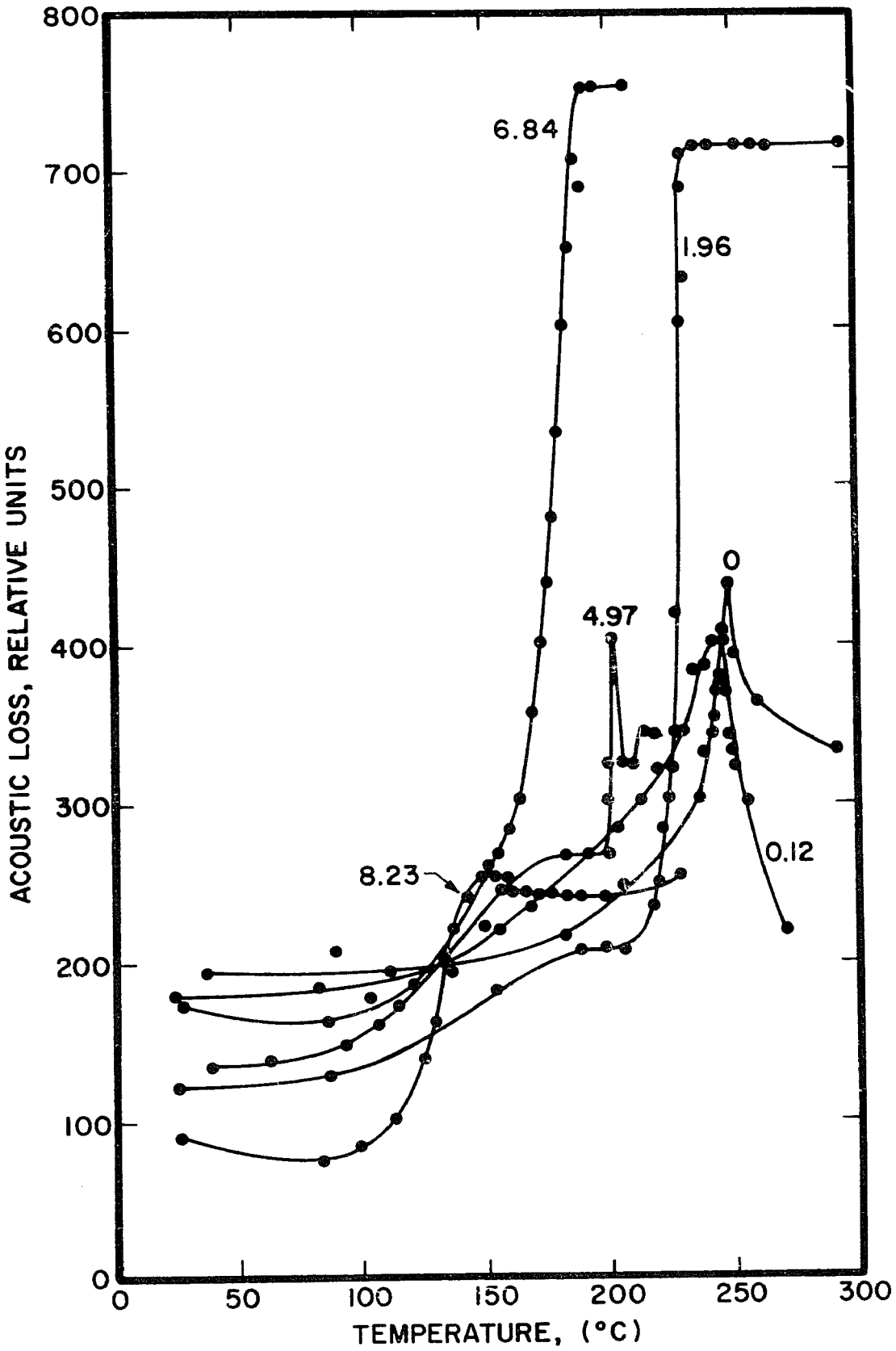
ACOUSTIC LOSS, RELATIVE UNITS
800
700
600
500
400
300
200
100
0
0
50
100
150
200
250
300
TEMPERATURE, (°C)
6.84
1.96
0
4.97
8.23
0.12

Figure 30

Young's Modulus as a Function of Temperature for a 1 Percent Lithium-11.5 Percent Magnesium-Nickel Oxide Alloy. Measurements Taken With 118.5 KC Crystals. Open Circles are Data Taken With Increasing Temperature, Closed Circles are Data Taken With Decreasing Temperature.

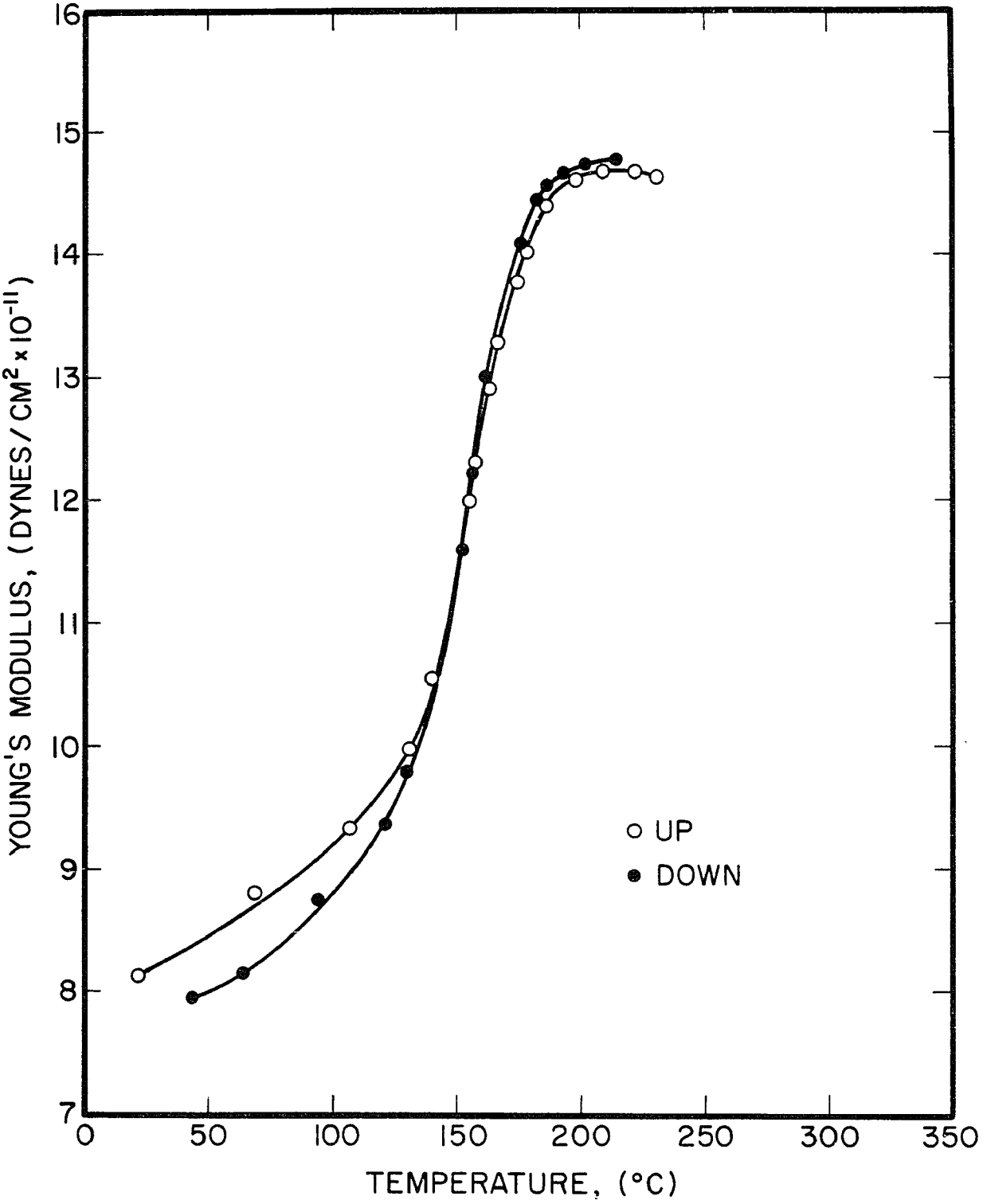
YOUNG'S MODULUS, (DYNES/CM^2 x 10^{-11})
16
15
14
13
12
11
10
9
8
7
0
50
100
150
200
250
300
350
TEMPERATURE, (°C)
UP
DOWN

Figure 31

Néel Temperature as a Function of Atomic Percent Lithium as Determined From the Maximum Slope of the Modulus Versus Temperature Curve of Figure 27. The Line was Determined by Least-Squares Analysis.

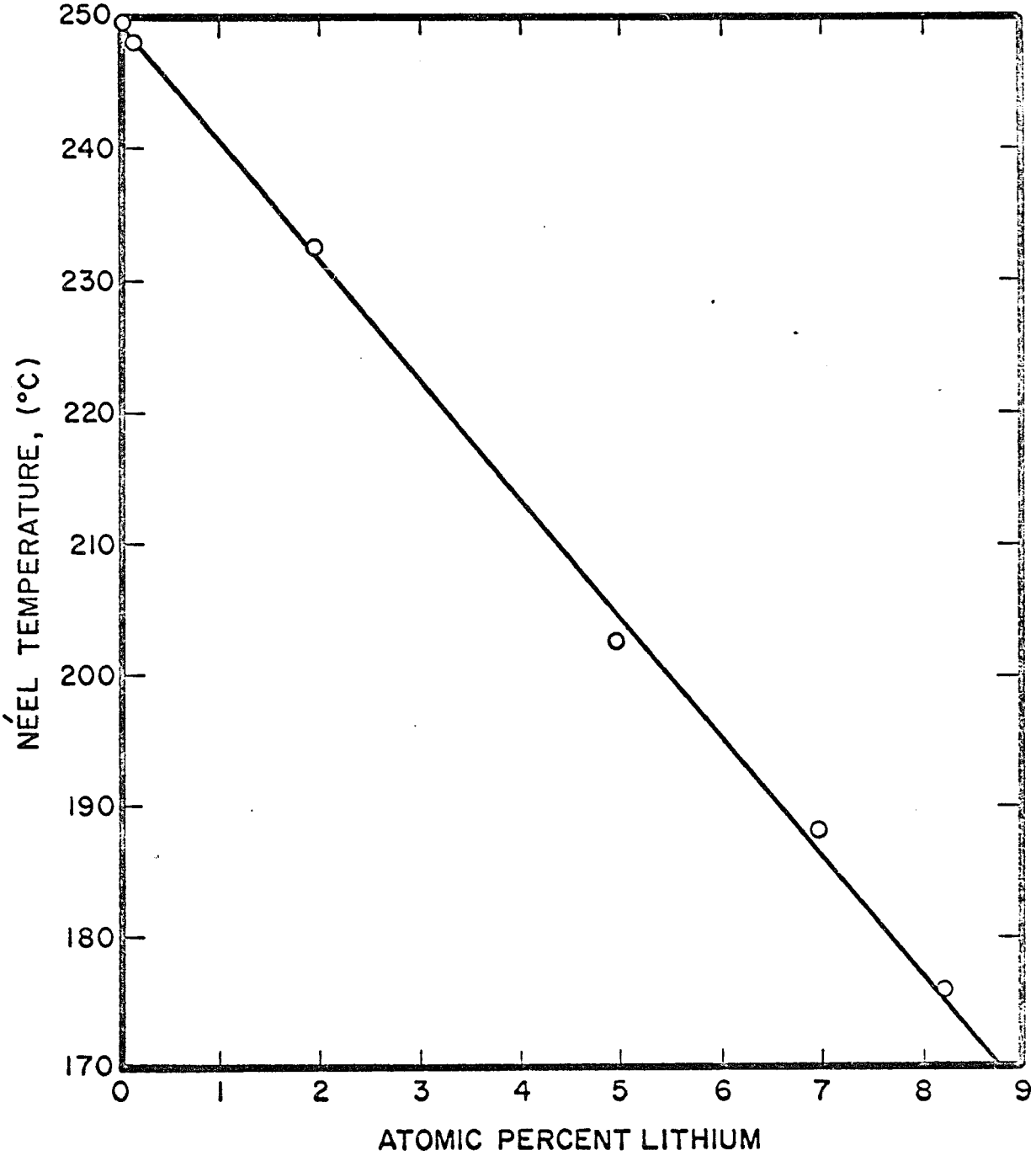
250
240
230
220
210
200
190
180
170
NÉEL TEMPERATURE, (°C)
0
1
2
3
4
5
6
7
8
9
ATOMIC PERCENT LITHIUM

Figure 32

Resistivity as a Function of Temperature for Each of the Lithium-Nickel Oxide Alloys Investigated. Each set of Points is Identified by the Lithium Content (Atomic Percent) of the Sample. Closed Symbols are Data Taken With Increasing Temperature, Open Symbols are Data Taken With Decreasing Temperature.

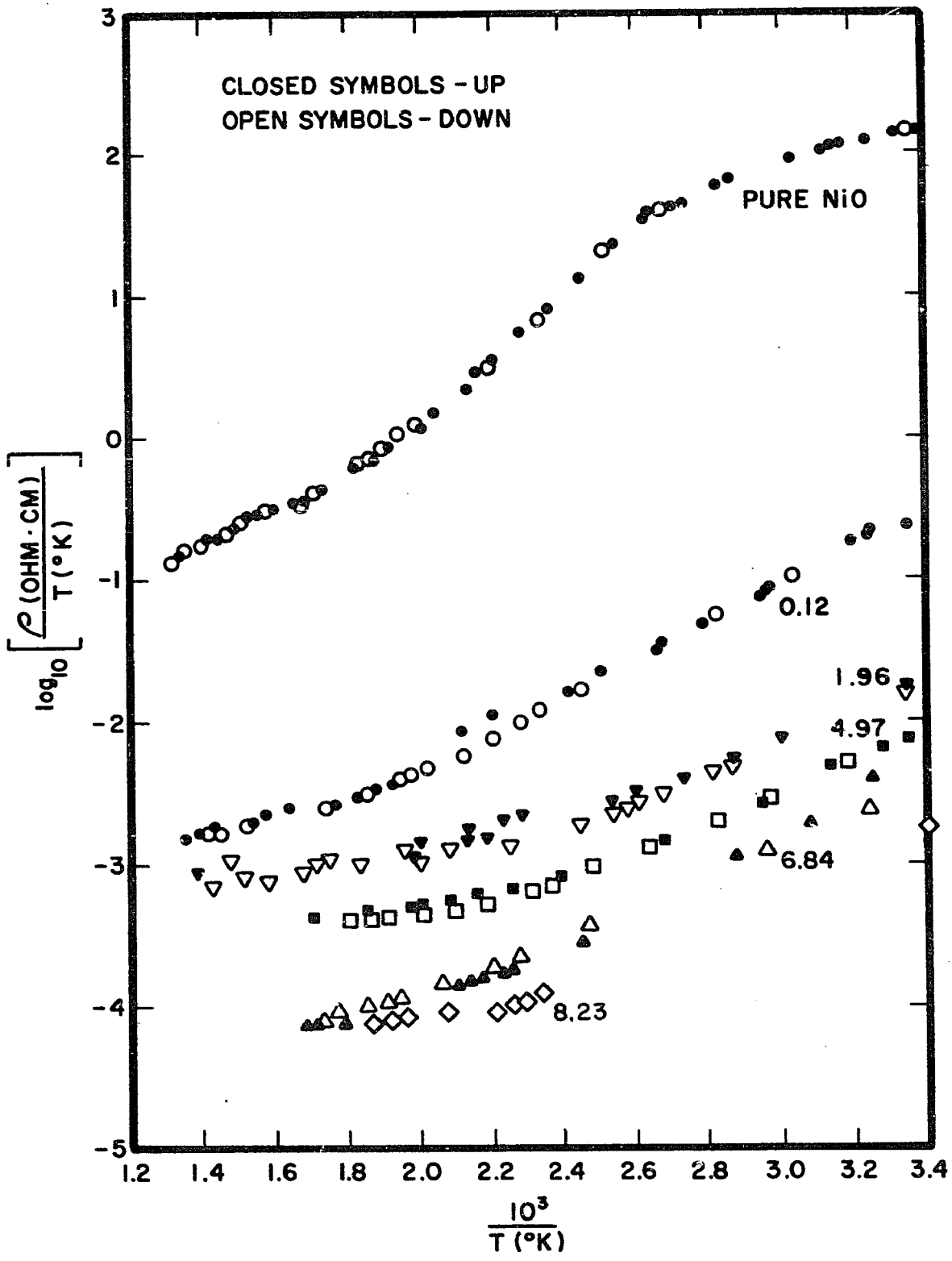
CLOSED SYMBOLS - UP
OPEN SYMBOLS - DOWN
PURE NiO
0.12
1.96
4.97
6.84
8.23
$\log_{10}\left[\frac{\rho\ (\Omega\cdot cm)}{T\ (^\circ K)}\right]$
$\frac{10^3}{T\ (^\circ K)}$
3
2
1
0
-1
-2
-3
-4
-5
1.2
1.4
1.6
1.8
2.0
2.2
2.4
2.6
2.8
3.0
3.2
3.4

Figure 33

General Form of the Resistivity Versus Temperature for Nickel Oxide.

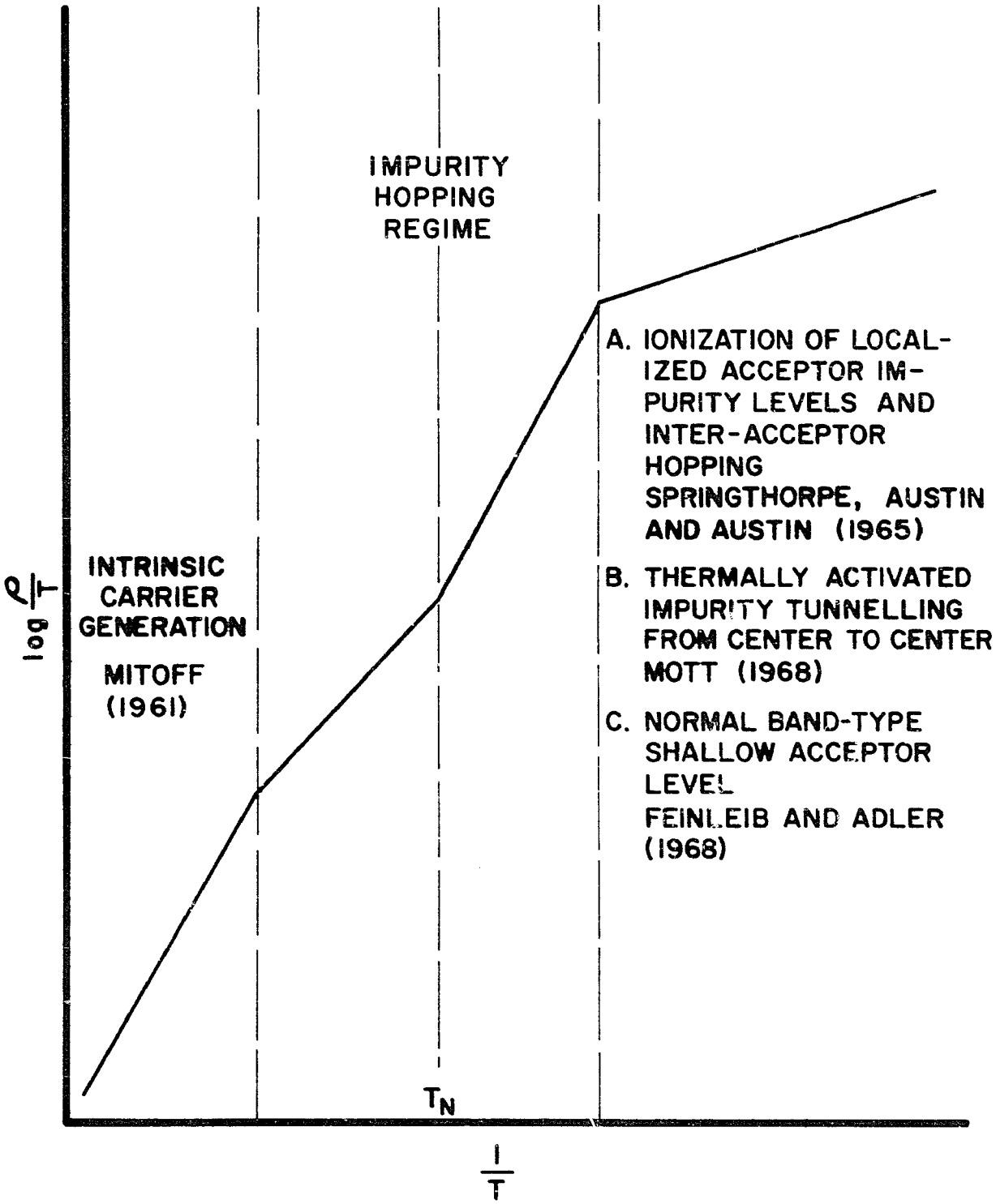
IMPURITY
HOPPING
REGIME
INTRINSIC
CARRIER
GENERATION
MITOFF
(1961)
A. IONIZATION OF LOCAL-
IZED ACCEPTOR IM-
PURITY LEVELS AND
INTER-ACCEPTOR
HOPPING
SPRINGTHORPE, AUSTIN
AND AUSTIN (1965)
B. THERMALLY ACTIVATED
IMPURITY TUNNELLING
FROM CENTER TO CENTER
MOTT (1968)
C. NORMAL BAND-TYPE
SHALLOW ACCEPTOR
LEVEL
FEINLEIB AND ADLER
(1968)
T_N
$\log \rho/T$
$\frac{1}{T}$

VITA

Michael Richard Notis was born in Brooklyn, New York on August 6, 1938. He attended Far Rockaway High School and was awarded a Grumman Aircraft Engineering Scholarship upon graduation. He attended Lehigh University from 1956 to 1960 and received a B.S. degree in Metallurgical Engineering. During these years he was a summer employee at Grumman Aircraft Engineering Company where he worked in piece parts manufacture, hydraulic line assembly, tool design, and metallurgical quality control departments.

In 1960 Mr. Notis was employed by the Western Electric Company in Allentown, Pennsylvania. He was soon transferred to Bell Telephone Laboratories as a participant in the Western Electric Development Engineering Program and was then promoted to Planning Engineer in 1963. He received his M.S. degree in Metallurgical Engineering at Lehigh University in October 1963, and took a leave of absence from Western Electric Company in order to return to Lehigh in July 1967.

Papers published by Mr. Notis include the "Effect of Growth Rate on Stacking Fault Density in Epitaxial Silicon Layers" in the Journal of Applied Physics, 35 (3) 695-697 (1964), and the "Decarburization of an Iron-Nickel-Cobalt Glass Sealing Alloy" in the Journal of the American Ceramic

Society, 45 (9) 412-416 (1962). He is a member of the Newtonian Society, the Society of Sigma Xi, American Society for Metals, American Society for Testing Materials, and the Metallurgical Society of A.I.M.E.

Mr. Notis was married to the former Ruth Ellen Zwiebel on August 30, 1959 and has three children, Beth, age 8, Mark Ian, age 5, and Jennifer Lynn, age 1.